MODEL-BASED OPTIMIZATION OF SIMULATED MOVING BED REACTOR OPERATIONS IN ISOLATION AND WITHIN AN OVERALL PROCESS

A Dissertation
Presented to
The Academic Faculty

by

Shan Tie

In Partial Fulfillment
of the Requirements for the Degree
Doctor of Philosophy in the
School of Chemical and Biomolecular Engineering

Georgia Institute of Technology
December 2017

MODEL-BASED OPTIMIZATION OF SIMULATED MOVING BED REACTOR OPERATIONS IN ISOLATION AND WITHIN AN OVERALL PROCESS

Approved by:

Dr. Yoshiaki Kawajiri, Advisor
School of Chemical and Biomolecular Engineering
Georgia Institute of Technology

Dr. Ryan Lively
School of Chemical and Biomolecular Engineering
Georgia Institute of Technology

Dr. Andreas Bommarius, Advisor
School of Chemical and Biomolecular Engineering
Georgia Institute of Technology

Dr. Megan Donaldson
Engineering and Process Science
The Dow Chemical Company

Dr. Matthew Realff
School of Chemical and Biomolecular Engineering
Georgia Institute of Technology

Date Approved: August 18, 2017

To my loved ones

ACKNOWLEDGEMENTS

I would like to thank my advisors, Dr. Yoshiaki Kawajiri and Dr. Andreas Bommarius, for giving me the opportunity to be their student. I have learned much from them both and I am grateful for their advice, support, and expertise throughout my graduate school experience.

Thank you to my committee members for reviewing my thesis and giving insightful suggestions and feedback to consider for my thesis project.

I am also grateful for my colleagues, Dr. Gaurav Agrawal, Dr. Balamurali Sreedhar, Dr. Jungmin Oh, and Dr. Hector Rubiera who taught and guided me and by laying the groundwork for my research. I am also thankful for the members of both the Kawajiri and Bommarius research groups for creating a friendly, learning atmosphere.

I am thankful to all the faculty and staff in School of Chemical and Biomolecular Engineering for creating a successful academic environment.

Finally, I would like to extend my thanks to my collaborators at the Dow Chemical Company for providing their expertise to the project and for the financial support through the UPI program.

TABLE OF CONTENTS

LIST OF TABLES

LIST OF FIGURES

LIST OF SYMBOLS AND ABBREVIATIONS

A_{cs}	cross-sectional area of the chromatographic column (m^2)
AA	acetic acid
b	adsorption equilibrium constant
C	liquid phase concentration (mol/L)
D_{ax}	axial dispersion coefficient (m^2/min)
EA	ethyl acetate
EtOH	ethanol
H	Henry's constant
k_1	forward reaction rate constant (L/mol min)
K_{eq}	equilibrium constant
K_m	mass transfer coefficient (min^{-1})
MW	molecular weight (g/mol)
L	column length (m)
N	number
$\dot{N}$	Molar flow rate (mol/min)
PM	1-methoxy-2-propanol
PMA	propylene glycol methyl ether acetate
PSA	pressure swing adsorber
q	average solid phase concentration (mol/L)
r	reaction rate (mol/L min)
SMBR	simulated moving bed reactor
t	time (min)

u	interstitial velocity in the column (m/min)
U_L	lower bound on volumetric flow rate (mL/min)
U_U	upper bound on volumetric flow rate (mL/min)
x	axial coordinate

Greek letters

ε	epsilon constraint method
ε_T	total void fraction
ζ	objective function for SMBR optimization
θ	parameter
v	stoichiometric coefficient
ξ	conversion
ρ	Tikhonov regularization weighting factor
φ	objective function for parameter estimation

Superscripts and Subscripts

comp	component
D	desorbent stream
eq	equilibrium
Ex	extract stream
exp	experiment
F	feed stream
i	component (AA, EA, PM, PMA, water, ethanol)
j	column number (1, 2, 3, 4)

k	experiment data point
m	model parameters
R	raffinate stream
rec	recycle stream
SS	superstructure configuration’s downstream recycle stream

SUMMARY

Simulated moving bed reactor (SMBR) is a process intensification alternative to conventional sequential integration of batch reactor and separator operations. Specifically, SMBR is a cyclic operation that is continuous in carrying out simultaneous reaction and chromatographic separation. This operation improves separation resolution, increases productivity, and reduces solvent consumption compared to the conventional operation. Additionally, SMBR is less energy-intensive compared to other reactive separation techniques such as reactive distillation. Furthermore, this operation can significantly improve the conversion of equilibrium-limited reactions by creating the driving force for the forward reaction.

Despite these benefits, the complexity in SMBR modeling and design is extremely challenging for industrial implementation. Determining the optimal SMBR operation only by an experimental approach is time intensive and requires human expertise and intervention. Within the past decade, work has been performed to find the optimal design and operation of SMBR utilizing a mathematical model; however, these investigations were focused on single-objective optimization, which lacks the analysis of trade-offs in SMBR operation, or used heuristic based algorithms, which could potentially miss the optimal solution.

This work demonstrates a practical and deterministic model-based approach to optimize an industrially relevant SMBR process and to identify the optimal SMBR operating parameters for an SMBR operation in isolation and within an integrated overall process. The SMBR operation is applied to an industry case study for the continuous production of a solvent, propylene glycol methyl ether acetate (DOWANOL™, PMA). PMA, a strong solvent, is an

industrially important intermediate product that is the second-most used ester and has many industry applications as the base for cleaners, paints, and coatings.

The first and second objectives of the study are to apply the model-based framework to the esterification and transesterification reaction routes of PMA production. The optimization formulation is a multi-objective problem to maximize both PMA productivity and the conversion of the limiting reactant. Several constraints were placed on product recovery and byproduct impurity. The initial SMBR models were determined by batch kinetic and single column reaction and separation experiments. Several SMBR experiments were conducted on the in-house SMBR unit. Outlet concentrations, determined from both model predictions and obtained from the SMBR experiments, were used to recalculate the model parameters. The corrected SMBR models were experimentally validated and then optimized to compare the performance of the two reaction routes for PMA production. These two objectives demonstrate that the simultaneous optimization and model correction (SOMC) method is able to determine a corrected model capable of accurately predicting experimental SMBR results and for determining optimal operating conditions. Moreover, the SOMC is robust and generalizable to different chemistries such that this method can extend beyond the case studies of esterification and transesterification production of PMA.

The final objective of the study is to determine the optimal SMBR operation within an overall process that includes two downstream units. The extract and raffinate streams are processed to improve product purity and recycle streams leaving the downstream units are returned to the SMBR to reduce solvent consumption. Three different operating schemes are evaluated—the standard, limited superstructure, and full superstructure configuration. The process is optimized to maximize the PMA productivity while conversion, product recovery,

byproduct content, and solvent to product ratio are process constraints. This work offers a more realistic overall process understanding that is representative of industrial SMBR operations.

CHAPTER 1. INTRODUCTION

Within the past decade, there has been growing societal and scientific concern for the impact of anthropological development and progress on the environment. Increasing attention has focused on how chemical processes affect resource consumption and waste generation. Process intensification has gained momentum as a way to achieve good product quality and quantity while balancing considerations for economic and environmental costs. Process intensification is the engineering of novel methods and equipment to reduce chemical plant footprint and to transform processes to render more compact, safe, energy-efficient, and environmentally sustainable plants. Such technologies have included new equipment (catalyst, microreactors) and methods such as hybrid separations and multifunctional reactors (chromatographic reactors, reactive distillation, reactive crystallization, reactive extraction, reactive membranes), and process-control methods [1].

There are implementation challenges for all hybrid reactive separations. The main challenge are: 1) technical gaps that include a lack of materials, lack of simulation and scale-up capability, and lack of validated process data; 2) implementation risks from a lack of information of the process economics and demonstrations/prototypes at reasonable scales; 3) barriers to technology transfer because the new technologies are always application specific and are hard to generalize. Finally, the limited degree of freedom because of the combined reaction and separation reduces the size of the feasible operation window and makes the selection of optimal operations difficult. Some process-specific challenges are: reactive adsorption faces challenges involving development of catalyst/adsorbents; reactive distillation suffers from challenges of proper boiling point

sequence and difficulty in providing residence time; membrane reactors face relatively high price of units [1].

Regardless of the barriers, the outlook for the process intensification methods is positive. Continued research and innovation in this area have allowed new developments in process materials, equipment, and design tools. Moreover, at the heart of any chemical engineering process is the production and purification of the desired product. Recently, there is increasing demands and new demand arising for high purity chemicals and biologics, especially in the pharmaceutical industry. Traditional methods of sequential reaction followed by downstream separation is no longer able to satisfy demands. A potential solution is reactive chromatography.

The following sections will explain the principles of reactive chromatography. This principle, which can be implemented as a single-column operation, is extended to simulated moving bed reactor (SMBR). Furthermore, its applications to the esterification and transesterification routes of PMA production and its potential for additional chemical reactions are discussed.

1.1 Principles of reactive chromatography

Reactive chromatography is a type of reactive separation process rooted in the fundamentals of chromatography. Chromatography is a commonly used technique in chemical engineering that separates component mixtures based on their individual adsorptive properties to the solid phase. The component mixture (feed) is carried through a column by a mobile, liquid phase (solvent/desorbent) and the components interact with the stationary, solid phase (resin/adsorbent). Separation of mixtures into individual components occurs due to the relative affinity of each component towards the adsorbent.

Weakly adsorbing components travel through the column faster and elute earlier whereas the strongly adsorbing components travel slower and elute later.

In reactive chromatography (Figure 1), reaction in addition to separation occurs in the column. Typically, reactive chromatography is implemented using a single solid phase that acts as both adsorbent and catalyst. There are variations such as using a mixed resin bed to perform the reaction and separation functions. In a single resin operation, when a mixture is fed into the column, the solid phase simultaneously catalyzes product formation and separates the product from its reactants. In equilibrium limited chemistries, the conversion increases because of Le Châtelier's Principle. The dual separation and reaction properties of the solid phase work together such that newly formed products are continuously removed from the reaction locus, thus driving equilibrium-limited reactions to the theoretical conversion of 100%.

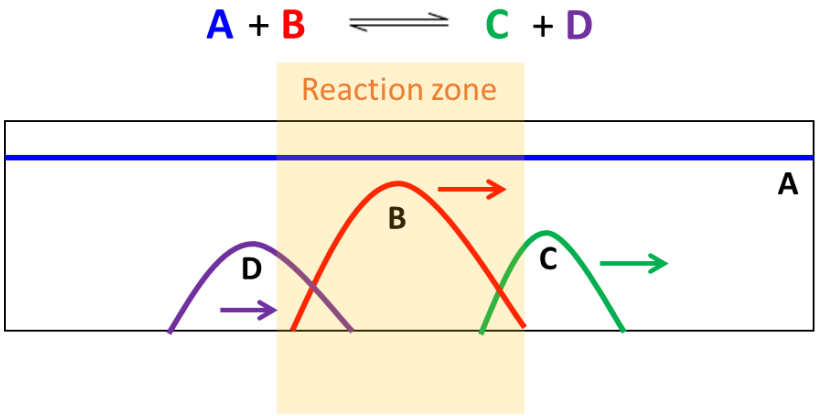

Figure 1 Schematic of reactive chromatography for the production of *C* and byproduct *D* from a reaction of *A* and *B*.

1.2 Principles of simulated moving bed reactor

The concept of a reactive chromatography process can be incorporated into a simulated moving bed system to create a continuous reactive chromatography process or

simulated moving bed reactor (SMBR). The reason the system is a "simulated" moving bed instead of a "true" moving bed (TMB) is because from an implementation standpoint, the equipment needed and the movement of the resin is difficult to achieve. Movement of the solid phase faces some technical challenges such as equipment abrasion, mechanical erosion of the resin material, and difficulty in maintaining a plug flow, especially in large diameter columns. To overcome these challenges, a simulated moving bed is favored. The continuous operation of SMBR (Figure 2) is realized by the "simulated" countercurrent flow of the solid phase with respect to the mobile phase by periodically and simultaneously switching the inlet and outlet streams in the direction of liquid flow [2]. There are two inlet ports for the desorbent and feed and two outlet ports for the extract and raffinate. The feed can be composed of a pure, single reactant or a mixture of components. The faster moving components elute from the raffinate while the slower moving components are removed from the extract.

The standard SMBR configuration consists of a minimum of four columns connected in a four-zone design—with one column in each zone. The zones are demarcated by the two inlet ports and the two outlet ports. Each zone's flow rate can be controlled independently yielding four control variables. Zones II and III are mainly responsible for the reaction and separating the products while zones I and IV regenerate the column by desorbing the adsorbed species. The regular switching of the port positions to simulate the countercurrent motion of the stationary phase is determined by the switching time, the fifth control variable. After start-up, an SMBR system reaches cyclic steady state (CSS) where the concentration profiles keep propagating through the four zones, but the profile developed within each given zone is identical between cycles. The aforementioned control

variables are crucial in determining productivity, product purity and recovery, and solvent consumption and thus require careful optimization for the SMBR operating strategy.

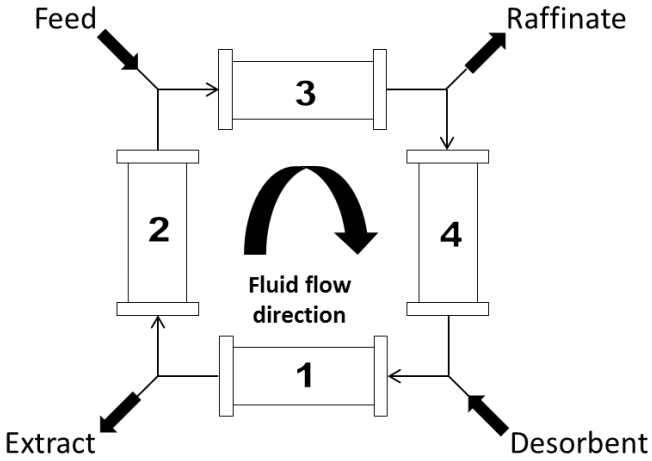

Figure 2 Schematic of a standard configuration in a simulated moving bed reactor (SMBR) operation.

SMBR has many operational advantages that can offer potential economic and environmental advantages compared to the conventional alternative of sequential integration of batch reactor and separator operations. Specifically, SMBR reduces capital cost because of the combined operation into one, exceeds equilibrium limited conversion because of the simultaneous reaction and separation, increases productivity due to the continuous operation, improves separation resolution due to the countercurrent operation, and reduces solvent consumption and waste generation because of the internal recycling of unconsumed reactant and desorbent [3]. Careful investigation is needed to determine how an SMBR operation can realize those advantages given a product and process.

Figure 3 illustrates the internal concentration profiles during two steps of an SMBR operation after having reached cyclic steady state. The example is of the reversible reaction between A and B to form C and D ($A + B \leftrightarrow C + D$). In the beginning of Step 1 (Figure

3A), desorbent is added into column 1, and feed into column 3. The reaction is catalyzed by the resin to form C and D. The two products separate from one another and the reaction locus. The slower moving component (D) is collected mainly at the extract, which is located at the end of column 1. The faster moving component (C) is collected at the raffinate, which is located at the end of column 3 (Figure 3B). After the given step time, the locations of all the inlets and outlets move in the direction of the liquid flow by one position (Figure 3C). The concentration profiles of all the components have also traveled through the columns accordingly and thus both outlets must move forward by one position to collect the products (Figure 3D).

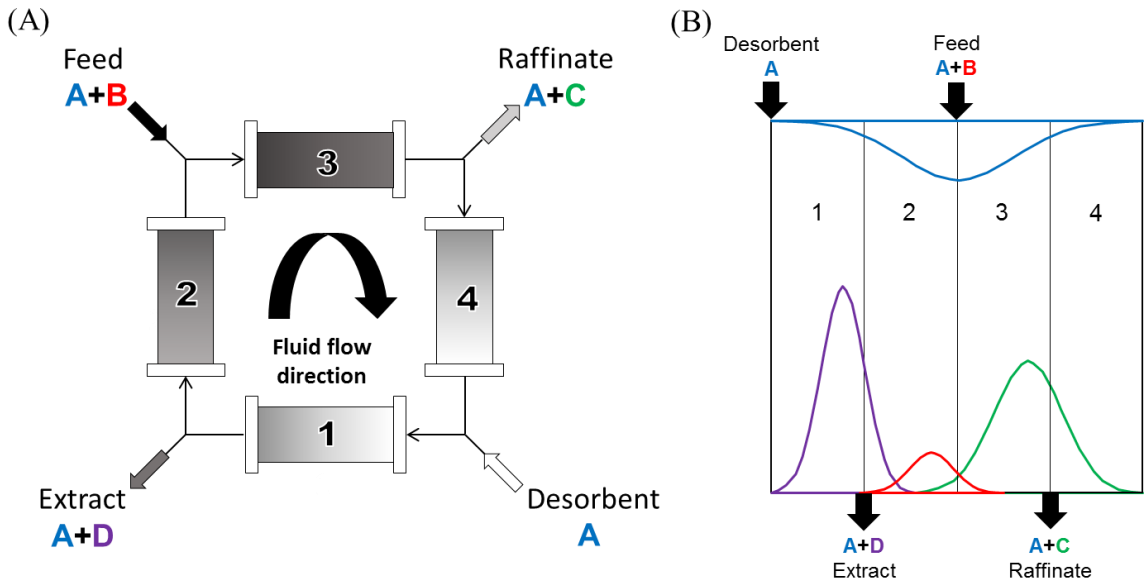

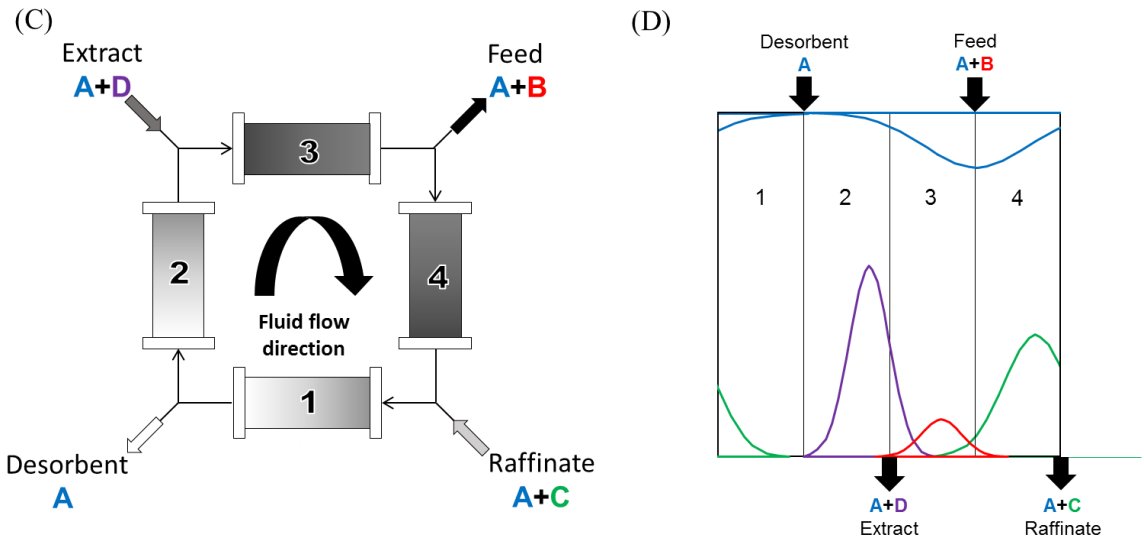

Figure 3 Schematic of SMBR process with the internal concentration profiles at cyclic steady state (CSS) for two consecutive steps: (A) step 1, (B) internal concentration profiles at the beginning of Step 1, and (C) step 2, and (D) internal concentration profiles at the beginning of Step 2.

1.3 Applications of SMBR

The advantages of SMBR have attracted attention especially for various industrial applications. Applications have included isomerization of glucose to fructose [4, 5], hydrogenation of mesitylene [6], hydrolysis [7], isomerization and separation of p-xylene [8], synthesis of methyl tertiary butyl ether [9], and esterification reaction involving esters [10, 11] and acetic acid [12-14]. Minceva *et al.* summarized the various SMBR applications [8]. Given the myriad of applications, we are not aware of any work, besides those done in our group [15-18], which has evaluated the SMBR production of glycol ether esters.

1.3.1 PMA production

This work applies simulated moving bed reactor (SMBR) operation to the production of propylene glycol methyl ether acetate (PMA). PMA, a strong solvent, is the second-most used ester and has many industry applications as the base for cleaners, paints,

and coatings [19]. In this study, we consider two potential reaction routes for PMA production, esterification and transesterification. The esterification route is catalyzed by a cation exchange resin (AMBERLYST^{TM} 15), between acetic acid and 1-methoxy-2-propanol to form PMA and the water byproduct (Figure 4A). On the other hand, the transesterification reaction route is preferentially catalyzed by an anion exchange resin (DOWEX^{TM} 22), between ethyl acetate and 1-methoxy-2-propanol to form PMA and the ethanol byproduct (Figure 4B). Both routes are equilibrium-limited in nature and would benefit from reactive separation methods that can drive reaction towards higher conversion.

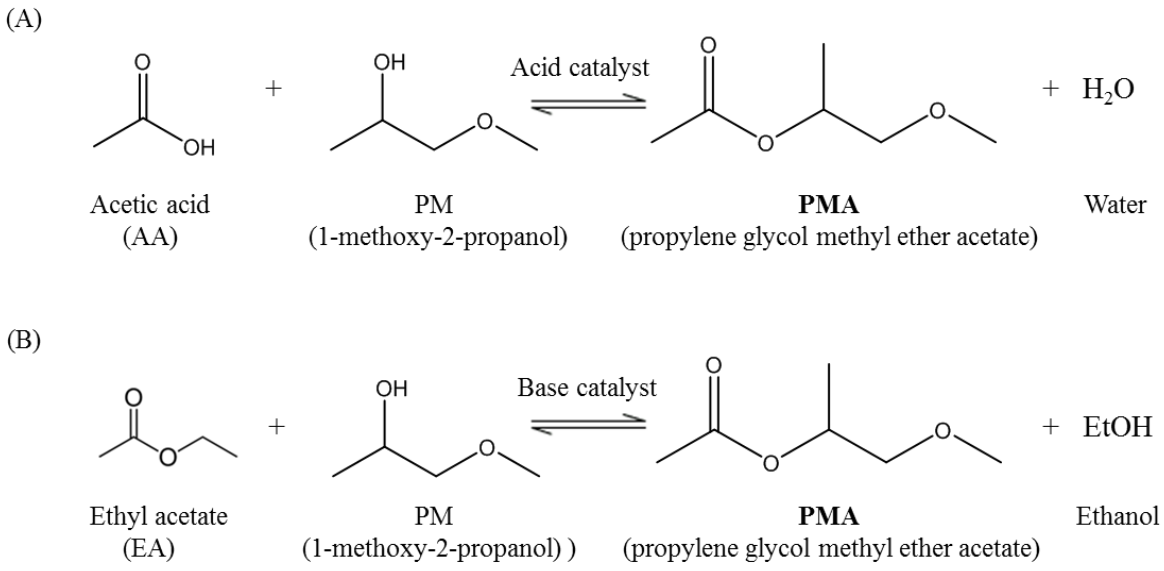

Figure 4 (A) Esterification reaction, catalyzed by AMBERLYST^{TM} 15, between acetic acid and PM to form PMA and water. (B) Transesterification reaction, catalyzed by DOWEX^{TM} 22, between ethyl acetate and PM to form PMA and ethanol.

1.3.1.1 State-of-the-art production methods for PMA

The conventional method for PMA production has been via the esterification route. One approach is the sequential reaction and purification [20]. PMA is produced in a reactor. The product stream is treated in a flash column to separate the product from the catalyst

and then by a secondary separation unit, distillation column, in which the PMA is collected from the bottoms (Figure 5). Another similar method replaces the reactor with reactive distillation followed by additional purification steps [21].

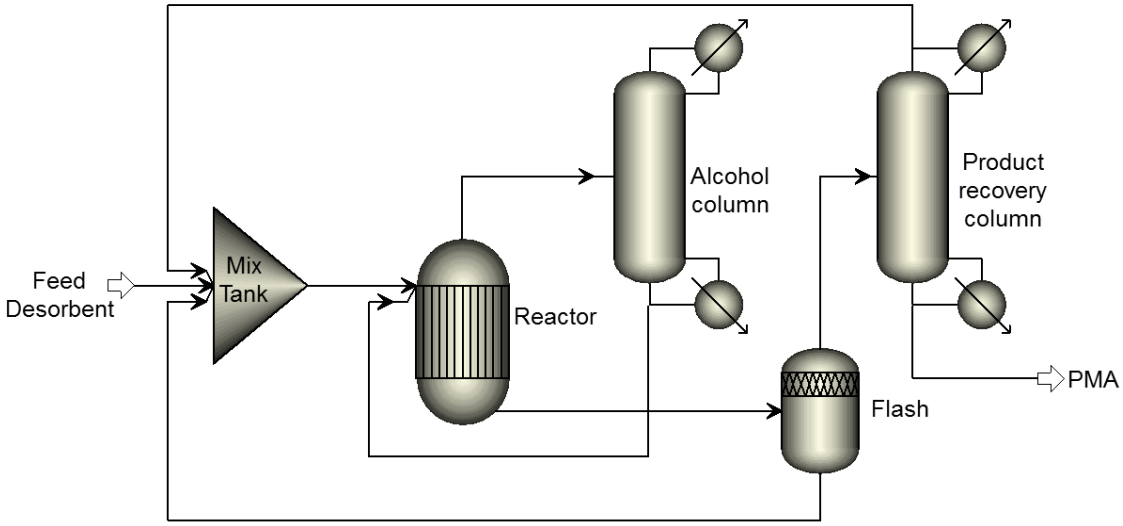

Figure 5 Reproduction of patent describing production of PMA by Johnson et al. [20].

CHAPTER 2. SCOPE OF THESIS

The overarching purpose of this work is to demonstrate that optimizing SMBR operations can be carried out in a systematic and deterministic way that is robust, reliable, and generalizable to different reaction chemistries. The approach is based on both experimental work performed on the SMBR unit as well as mathematical modeling and optimization methods. The three objectives in this thesis are:

1. Optimize the SMBR operation for the esterification route of PMA production using a model-based framework
2. Determine if the model-based framework can be applied to the transesterification route of PMA production and compare the optimized operation between the two reaction routes
3. Optimize an overall process for the esterification route of PMA production

The first objective is the topic for CHAPTER 5, where the esterification route for PMA production is optimized for SMBR operation. For the production of PMA, Agrawal et al. [15] developed an SMBR model and a multi-objective optimization framework to determine the optimal operation of the SMBR. An initial model is defined from model parameters that were calculated from batch, single column chromatography experiments (hereon referred to as non-SMBR experiments). A multi-objective optimization problem is formulated to maximize the productivity of PMA and maximize the conversion of the esterification reaction. A Pareto plot was constructed to analyze the trade-off between productivity and conversion. In this work, the initial model and multi-objective optimization study are validated experimentally using an in-house SMBR unit.

Concentration data from both the experimental SMBR operations and from model determinations are used systematically to correct the initial SMBR model structure and refine model parameters. By comparing the model and experimentally obtained species' concentrations, the corrected SMBR model yields a significantly better model-to-experiment match than the initial SMBR model.

The second objective is presented in CHAPTER 6, which extends the model-based framework to optimize SMBR operation for the transesterification route of PMA production. Similar to the esterification work, initial model parameters were calculated from batch kinetic and single column chromatography experiments by Oh et al. [17, 18]. A multi-objective optimization problem was formulated to maximize the productivity of PMA and maximize the conversion of the transesterification reaction. Additional process constraints including PMA recovery and ethanol content in the raffinate were implemented. Parameter recalculation was conducted using model predicted and experimental concentrations of the SMBR operation. The corrected SMBR model for transesterification is optimized and compared against the optimized operations for esterification.

It is important to note that the model-based framework is designed for finding optimal operating conditions and model parameter values at a process development stage. Therefore, it does not deal with real-time system perturbations and unanticipated system fluctuations.

The final objective is presented in CHAPTER 7, in which the SMBR operation is optimized for the esterification route of PMA production within an overall process. The proposed overall flowsheet consists of the SMBR unit followed by two downstream units. Specifically, the extract and raffinate streams leaving the SMBR are processed further to

improve product purity, and streams exiting the downstream units are recycled back into the inlets of the SMBR unit to reduce solvent consumption and waste generation. The objective function is to maximize the PMA productivity. Several process constraints are placed on solvent use, conversion, and product purity and recovery. Additionally, three different SMBR configurations are explored—standard, limited superstructure, and full superstructure. Specifically, we explore the superstructure of how the downstream recycle stream can be connected to the inlet of the SMBR as well as how the feed, extract, and desorbent streams can be optimally configured.

Altogether, this work tries to approach the design and operation of SMBR, in isolation or within an overall process, from a systematic, model-based approach based on both model prediction and experimental validation. Such an approach would eliminate the reliance on heuristic methods that could potentially miss the optimal solution or dependence on experts' intervention and intuition from time- and resource-intensive trial-and-error approaches to understand the operating solution space. This work expects to render SMBR implementation a more tractable and accessible operation and to expand its potential for application in academia and industry.

CHAPTER 3. MATERIALS AND EXPERIMENTAL METHODS

3.1 Materials

PM (1-methoxy-2-propanol, >99%), PMA (propylene glycol methyl ether acetate, >99%), and ethyl acetate (HPLC grade, 99.5+%) were purchased from Alfa Aesar while the acetic acid (99%) was purchased from BDH Chemicals. All chemicals were used without further purification

3.2 Resin preparation

3.2.1 AMBERLYST™ 15—Esterification

The sulfonated cation exchange resin, AMBERLYST™ 15, used for the esterification studies was obtained from the Dow Chemical Company in a wet condition. The resin was dried at 373.15 K for 12 h and then sieved. Resin particle sizes between 500-700μm were used for the SMBR experiments. Table 1 is a reproduction of the resin properties provided by the Dow Chemical Company.

Table 1 Physical and chemical properties of AMBERLYST™ 15 [22].

Type	Strong acid cation
Matrix type	Styrene-Divinylbenzene (Macroreticular)
Operating pH	0-14
Ionic form	H+
Concentration of active sites	≥ 1.7 eq/L
Moisture (%)	52-57
Max. operating temperature (K)	393.15
Surface area (m^2/g)	53
Total pore volume (cm^3/g)	0.40
Average pore diameter (Å)	300
Bulk density (g/L)	770

3.2.2 DOWEX™ 22—Transesterification

The Type II anion exchange resin, DOWEX™ 22, for the transesterification studies were obtained from the Dow Chemical Company in the Cl^- form. The resin was ionically exchanged into the OH^- form following the same packing procedure as described previously [15, 16]. The preparation of the resin is summarized briefly as follows: the resin was flushed with 5 wt% of NaOH solution for 12 bed volumes (BV) at 0.1 BV/min, followed by DI water rinse at 18 BV at 0.1 BV/min and finally 18 BV of PM at 0.1 BV/min. Table 2 below is a reproduction of the resin properties provided by the Dow Chemical Company.

Table 2 Physical and chemical properties of DOWEX™ 22 [23].

Type	Strong base anion, Type II
Matrix type	Styrene-Divinylbenzene (Macroporous)
Operating pH	0-14
Ionic form	Cl-
Concentration of active sites	≥ 1.2 eq/L
Moisture (%)	48-56
Max. operating temperature (K)	318.15
Surface area (m^2/g)	53
Bulk density (g/L)	1100

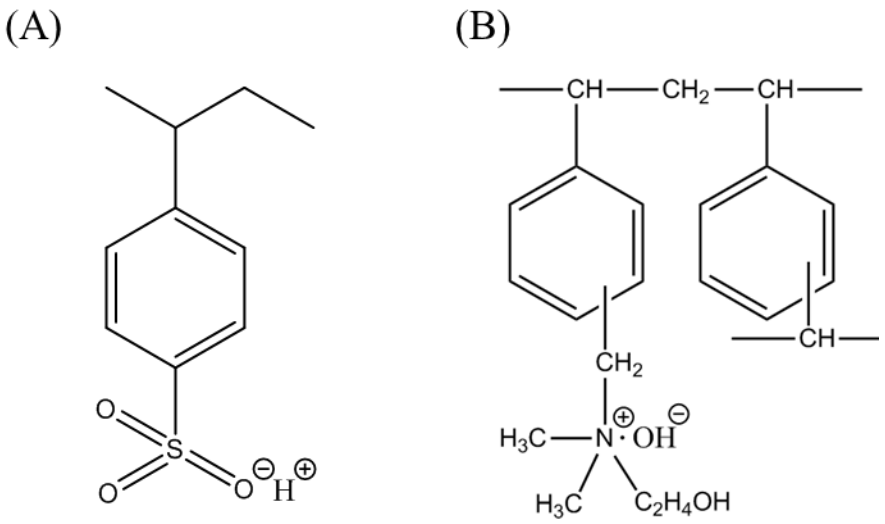

Figure 6 Chemical structure for monomers of (A) AMBERLYST^{TM} 15 and (B) DOWEX^{TM} 22.

3.3 Column packing

Four stainless steel columns (ST-100500, Chrom Tech Inc.) with 50 cm length and internal diameter of 1 cm were used for the SMBR experiments. The columns were packed with resin using the slurry technique. The AMBERLYST^{TM} 15 was made into a slurry in acetic acid while DOWEX^{TM} 22 was made into a slurry in PM. Each SMBR column was connected to a packing column, the slurry resin was slowly added, and the system underwent three cycles of fluidization and settling before the resin bed was allowed to rest, uniformly inside the SMBR column and the column ends were sealed off. Following the column packing, the consistency of the column packing was verified by quantifying the pressure drop, the retention time and band broadening properties of PMA, as well as by conversion from a pulse injection experiment in a reactive chromatography column.

3.4 SMBR unit

The SMBR unit (Figure 7, Figure 8), built in-house, is in a standard four-zone SMB configuration. The entire system (pumps, valves, and detector) is controlled by a MATLAB based graphical user interface developed in house. A single stainless steel column was used for each of the four SMBR zones. Three preparatory scale dual piston pumps (P-1100-CF, Chrom Tech Inc.) were used for the desorbent, extract, and recycle streams. A constant pressure, dual piston pump (P-1536-CP, Chrom Tech Inc.) was used for the feed stream. The switching of the inlet and outlet port locations was controlled by four dead end (SD) valves (Valco Instruments Co. Inc.) and the recycle stream flow path was controlled by flow through selector (SF) valve (Valco Instruments Co. Inc.) and one more SD valve. Temperature of the four columns was maintained inside an oven (CH-460 Column Heater, Eppendorf) with temperature control (TC-50 Temperature Controller, Eppendorf). All tubing was Teflon tube with an outer diameter of 1/16 inch. The raffinate line passed through a refractive index detector (Shodex RI-102, Showa Denko K.K.) to monitor the development of a cyclic steady state concentration profile of the product. Readings for pump pressure, flow rate, valve position, and refractive index detector values for the raffinate outlet were recorded in real time.

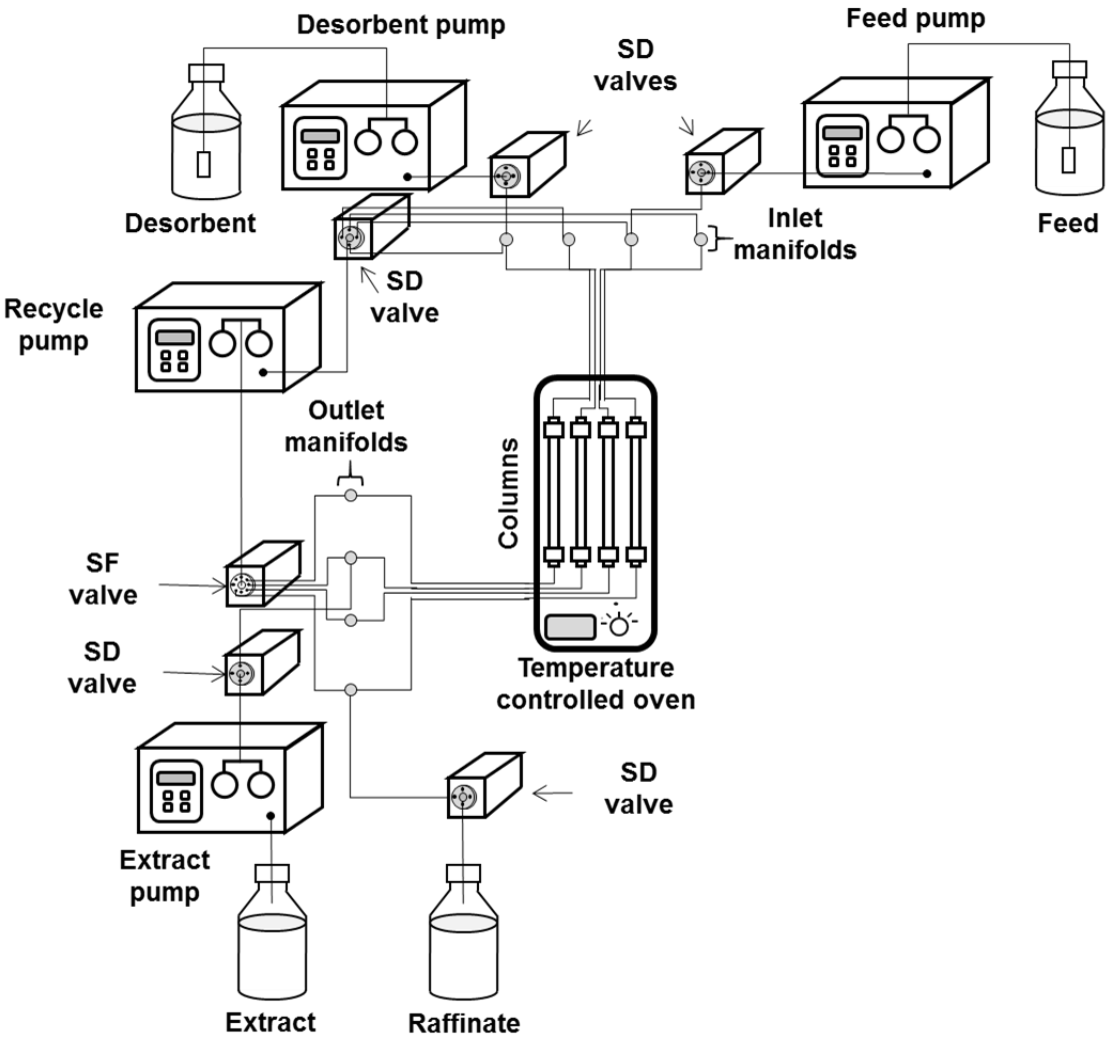

Figure 7 Schematic of the SMBR unit.

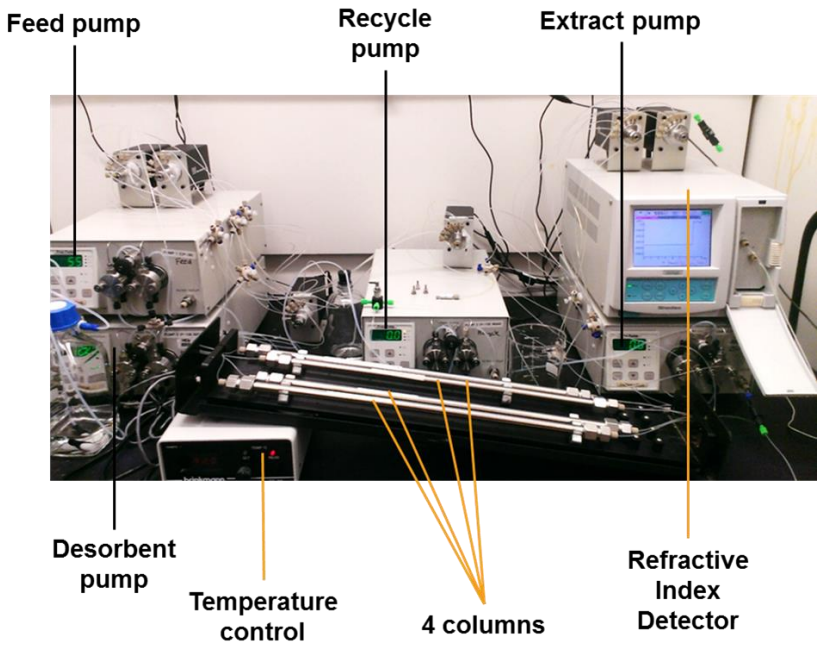

Figure 8 Actual SMBR unit.

3.5 SMBR operations

Before the start of every SMBR experiments, the entire system is flushed with PM until the composition of the outlets (extract and raffinate) are pure PM with no detectable levels of water, as confirmed by gas chromatography (GC) measurements. The reactants and desorbent are also check via GC to ensure there is no detectable levels of water. For the transesterification reaction, water levels >0.05 vol% have dramatically decreased productivity and conversion. Thus dry molecular sieve 3Å is added to all inlet bottles for the feed and desorbent to ensure no water accumulates in the solutions over the SMBR operation. Approximately a quarter of the total container volume of sieve is added.

The SMBR operating conditions are selected and monitored via the MATLAB controlled interface. After reaching cyclic steady state (CSS), extract and raffinate streams were collected in graduated cylinders over a cycle in a non-disruptive manner. The internal

recycle stream at the end of zone IV was sampled only after completing all other sampling since the liquid concentrations are disturbed when the recycle stream is sampled. In our study, it took nearly six cycles to reach CSS. CSS was confirmed by comparing the concentrations of all components in the raffinate and extract streams to those after twenty cycles.

3.6 GC analysis

Experimental concentrations for each component were determined for the extract and raffinate streams using a Shimadzu gas chromatography (GC) system, GC-2010. The machine is equipped with a flame ionization detector and a thermal conductivity detector. The column used in the GC analysis is a ZB-1 (Phenomenex) capillary column with dimensions 60 m x 0.32 mm x 1.00 μm. A single method was developed for analysis of all components. A calibration curve was constructed from samples made from known concentrations and the curves were used to determine the concentrations of experimental samples. For more details on the GC method, see [16].

CHAPTER 4. MODELING AND OPTIMIZATION

This section is dedicated to providing the mathematical model and the optimization methods used for the SMBR operation in isolation and within an overall process.

4.1 Model-based framework

The model-based framework we propose is called simultaneous optimization and model correction (SOMC). As the name suggests, this method allows for one to correct and optimize the model at the same time. Figure 9 below illustrates the steps involved in SOMC.

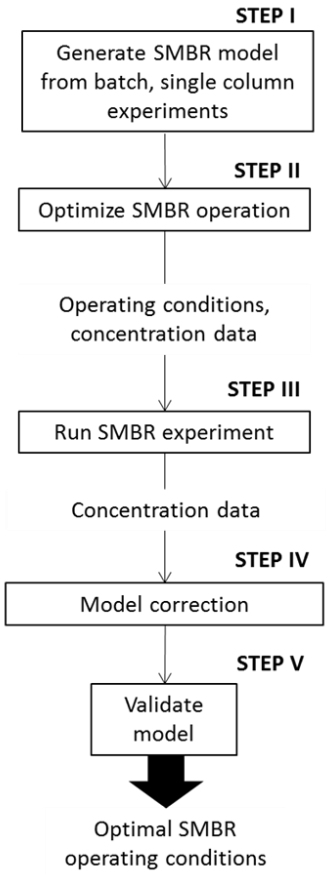

Figure 9 Simultaneous optimization and model correction (SOMC) scheme.

The first step begins with the SMBR model (Section 0) and initial model parameter values. These model values are determined from batch kinetic or single column chromatography experiments. In Step II, the initial SMBR model is optimized (Section 4.3) and the solution gives the operating conditions and the concentration values predicted by the model from the extract and raffinate outlets. In Step III, the SMBR experiments (Section 3.5) are conducted and experimental concentration values are obtained. In Step IV, using the concentration values from experiments and model predictions, a least-square minimization is performed to recalculate the model parameter values (Section 4.4). In Step V, the corrected model is validated experimentally and then the SMBR model can be re-optimized to give the operating conditions and the accurate concentration predictions.

4.2 Modeling of SMBR

We consider a pseudo-homogenous reaction mechanism and a transport dispersive model with a linear driving force for the solid phase. The axial dispersion of all components is captured by a lumped dispersion coefficient, D_{ax}, and diffusion into the resin particle by individual components is approximated by individual mass transfer coefficients, $K_{m,i}$. The transesterification reaction is assumed to occur only in the solid phase, which is confirmed by our experimental observation that the reaction does not proceed in the absence of the catalyst.

The main assumptions made in this study are the following: (1) the radial distribution of the liquid concentration can be ignored, (2). the total void fraction ε_T is constant, (3) the adsorptive retention of components and reaction occurs in the solid phase (ion exchange resin), the volume fraction of which is given by $1-\varepsilon_T$, (4) liquid velocity varies with liquid composition, (5) the linear driving force (LDF) model describes the mass

transfer between the liquid and solid phases, (6) the activity coefficient of each component is unity in reaction equilibrium and kinetics, and (7) both reaction routes are reversible, first-order reactions with respect to each component. Under these assumptions, the model equations are given as follows.

Mass balance in the liquid phase:

$$\frac{\partial C_i^j(x,t)}{\partial t} + \frac{(1-\epsilon_T)}{\epsilon_T} K_{m,i}\left(q_i^{j,eq}(x,t) - q_i^j(x,t)\right) + \frac{1}{\epsilon_T}\left(u^j(t)\frac{\partial C_i^j(x,t)}{\partial x} + C_i^j(x,t)\frac{\partial u^j(t)}{\partial x}\right) = D_{ax}\frac{\partial^2 C_i^j(x,t)}{\partial x^2} \quad (1)$$

where C_i^j and q_i^j are the concentration in the liquid and the solid phase, respectively, ϵ_T is the total void fraction, $u^j(t)$ is the superficial velocity of column, D_{ax} is the overall axial dispersion coefficient, $K_{m,i}$ represents the individual mass transfer coefficients, x is the axial distance and t is the time. The superscript j represents the j^{th} column while subscript i refers to the component index. The time variant velocity term is necessary to describe the dynamics of the system. From previous work [24], we assumed that the liquid volume remains constant and thus we assume the volumes are additive:

$$\sum_{i=1}^{N_{Comp}} (C_i^j(x,t)A_{cs}dx)v_i = A_{cs}d \quad (2)$$

where C_i is the concentration of each component, v_i is the molar volume of each component, A_{cs} is the cross sectional area in each column, and dx is an infinitesimally small slice along the length of the column. Dividing both sides by $A_{cs}dx$ gives:

$$\sum_{i=1}^{N_{Comp}} C_i^j(x,t)v_i = 1 \quad (3)$$

Mass balance in the solid phase:

$$\frac{\partial q_i^j(x,t)}{\partial t} = K_{m,i}\left(q_i^{j,eq}(x,t) - q_i^j(x,t)\right) + \nu_i\, r^j(x,t) \tag{4}$$

where $q_i^{j,eq}$ is the concentration in the solid phase that is in equilibrium with the liquid phase, ν_i is the stoichiometric coefficient of the i^{th} component in the reaction and r^j is the net reaction rate in the j^{th} column.

We employ slightly different adsorption equilibriums between the solid and liquid phases between the esterification and transesterification routes.

For the esterification route, the isotherms are represented by the following equations:

$$q_i^{j,eq}(x,t) = H_i\, C_i^j(x,t) \tag{5}$$

$$i = AA, PM, PMA, Water, \quad j = 1, \dots, N_{Column}$$

For the transesterification route, the isotherms are represented by the following equations:

$$q_i^{j,eq}(x,t) = H_i\, C_i^j(x,t) \quad i = EA, PM, \quad j = 1, \dots, N_{Column} \tag{6}$$

$$q_i^{j,eq}(x,t) = \frac{H_i\, C_i^j(x,t)}{1 + b_i C_i^j(x,t)} \qquad i = PMA, EtOH \quad j = 1, \dots, N_{Column}$$

where H_i is the Henry constant. The symbols $AA, EA, PM, PMA, Water, EtOH$ refer to acetic acid, ethyl acetate, 1-methoxy-2-propanol, propylene glycol methyl ether acetate, water, and ethanol respectively. N_{Column} refers to the total number of columns. For the esterification case, all components could be modeled with the linear isotherm and it was also chosen for the sake of model simplicity. In contrast, for the transesterification route,

ethanol and PM can be sufficiently modeled by a linear adsorption isotherm; however, PMA and ethanol demonstrated nonlinear adsorption behavior and are better characterized by a Langmuir isotherm.

The net reaction rate of the esterification reaction catalyzed by a heterogeneous acid is given by the second-order model:

$$r^j = k_1\left(q_x^j q_{PM}^j - \left(\frac{1}{K_{eq}}\right) q_{PMA}^j q_Y^j\right) \tag{7}$$

where k_1 is the forward reaction rate constant, K_{eq} is the reaction rate equilibrium constant and r^j is the reaction rate in the j^{th} column. The subscripts, *x*, represents the limiting reactant, either acetic acid or ethyl acetate, and *y*, represents the byproduct, either water or ethanol depending on the reaction route.

The above model equations (1-7) describe the concentration profiles in a single-column chromatographic reactor. To extend these equations to describe an SMBR operation, flow and mass balance equations for multiple columns are defined. Flow and mass balance equations are given by:

$$u^{j+1}(t) = u^j(t) - \left(u_R^j(t) + u_{Ex}^j(t)\right) + (u_D^{j+1}(t) + u_F^{j+1}(t)) \tag{8}$$

$$C_i^{j+1}(0,t)\, u^{j+1}(t) = C_i^j(L,t)\left(u^j(t) - u_{Ex}^j(t) - u_R^j(t)\right) + C_{i,F} u_F^{j+1}(t) \tag{9}$$

where $u_R^j(t)$, $u_{Ex}^j(t)$, $u_D^j(t)$ and $u_F^j(\mathrm{t})$ are the velocities of raffinate and extract outlet streams, desorbent and feed inlet streams, respectively. These values are positive only if raffinate, extract, desorbent, or feed is withdrawn from or fed to column *j*, and zero otherwise. The concentration of the i^{th} component in the feed is represented by $C_{i,F}$ and the

column length is represented by L.

Finally, a cyclic steady state (CSS) constraint is enforced. At CSS, the concentration profiles at the beginning of the step in the j^{th} column are identical to concentration profiles at the end of the step in the $j+1^{th}$ column. The formulation is written as:

$$C_i^j(x,0) = C_i^{j+1}\left(x, t_{step}\right) \quad j = 1, \dots, N_{Column} - 1 \tag{10}$$

$$q_i^j(x,0) = q_i^{j+1}\left(x, t_{step}\right) \quad j = 1, \dots, N_{Column} - 1 \tag{11}$$

$$C_i^{N_{Column}}(x,0) = C_i^1\left(x, t_{step}\right) \tag{12}$$

$$q_i^{N_{Column}}(x,0) = q_i^1\left(x, t_{step}\right) \tag{13}$$

where t_{step} is the step time and i is the individual components.

There are 12 model parameters for esterification and 14 model parameters for transesterification. The following parameters, ε_T, K_{eq}, k_1, H_i, D_{ax}, K_i, are used in both reaction routes whereas b_{PMA} and b_{EtOH} are exclusively for the transesterification route. All initial parameter values are determined from three different types of experiments: batch kinetic reaction experiments, unreactive chromatographic pulse tests, and single-column reactive chromatography experiments [15-18]. In our previous study, a tracer, dextran, was injected into a single chromatography column to estimate the interparticle void fraction. The reaction equilibrium constant K_{eq} and the forward reaction rate k_1 were obtained from a well-stirred batch reactor experiment. All remaining parameters were estimated

simultaneously by fitting the model equations for a single-column reactive chromatography model to unreactive pulse tests and single-column reactive chromatography experiments.

4.3 Optimization strategy for SMBR

The SMBR model presented earlier is integrated into a multi-objective optimization problem. This formulation, a modified version of the one presented by Tie *et al.* [24], is summarized below, where six operating parameters–switching time (t_{step}), feed concentration, plus four zone flow rates ($u^j, j = 1,2,3,4$)–are optimized.

Maximize PMA production rate (g/hr):

$$max\ \zeta_1 = \frac{A_{cs}\, MW_{PMA}}{t_{step}} \sum_{j=1}^{N_{Column}} \int_0^{t_{step}} C_{PMA}^j(L,t)\, u_R^j(t)\, dt \tag{14}$$

where ζ_1 is the first objective function, A_{cs} is the area of cross-section of the chromatographic column, MW_{PMA} is the molecular weight of PMA, and t_{step} is the switching time. Note that the production rate is defined by the amount of PMA eluting from the raffinate stream only.

The maximize conversion of the limiting reactant is:

$$max\ \zeta_2 = 1 - \frac{\sum_{j=1}^{N_{Column}} \int_0^{t_{step}} (C_X^j(L,t)\, u_R^j(t) + C_X^j(L,t)\, u_{Ex}^j(t))\, dt}{\sum_{j=1}^{N_{Column}} \int_0^{t_{step}} C_{AA,F}\, u_F^j(t)\, dt} \tag{15}$$

where ζ_2 is the second objective function. Several constraints are defined for product recovery and byproduct content in the raffinate stream.

A constraint for minimum PMA recovery in the raffinate stream, which must be at least 90% is:

$$\frac{\sum_{j=1}^{N_{Column}} \int_0^{t_{step}} C_{PMA}^j(L,t)\, u_R^j(t)\, dt}{\sum_{j=1}^{N_{Column}} \int_0^{t_{step}} (C_{PMA}^j(L,t)\, u_{Ex}^j(t) + C_{PMA}^j(L,t)\, u_R^j(t))\, dt} \geq 0.9 \tag{16}$$

where C_{PMA}^j is the concentration of PMA in any of the j zones.

Additionally, a constraint for maximum byproduct (water or ethanol) content in the raffinate outlet (wt%) is defined as:

$$\frac{\sum_{j=1}^{N_{Column}} \int_0^{t_{step}} MW_y\, C_y^j(L,t)\, u_R^j(t)\, dt}{\sum_i \left(\sum_{j=1}^{N_{Column}} \int_0^{t_{step}} MW_i\, C_i^j(L,t)\, u_R^j(t)\, dt\right)} \leq 1\% \tag{17}$$

where y is either water or ethanol depending on the reaction route. In this constraint, the byproduct content in the raffinate is enforced to be less than 1 wt% for downstream process.

We also introduce constraints on the zone flow rates to obtain sensible operating conditions and to avoid an excessive pressure drop. The symbols U_L and U_U refer to the lower and the upper bounds.

Bounds on the zone flow rates:

$$U_L \leq A_{cs} u^j(t) \leq U_U \tag{18}$$

The upper bound is decided based on the maximum pressure drop that can be experienced by the pumps. In this study, U_L and U_U are set to values corresponding to 0 mL/min and 13.08 mL/min (the upper bound corresponds to a linear velocity of 10 m/hr), respectively. We confirm that the flow rates in the optimal operations do not reach either of the flow rate bounds.

The optimization of the two objectives is achieved by using an epsilon-constrained method [25]. In this approach, maximization of ζ_2 (Eq. 15) is replaced by the following constraint:

$$\zeta_2 \geq \varepsilon \tag{19}$$

By varying the value of ε and repeatedly solving the optimization problem (Eq. 19), a solution set that maximizes PMA production against different conversions is obtained.

The optimization formulations (Eq. 19) form a PDE (partial differential equation) constrained optimization problem that is discretized over time and space to form a system of algebraic equations. The spatial domain is discretized into 40 finite elements. The temporal domain is discretized using Radau collocation where one step is discretized into five finite elements and three collocation points. This system of equations forms a nonlinear programing (NLP) problem that is implemented in AMPL (A Mathematical Programming Language) [26]. The NLP problem is solved using an interior point solver, IPOPT 3.12 [27].

4.4 Model correction

An inverse method is used to estimate the new model parameters. The accuracy of the predicted concentration depends on the values of the model parameters. We used a simple least-square technique that minimizes the objective function by correcting the parameter values. The objective function, Φ, is formulated as:

$$\phi = \min_{\theta_m} \sum_{k=1}^{N_{exp}} \sum_{i=1}^{N_{comp}} (C_{i,k}^{model} - C_{i,k}^{exp})^2 + \rho \sum_{m=1}^{N_{param}} \left(\frac{\theta_m^{model} - \theta_m^{initial}}{\theta_m}\right)^2 \tag{20}$$

Subject to equations 1-13

where C_i refers to the individual component's concentration averaged over a cycle in the raffinate and extract outlets and the averaged concentration over a step in the recycle stream, the subscript *k* refers to the experiment index, the superscript *exp* refers to the

experimental values, N_{exp} refers to the total number of experiments, and N_{comp} refers to the total number of components. In the second term, N_{param} refers to the total number of parameters in the SMBR model and θ_m refers to the individual parameters. The superscripts *model* and *initial* refer to the values predicted from the SMBR model and the values obtained from the initial non-SMBR experiments. The term $\frac{\theta_m^{model}-\theta_m^{initial}}{\theta_m}$ is non-dimensionalized. The objective function (Eq. 20) contains two terms; first is the sum of squares of the concentration difference between the model predictions and experimental observations, and the second is known as a Tikhonov regularization [28] term that constrains the new parameter estimations from deviating to unrealistic values. The experimental values C_i^{exp} are obtained from SMBR experiments. After reaching cyclic steady state (CSS), both raffinate and extract products were sampled over a cycle in a non-disruptive manner. The same sampling approach was employed by Sreedhar and Kawajiri [29], and Agrawal *et al.* [15] for parameter correction for the SMB separation problems. All collected samples are analyzed using the method described in Section 2.3.3.

In Eq. 20, the Tikhonov regularization terms are a way to reduce the non-uniqueness in ill-posed parameter estimation problems [17]. Additionally, these terms modulate how much the new parameter values differ from the initial values. Note that these terms are the weighted sum of the difference between the new model parameters against the parameter values obtained from non-SMBR experiments. A large value of ρ weights the Tikhonov terms more heavily in the objective function and thus restricts the new parameter values from large deviations from the original values. Conversely, a small ρ weights the model deviation less strongly and allows for greater deviations in parameter values from the initial values. A balance must be struck between having model parameters

that can accurately fit experimental results as well as be physically reasonable and predictive.

4.5 Modeling of overall flowsheet

Modeling and optimization of the SMBR within an overall flowsheet is performed only for the esterification route; thus, the following presentation of the overall flowsheet applies only to the esterification SMBR model.

4.5.1 Structure of the overall flowsheet

The structure of the overall flowsheet (Figure 10) consists of an SMBR unit followed by two downstream separation units, a distillation column and a hot gas pressure swing adsorber (PSA). The SMBR is operated as a conventional, 4-zone SMBR. The desorbent is PM and the feed is a mixture of acetic acid and PM. The extract stream from the SMBR unit contains mainly PM with trace amounts of water, PMA, and unreacted acetic acid. The raffinate stream from the SMBR unit contains mainly PM and PMA with trace amounts of acetic acid and water. The raffinate stream first enters a buffer tank before entering a distillation column for product recovery. The distillation column recovers pure PMA in the bottoms, without sacrificing any PMA into the overhead stream, where all the PM, trace acetic acid and water are recovered. The Distillation overhead stream mixes with the extract stream exiting the SMBR in a buffer tank before being processed further in the hot gas PSA. We have a performance assumption on the hot gas PSA such that water is completely recovered in the waste stream (*PSA waste*). The purified stream exiting the hot gas PSA can be purged (*PSA purge*) or recycled (*PSA recycle*) into the SMBR. We examined three recycling structures, a standard configuration (Figure 11A) and two

superstructure configurations (Figure 11B and C). We conduct a comprehensive analysis of the standard and superstructure performance based on the problem formulation outlined in Section 4.6.

The purification of the raffinate stream for PMA is through simple distillation. The decision to employ this separation technique has been well-established for industrial use at manufacturing scales and PMA production and separation is described by the patents from Johnson et al. [20], Kametaka et al. [21], and M. Canonge and Joly [30].

Purification of the extract stream is through hot gas PSA. Compared to the conventional means (Section 1.3.1.1), the PSA demonstrates better energy and cost efficiency at industrial scales, high selectivity, and high throughput [31]. Additionally, 3Å zeolite adsorbents have become the industry standard and are highly cost-effective [31, 32].

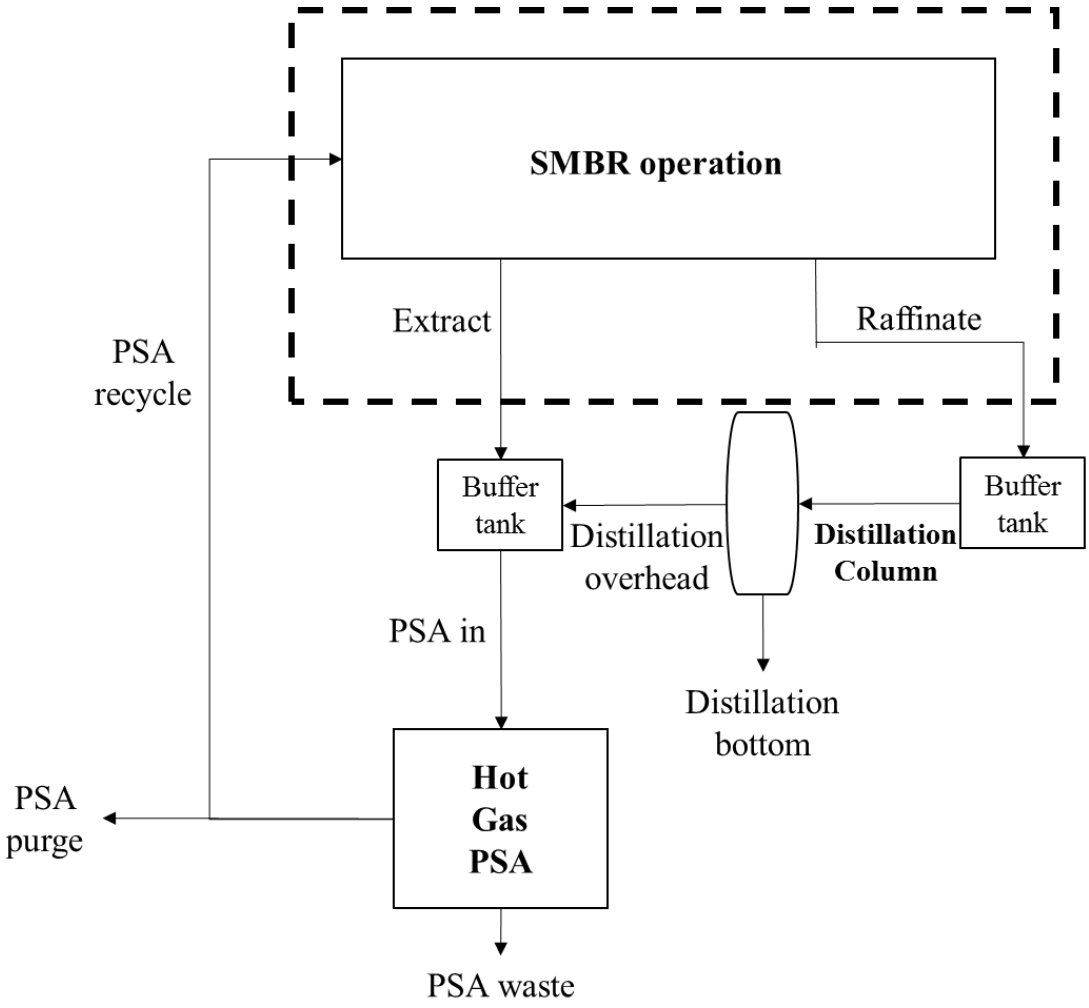

Figure 10 Schematic for the flowsheet for PMA production. The area inside the dashed box is described in more detail in Figure 11.

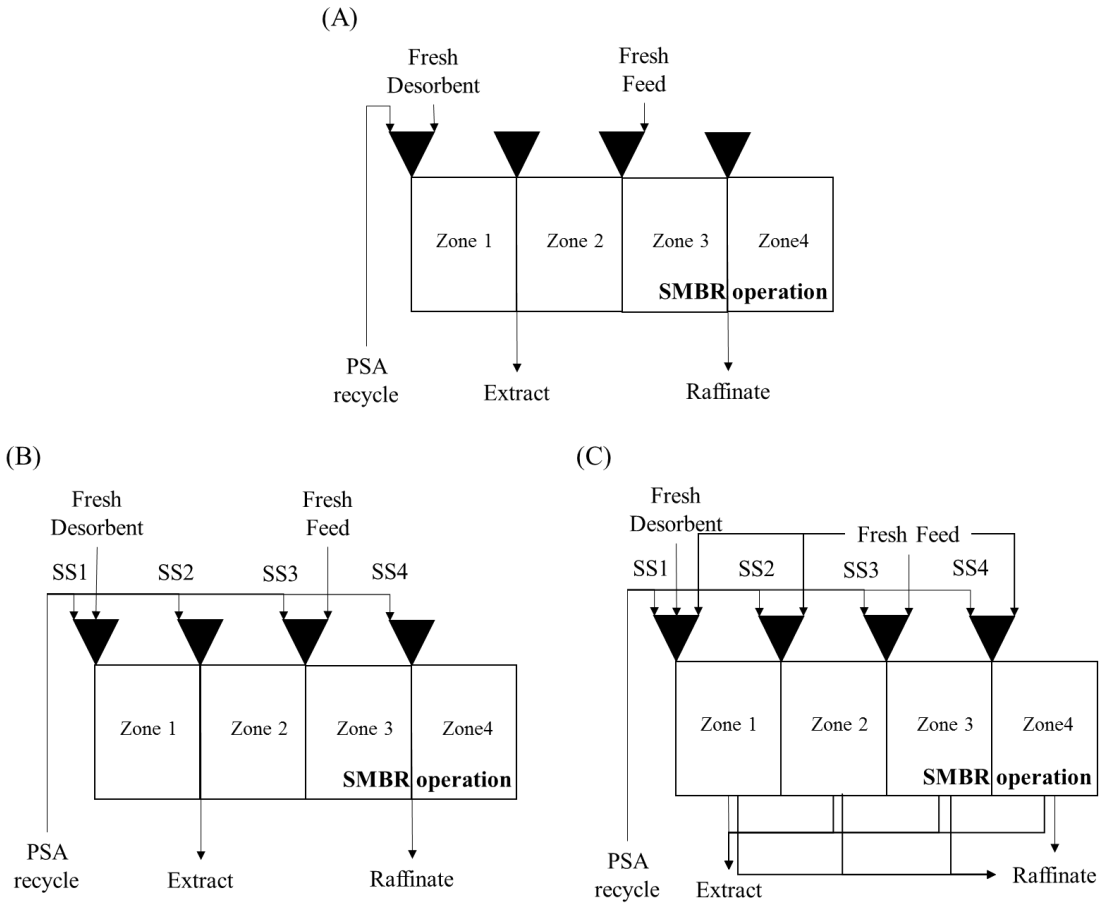

Figure 11 Detailed schematic of the stream configurations around the SMBR for the (A) standard, (B) limited superstructure, and (C) full superstructure configuration.

The key difference between the standard and superstructure configurations (Figure 11) is the integration of the *PSA recycle* stream with the SMBR unit. In the standard configuration, the *PSA recycle* stream is integrated into the SMBR only through the zone 1 inlet port. On the other hand, in the superstructure configurations, the *PSA recycle* stream splits into four potential streams, one for each of the four zones of the SMBR (*SS1*, *SS2*, *SS3*, *SS4*) and is simultaneously supplied to any of the four zones of the SMBR. The added difference between the full superstructure (Figure 11) and the other configurations is that

the fresh feed, extract, and raffinate streams, instead of being fixed, can be added or removed from any of the four zones.

4.5.2 Assumptions of the overall flowsheet

Our study set out to examine how the SMBR unit operates within the context of a larger plant process and to gain a better understanding of the phenomenon that govern an overall process; therefore, the process assumptions we made for the downstream units reflect realistic yet simplistic representations of the true operations. Table 3 contains a list of the operational assumptions, where $\dot{N}$ represents the molar flow rate and the subscript specifies the component followed by the stream. In particular, we assumed that the PSA waste is 100% water, and distillation column is able to purify PMA at 100% purity and 100% recovery.

Table 3 List of assumptions for the overall process.

1.	extract stream leaving the SMBR enters a buffer tank before further processing in the hot gas PSA
2.	raffinate stream leaving the SMBR enters a buffer tank before further processing in the distillation
3.	water stream leaving the hot gas PSA is pure water, $\dot{N}_{water,\ PSA} = 0$
4.	recycle stream leaving the hot gas PSA has the following molar flow balance: • $\dot{N}_{AA,\ PSA} = \dot{N}_{AA,\ extract} + \dot{N}_{AA,\ Distillation\ overhead}$ • $\dot{N}_{PM,\ PSA} = \dot{N}_{PM\ ,extract} + \dot{N}_{PM,\ Distillation\ overhead}$ • $\dot{N}_{PMA,\ PSA} = \dot{N}_{PMA,\ extract} + \dot{N}_{PMA,\ Distillation\ overhead}$
5.	PMA stream leaving the bottoms of the distillation is pure, $\dot{N}_{PMA,\ Distillation\ overhead} = 0$
6.	recycle stream leaving the overhead of the distillation has following molar flow balance: • $\dot{N}_{AA,\ Distillation\ overhead} = \dot{N}_{AA,\ raffinate}$ • $\dot{N}_{PM,\ Distillation\ overhead} = \dot{N}_{PM,\ raffinate}$ • $\dot{N}_{water,\ Distillation\ overhead} = \dot{N}_{water,\ raffinate}$

4.5.2.1 Downstream buffer tanks

There are two downstream buffer tanks, one for extract and raffinate streams. They are important to maintain a constant, time-averaged concentration for the streams to be processed in either the hot gas PSA or distillation column.

4.5.2.2 Feasibility of downstream units

We assume some performance capabilities for the distillation column and hot gas PSA (Table 3) that simply our calculations. The validity of these assumptions are assessed through both Aspen simulations, sensitivity analysis, as well as some literature evidence that are presented in Section 7.4.1.

4.6 Optimization strategy for overall flowsheet

The optimization problem is formulated as a single objective optimization problem with the objective function defined as the overall productivity PMA (kg/L/day).

Maximizing overall PMA productivity (kg/L/day):

$$\max \zeta_1 = \frac{N_{PMA,Distillation\ bottom} MW_{PMA}}{V_{SMBR}} \tag{21}$$

where ζ_1 is the objective function, N_{PMA} is the molar flow rate of PMA leaving the distillation bottoms, MW_{PMA} is the molecular weight of PMA, and V_{SMBR} is the volume of the SMBR.

Process constraints are also implemented. One is for the single-pass SMBR conversion of acetic acid (%):

$$1 - \frac{\sum_{j=1}^{N_{Column}} \int_0^{t_{step}} (C_{AA}^j(L,t)\, u_R^j(t) + C_{AA}^j(L,t)\, u_{Ex}^j(t))\, dt}{\sum_{j=1}^{N_{Column}} \int_0^{t_{step}} C_{AA,F}\, u_F^j(t)\, dt} \quad (22)$$

where $C_{AA}^j$is the concentration of acetic acid in Zone j, and u_R^j, u_{Ex}^j, and u_F^j are the flowrates in the raffinate, extract, and feed respectively. The different SMBR conversions evaluated are: 70%-99%.

Another process constraint is the excess solvent ratio (mol/mol), which is defined as:

$$\frac{N_{PM,Fresh\ Feed}}{N_{PMA,Distillation\ bottom}} \quad (23)$$

The excess solvent ratio is 1.0 when unreacted PM is recycled without any loss (i.e. the flow rate of the *PSA purge stream* is zero). Therefore, the lower limit is 1 because even at 100% conversion, the molar amount of PMA produced will never exceed the molar amount of PM fed into the overall process. On the other hand, this value can become greater than 1.0 when PM is discarded into the *PSA purge* stream, and fresh PM must be supplied in excess to compensate this loss. This scenario arises when the overall conversion is not 100% and therefore, there is more PM supplied than the amount of PMA produced. In this work, the excess solvent ratio is evaluated at values from 1.2 to 8.

The same constraints for minimum PMA recovery and maximum water content in the raffinate stream are applied to the overall flowsheet such as that presented in Section 4.3 in equations 16 and 17, respectively.

A constraint for maximum water content, which can be at most 10 wt% of the raffinate

stream, defined as:

$$\frac{\sum_{j=1}^{N_{Column}} \int_0^{t_{step}} C_{Water}^{j}(L,t)\, u_R^j(t)\, dt}{\sum_{j=1}^{N_{Column}} \int_0^{t_{step}} (C_{Water}^{j}(L,t)\, u_{Ex}^j(t) + C_{Water}^{j}(L,t)\, u_R^j(t))\, dt} \leq 0.1 \tag{24}$$

where C_{PMA}^{j} is the concentration of PMA in any of the *j* zones.

We also apply constraints on the zone flow rates with lower and upper bounds (U_L and U_U) such as those in Section 4.2.

To analyze and compare process performance, we compare the different configurations to gain some insight into the operating cost. We define a parameter as the operating cost (OC) proxy:

$$operating\ cost\ (OC)\ proxy = \frac{U_{PSA\ in} A_{cs}}{N_{PMA,Distillation\ bottom} MW_{PMA}/\rho_{PMA}} = \frac{\sum_{i=PM,AA,PMA,water} N_{i,PSA\ in} MW_i/\rho_i}{N_{PMA,Distillation\ bottom} MW_{PMA}/\rho_{PMA}} \tag{25}$$

where $U_{PSA\ in}$ is the linear flow rate of the PSA inlet stream; A_{cs} is the cross-sectional area of the SMBR; N_{PMA} is the molar flow rate of PMA leaving the distillation bottoms; MW_{PMA} is the molecular weight of PMA; ρ_{PMA} is the density of PMA. The numerator is the volumetric flow rate of the *PSA in* stream, which is the sum of *Distillation overhead* and *Extract* streams. It can be seen that the OC proxy is the ratio of the volume of all recycled components to the volume of PMA in the product stream. The OC proxy should serve as an indicator of the operating cost normalized by the revenue from PMA sales.

Additionally, we define some ratios to compare the performance of the limited superstructure to the standard configuration:

$$productivity\ ratio = \frac{Limited\ Superstructure\ configuration\ productivity}{Standard\ configuration\ productivity} \quad (26)$$

$$OC\ proxy\ ratio = \frac{Limited\ Superstructure\ configuration\ OC\ proxy}{Standard\ configuration\ OC\ proxy} \quad (27)$$

CHAPTER 5. SMBR OPTIMIZATION FOR ESTERIFICATION

5.1 Motivation

In standard SMBR operation, the operating variables are the four zonal flow rates, the feed composition, and the time for valve switching. The desired performance of the SMBR system depends on identifying the optimal operating conditions.

The complexity in SMBR modeling and design is extremely challenging for industrial implementation. Within the past decade, several studies reported the optimal design and operation of SMBR [10, 12]. In general, there are two major approaches for optimizing SMBR operations. The first is using shortcut methods derived from the TMB process. The shortcut method refers to the triangle theory, which uses a graphical approach to find operating conditions. The disadvantage of this method is that it assumes only convection and adsorption behavior in the system (neglects diffusion and reaction), and therefore can only give initial guesses for the feasible operating space. Furthermore, the approach cannot calculate explicit predictions for product purity. Finally, the theory is based on TMB operations and therefore in conditions in which the TMB is insufficient to describe SMB operation, such as fewer columns and high concentration ranges, the theory is not accurate. The second major approach is using model simulation and numerical optimization. In this approach, the SMBR process is defined by realistic process models and optimized for the objective function. Dünnebier *et al.* [12] presented a method for numerical optimization for SMBR operations. However, his approach lacked any method for model correction to address model mismatch. Furthermore, his approach emphasizes a single-objective function problem. Azevedo and Rodrigues [4] also formulated a single

objective maximization problem on enzyme productivity using the triangle theory design heuristics for zone flow rates. By analyzing a system that has only one objective function, the behavior of the SMBR operation cannot be evaluated in realistic scenarios and the trade-off relationships between competing objectives cannot be observed. Lode *et al.* [10] formulated a multiple objective optimization problem to maximize productivity and minimize desorbent requirement; however, his approach relied on the triangle theory to guide their design space and examined sugar inversion. All of these prior methods have either relied on heuristics or relied on model-based optimization without correcting for any model mismatch. These methods risk either missing the optimal solution and/or requiring human expertise and thus being time- and resource-intensive.

Several factors motivated the study of PMA production via the esterification route. Due to the formation of multiple azeotropes, conventional method of PMA production such as sequential batch reaction followed by distillation encounters separation challenges. Additionally, PMA's conversion is equilibrium-limited and would benefit from SMBR's capabilities of driving reaction in the forward direction. Finally, several studies on the esterification reaction [33] in reactive chromatography [34, 35] and SMBR [10, 12, 13] operations provided literature references for our model development. These factors make PMA an ideal candidate for production using SMBR.

5.2 Results

5.2.1 SMBR optimization

The results from the optimization problem given by Eq. 19 are discussed based on the initial model parameters taken from Agrawal *et al.* [15]. Three different values, 0.7,

0.8, and 0.85, were chosen for ε in Eq. 19 while solving the maximization problem for ζ_1 (Eq. 14). These values for ε correspond to 70%, 80%, and 85%, which we believe are within a range of practical interest. Each optimal solution of this optimization problem lies on the Pareto front of the multi-objective optimization problem (Figure 12). The operating conditions from this multi-objective optimization analysis are shown in Table 4.

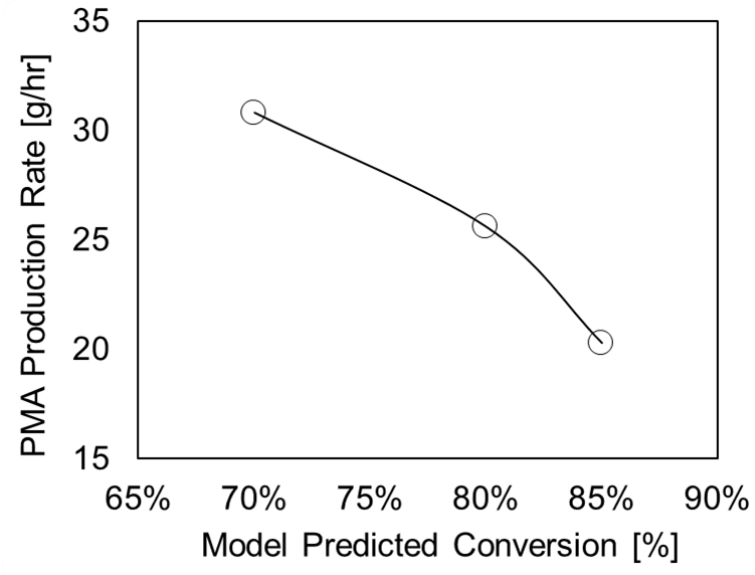

Figure 12 Pareto plot: model predicted PMA production rate against conversion of acetic acid.

Figure 12 shows the Pareto front between PMA production rate (Eq. 14) and conversion (Eq. 15). There is a trade-off relationship between these two objectives. To achieve higher conversion, the residence time must increase inside the SMBR. This leads to a slower flow rate and longer switch time, as can be observed in the optimal operating conditions listed in Table 4. The slower flow rate results in the lower production rate as conversion increases. Specifically, the desorbent flow rate decreases from 6.00 mL/min to 3.20 mL/min as conversion increases from 70% to 85%. A similar trend can be observed

for the extract, feed, and recycle flow rates. Additionally, the switch time increases as conversion increases; for example, the switch time increases from 18.6 min to 29.3 min as conversion increases from 70% to 85%.

Table 4 Optimal operating conditions form SMBR from the multi-objective optimization analysis for maximizing PMA production rate and acetic acid conversion. The flow rates were rounded off to the nearest 0.1 ml/min when implemented experimentally.

Parameters	70% Conversion	80% Conversion	85% Conversion
Desorbent Flow rate [mL/min]	6.00	4.00	3.20
Extract Flow rate [mL/min]	5.80	3.80	3.10
Feed Flow rate [mL/min]	1.27	0.89	0.72
Recycle Flow rate [mL/min]	0.70	0.50	0.40
Switch Time [min]	18.6	24.5	29.3

5.2.2 SMBR experiments

The SMBR operating conditions listed in Table 4 are implemented experimentally on the SMBR unit. After reaching cyclic steady state, concentration samples are collected for each step of cycles 7 and 8. The concentrations are determined by GC. Figure 13 graphs the four component concentrations from the extract and raffinate streams at all three conversion conditions. The 45-degree line serves as a reference; any points lying on the line is exactly fitting experimental results. The comparison of experimental and model concentrations suggests that the trend of the concentrations is captured well by the model. To quantify the model accuracy, we define the squared error of the concentration:

$$SE = \sum_{k=1}^{N_{exp}} \sum_{i=1}^{N_{comp}} (C_{i,k}^{model} - C_{i,k}^{exp})^2 \tag{28}$$

These observations demonstrate that the initial approach to determine model parameters is a promising method for developing a preliminary SMBR model. Water concentrations were predicted relatively accurately, while the discrepancy is more noticeable for the remaining components. The mismatch for acetic acid, PM, and PMA motivates parameter correction as discussed below.

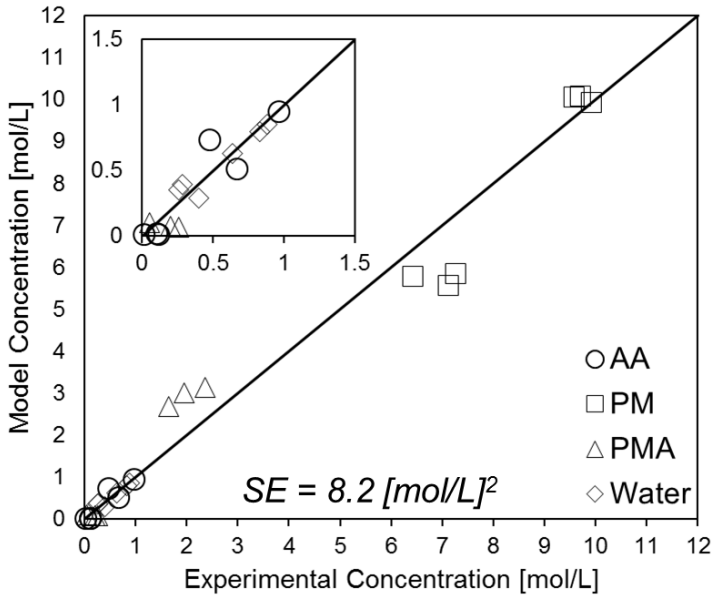

Figure 13 Model predictions against experimentally observed concentration values for acetic acid, PM, PMA and water in the *initial model*.

5.2.3 SMBR parameter estimation

To improve the model fitting, parameter estimation was carried out using the concentration results obtained from the SMBR experiments. There are twelve model parameters: ε_T, K_{eq}, k_1, H_{AA}, H_{PM}, H_{PMA}, H_{water}, D_{ax}, K_{AA}, K_{PM}, K_{PMA}, and K_{water}. The objective function used to correct for the model parameter is:

$$\phi = \min_{\epsilon_T, D_{ax}, K_{eq}, k_1, H_i, K_i} \sum_{k=1}^{N_{exp}} \sum_{i=1}^{N_{comp}} (C_{i,k}^{model} - C_{i,k}^{exp})^2 \; + \rho \sum_{m=1}^{N_{param}} \left(\frac{\theta_m^{model} - \theta_m^{initial}}{\theta_m^{unity}}\right)^2 \quad (29)$$

$$\theta = \left(\varepsilon_T, D_{ax}, K_{eq}, k_1, H_{AA}, H_{PM}, H_{PMA}, H_{water}, K_{AA}, K_{PM}, K_{PMA}, K_{water}\right)$$

Subject to equations 1-13

The term $\boldsymbol{\theta_m^{unity}}$ is equal to 1 and it indicates that each $\boldsymbol{\theta_m^{model} - \theta_m^{initial}}$ is non-dimensionalized by normalizing the parameter difference by a parameter value of 1. An appropriate Tikhonov weighting parameter, $\boldsymbol{\rho}$, from the objective function (Eq. 29) was determined by trial and error in such a way that the optimal solution gives the best balance between model fitting and parameter deviations from the initial values [36]. After some trial-and-error runs, the value of ρ was chosen to be 0.1.

Table 5 summarizes the SMBR parameter values from the *initial model* and the *corrected model*. The changes of recalculated parameter values are reasonable compared to the initial values, and are within the same order of magnitude from those in other esterification studies [10, 11, 13, 14].

Table 5 Summary of SMBR parameter calculations.

	Total void fraction	**Reaction**		**Adsorption (Henry's Constant)**				**Dispersion and Mass Transfer**				
Parameter	ε_T	K_{eq}	k_1 $[\frac{L}{mol\ min}]$	H_{AA}	H_{PM}	H_{PMA}	H_{water}	D_{ax} $[\frac{m^2}{min}]$	K_{AA} $[\frac{1}{min}]$	K_{AA} $[\frac{1}{min}]$	K_{AA} $[\frac{1}{min}]$	K_{AA} $[\frac{1}{min}]$
Initial model	0.334	0.864	0.196	0.474	0.226	0.001	1.65	2.74×10^{-4}	0.350	1.77	1.51	0.286
Corrected model	0.518	0.863	0.175	0.591	0.187	0.001	1.66	1.11×10^{-5}	0.375	1.77	1.51	0.184

These results reveal that the values of the Henry's constant for AA and PM (H_{AA}, H_{PM}) must change to improve model fitting. There are some potential sources to account for the changes in these parameters. First, the dead volume effects in the SMBR unit (column connection tubing, valves, and pumps) can be lumped into the Henry's constants [37]. Second, variance (error and noise) in the measurement can also lead to the different values; the initial parameter values were determined from only a few single-column experiments, where the estimated parameters may have been influenced by the measurement variance. On the other hand, the recalculated parameter values were based on multiple SMBR experiments involving multiple columns. These observations suggest that the single column experiments used to determine the initial Henry's constants provided a good initial guess, which could be improved from experimental data from the SMBR unit.

The mass transfer coefficient of water (K_{water}) was the only mass transfer coefficient to change of all the species. The changes in these coefficients may be due to the strong correlations with the axial dispersion and the Henry's constants. Additionally, water is affected by other factors that are difficult to control experimentally. Specifically, PM is very hygroscopic and absorbs water from the atmosphere very easily during the experiment and sample analysis, which makes quantification of water produced by the reaction a very difficult task. To minimize the amount of water adsorbed during sampling and analysis, all openings to sample containers were sealed and complete samples were immediately analyzed by GC.

The corrected value of the total void fraction, $\varepsilon_T = 0.518$, is significantly larger than its initial value from our previous study, 0.334, which was obtained by an injection of

dextran through a single-column chromatography. We found that this increase was crucial to obtain a reasonable fit of the model to the experimental data. A potential interpretation for this increase is that the initial value measured by dextran represents the interparticle porosity ε_b, while the corrected one represents the total porosity ε_T. This interpretation indicates that the retention of the components and reaction occur on the resin surface, not in the resin pores. This interpretation aligns well with the following correlation [38]:

$$\varepsilon_T = \varepsilon_b + (1 - \varepsilon_b)\varepsilon_p \tag{30}$$

which gives an estimate of ε_T = 0.547, obtained with the value of the intraparticle porosity, ε_p = 0.32, given by the manufacturer [39] and the above assumption, ε_b = 0.334. Additionally, it was determined from our single column swelling ratio experiments that the resin shrinks to a larger extent in acetic acid and PMA than in PM and water. Thus, during SMBR operations, the total void fraction can change locally due to the osmotic pressure difference caused by the internal column concentration. Modeling the relationship between the liquid composition and void fraction would increase the model complexity and is outside the scope of this work, and therefore, we treated the ε_T term as a constant. We finally note that the treatment of the void fraction in this study is somewhat empirical, and do not intend to analyze any fundamental mechanism from our parameter correction.

The sensitivities of all parameters were analyzed by perturbing each parameter individually by 20% while all other parameters were unchanged (Figure 14). There are several sensitive parameters, ε_T, k_1, H_{AA}, and H_{PM}, that can cause noticeable increase in the squared error (*SE*) of the concentration (Eq. 28). These parameters are also the same

parameters that changed by more than 10% from their *initial model* to the *corrected model* values.

We also note some parameters are relatively insensitive. The axial dispersion coefficient D_{ax}, which decreased from its initial value by one order of magnitude, has virtually no influence on the *SE*. We confirmed that ignoring the axial dispersion term from Eq. 1 by setting the coefficient to 0 causes negligible changes. This observation is distinctly different from the work for single-column reactive chromatography in Agrawal *et al.* [15]; in their work, the axial dispersion was critical to allow for better model fitting. In their single-column experiments, the feeding strategy was a pulse-injection of reactants (acetic acid and PM). As this sharp pulse travels through the column, the influence of the axial dispersion on the observed chromatograms was more distinct, and thus a more precise mass transfer model was necessary that evaluates axial dispersion individually. On the other hand, in the SMBR system, a continuous, cyclic feeding strategy causes a broadening of concentration profiles throughout all four zones, and thus such a precise mass transfer model that considers axial dispersion separately was not necessary. We finally note that the insensitivity of H_{PMA} was caused by the small magnitude of the parameter itself (0.001).

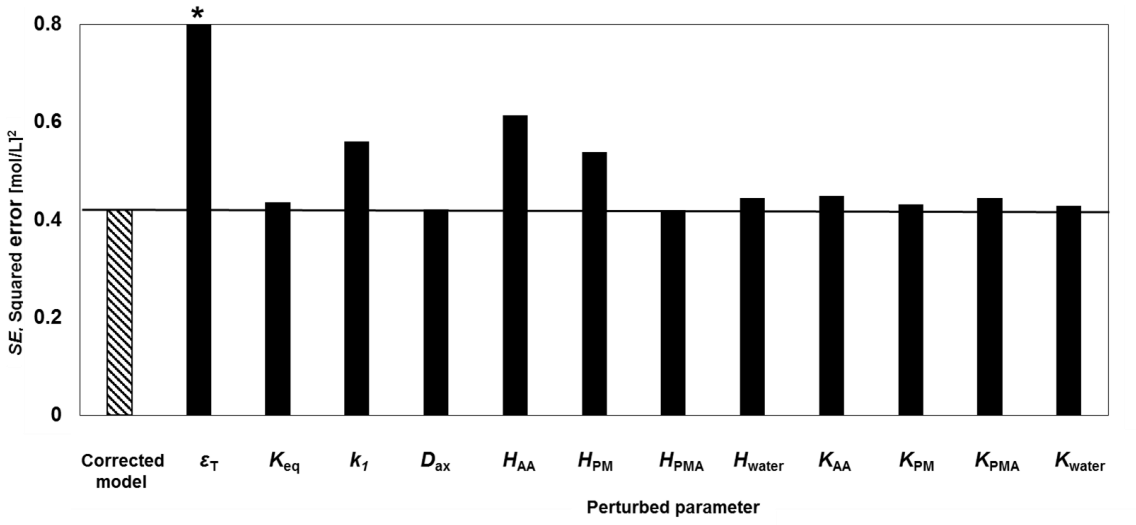

Figure 14 Summary of the sensitivity analysis. Each parameter was perturbed by 20% while all other parameters were unchanged. The total squared error of the concentration is reported for the *corrected model* along with each perturbed parameter. The asterisk above the bar for $\boldsymbol{\varepsilon_T}$ indicates the value extends beyond the maximum y-axis value.

Figure 15 graphs the four component concentrations from the extract and raffinate streams at all three conversion conditions. As can be seen for all four components, the *corrected model* has more data points lying on or near the reference line than the *initial model* (Figure 13) indicating that the *corrected model* has improved the model match. The values of squared error (*SE*) listed for each plot quantifies the squared error of the concentration for the *initial* and *corrected* models.

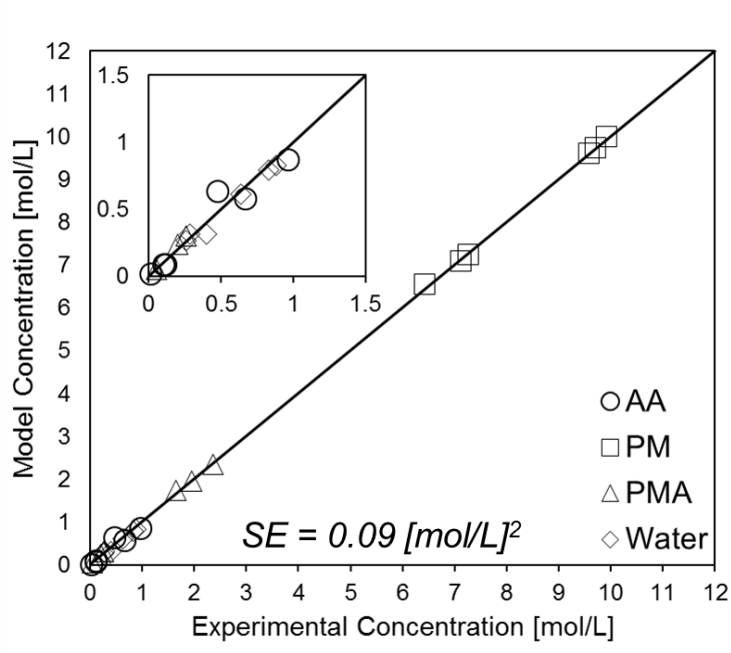

Figure 15 Model predictions against experimentally observed concentration values for acetic acid, PM, PMA and water in the *corrected model*.

The conversion plot (Figure 16) graphs the conversion determined by the model against the conversion obtained experimentally. The SMBR operations are optimized using the experimental operating conditions and the conversion results are obtained from the *initial model* and *corrected model*. The 45-degree line serves as the reference line for a completely accurate model. The *corrected model* resolves some of the mismatch seen in the *initial model*; the poorest fitting for both models occurs at the lower conversion, 70%, but the mismatch is reduced after the parameter correction.

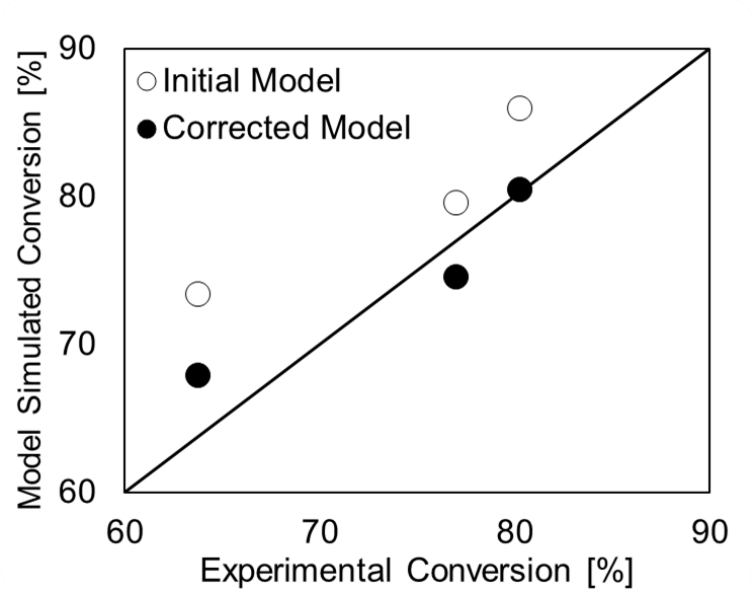

Figure 16 Comparison of model predictions against experimentally observed conversion of acetic acid.

5.2.4 Model validation

To verify the improved accuracy of the new model, a validation experiment was performed following the parameter estimation. The SMBR operating conditions listed in Table 6 were determined by optimizing the *initial model* to maximize PMA productivity and to achieve a conversion of 95%. We acknowledge that the model validation can be done by optimizing the *corrected model*; however, we chose to optimize the *initial model* to maintain the consistency of the SMBR model used to determine the operating parameters for the 95% conversion to those of the prior three conversions. This conversion was chosen to test the accuracy of the model's predictability for an extrapolation from the conversion range of 70% to 85%.

Table 6 Experimental operating conditions for maximized PMA production rate and 95% acetic acid conversion

Operating parameters	Optimal value for 95% conversion
Desorbent Flow rate [mL/min]	1.60
Extract Flow rate [mL/min]	1.60
Feed Flow rate [mL/min]	0.38
Recycle Flow rate [mL/min]	0.20
Switch Time [min]	51.3

Figure 17 compares the experimental observations and model predictions. In general, the *corrected model* shows an overall better prediction of the experimental outcomes than the *initial model*. The only exception to this observation is for the water concentration in the raffinate stream (Figure 17B); however, as mentioned earlier, water measurements are lower due to the ease of water adsorption by PM.

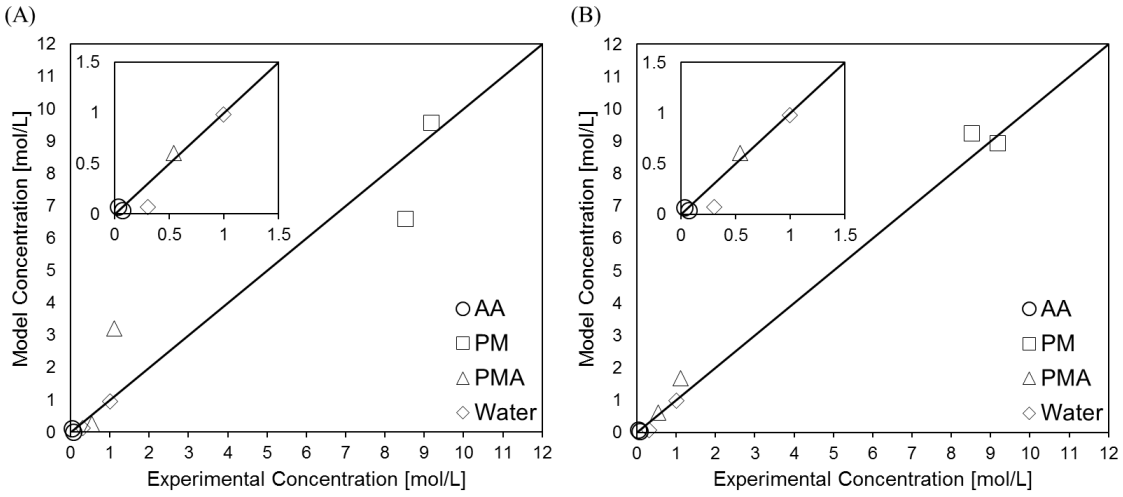

Figure 17 Comparison of the 95% conversion experiment to the predictions for (A) *initial model* and (B) *corrected model*.

The *corrected model* is also able to predict the production rate for each conversion experiment (Figure 18A). The *corrected model* successfully captures the trade-off relationship between production rate and conversion (Figure 18B) that was observed

experimentally. This trade-off (Figure 12) was discussed earlier in Section 5.2.1—at a higher conversion, the production rate is lower due to lower flow rates, which were necessary to increase the residence time.

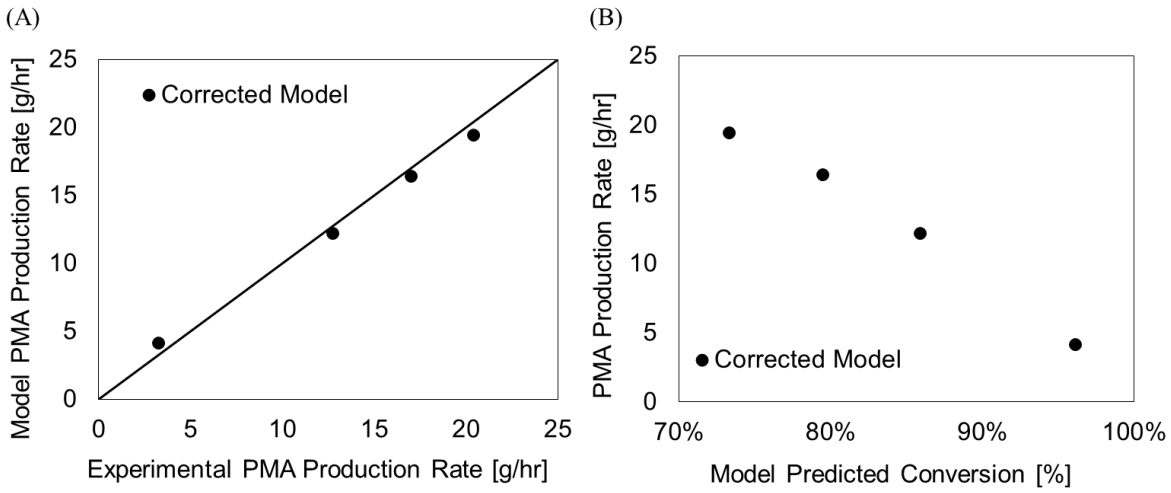

Figure 18 (A) Plot of the corrected model against the experimental results for PMA production rate. (B) Pareto plot of PMA production rate against conversion predicted by the model.

5.2.5 Potential sources of model mismatch

There are several potential sources of modeling errors that are causing the remaining model mismatch. First, as discussed in Section 0, changes in the void fractions due to shrinking and swelling of the resin can contribute to model error. Second, the changes in the liquid volume due to local changes in composition can also cause some model mismatch (further discussion in Section 5.2.5.1). Third, the assumption of second order kinetics may not be exact. A different reaction order will affect the reaction rate and thus the calculation of conversion and PMA production rate. Furthermore, the kinetic equilibrium assumes ideal component behaviors. If the non-ideality is significant, then a model that includes the activity coefficient of each component is necessary. This reaction

equilibrium would also affect the reaction rate and the determination of conversion and PMA production rate. Finally, a linear isotherm is assumed. This model is valid for dilute systems; however, at either low (70%) or high (95%) conversions, there are either high concentrations of unreacted acetic acid or formed PMA, respectively. These higher component concentrations would undermine the dilute system assumption and thus any existing nonlinear adsorption behavior would need to be described with a nonlinear isotherm such as a Langmuir model [40].

5.2.5.1 Analysis of liquid volume change

The liquid velocity may vary due to: (A) changes in the molar volume of each component due to reaction, and (B) excess volume that is dependent on the liquid composition. These two potential sources contribute to the volume change and are investigated individually.

To quantify the change in molar volume due to the reaction (A), we define the following (apparent) average molar volume for a stoichiometrically balanced mixture:

$$V_{avg}(\xi) = \frac{1}{N_{React}} \sum_{i \epsilon React} (1-\xi) v_i V_i + \frac{1}{N_{Prod}} \sum_{i \epsilon Prod} \xi v_i V_i$$
$$React = \{AA, PM\} \qquad (31)$$
$$Prod = \{PMA, water\}$$

where $V_{\text{avg}}(\xi)$ is the apparent average molar volume for a given conversion ξ, V_i is the molar volume of component i, N_{React} is the number of reactants, N_{Prod} is the number of products, *React* is the set of all reactants, and *Prod* is the set of all products. For the reaction in this study given in Figure 2, the change of $V_{\text{avg}}(\xi)$ for $0 \leq \xi \leq 1$ is within 0.2%. These calculations indicate that the influence of the molar volume change due to reaction is negligible.

We also investigated the influence of the excess molar volume (B), which depends on the liquid composition. We define the apparent molar volume as follows:

$$V_{\text{apparent}} = \sum_{i=1}^{n} x_i V_i \tag{32}$$

where x_i is the mole fraction of component i. On the other hand, the volume that can be observed may include excess volume as follows:

$$V_{\text{observed}} = \sum_{i=1}^{n} x_i V_i + V^E \tag{33}$$

where V^E is the excess volume [41]. It should be noted that V^E is a function of the composition x_i, and quantifying or modeling V^E at all potential values of x_i in a quaternary mixture would require substantial experimental effort. In this study, we investigated this influence only at some representative compositions; more specifically, the compositions at the end of each zone that were calculated by the SMBR model (Figure 19), and V_{observed} was measured experimentally at those compositions.

Table 7 summarizes the results from the experiments, where V_{observed} was measured at 25˚C. It can be seen that a maximum volume decrease of 3.1% is observed and is attributed to the excess volume, V^E. This finding is corroborated by an excess volume study [42] between water and PM. It is noted that measurement errors were observed to be less than 0.4%. We suspect this volume change contributed to the remaining model error observed in Section 5.2.3, and modifying the model to include this volume change effect may improve the accuracy. Such a modification would require substantial experimental effort to quantify the excess volume V^E in quaternary mixtures, and was not carried out in this study.

Table 7 Volumetric ratio of the samples from the mixing experiment.

	x_{AA}	x_{PM}	x_{PMA}	x_{water}	$\frac{V\text{observed}}{V\text{apparent}}$
End of Zone I	0	0.820	0	0.180	0.969
End of Zone II	0.090	0.550	0.180	0.180	0.979
End of Zone III	0	0.820	0.180	0	0.985

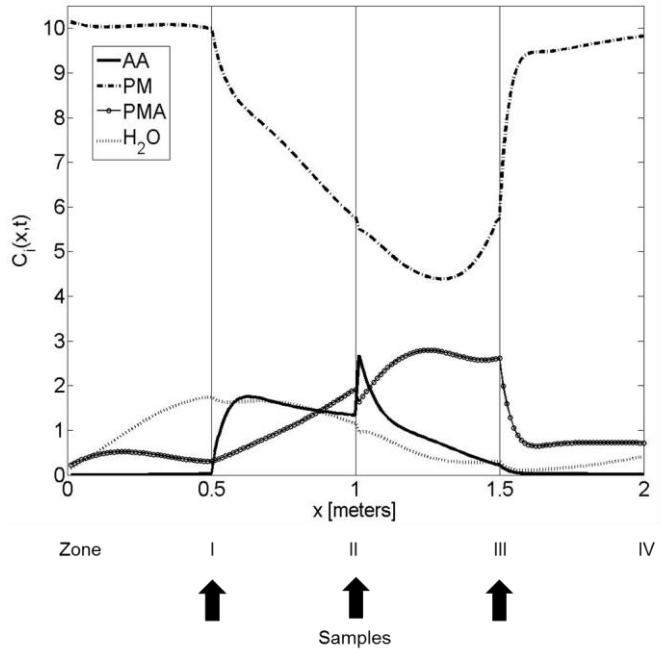

Figure 19 Liquid concentration profiles of all four components as a function of column length (x-axis, in meters) as determined by the model for the conversion of 95%. The operating condition is given in Table 7. The arrows mark the compositions tested for the experimental analysis of mixing effects on volume.

5.3 Conclusions

A model-based approach was used to develop an optimal operation for the SMBR system. Utilizing the model developed in the previous work [15], the SMBR model was optimized and the resulting optimal operating conditions obtained were implemented for

three different SMBR experiments at different acetic acid conversions. Comparison of the experimental results to the model simulation showed that the *initial model* was reasonably accurate. The model mismatch was expected considering that initial SMBR parameters were obtained not from SMBR experiments but from different kinds of experiments such as batch stir-tank reactor and single column chromatography experiments.

Using the method of least-square minimization, the experimental data and simulation results were used to correct the model parameters by minimizing the model mismatch of extract and raffinate streams. A Tikhonov regularization was used to deal with the ill-conditioned parameter estimation problem and to bind the newly calculated parameters more closely to the values obtained from previous non-SMBR experiments. This method determined a new set of model parameters that show better overall fit to all experimental SMBR data than the parameter set from the *initial model*. The *corrected model* was developed for a conversion range of 70% to 85%, and the model's predictive accuracy was validated outside that range at 95% conversion.

CHAPTER 6. SMBR OPTIMIZATION FOR TRANSESTERIFICATION

6.1 Motivation

Transesterification has many applications demonstrated both in laboratory and industrial scales. In laboratory uses, this organic reaction can be used to prepare esters and polymerization, specifically ring openings of lactones [43]. In industry, transesterification reactions are performed for production of paint components through the curing of alkyd resins [44]. Additionally, transesterification is important for the production of esters of oils and fats [45]. Most recently, with growing interest in environmentally sustainable fuel sources, the potential of biodiesel, fatty acid methyl ester (FAME) production, which is derived from the transesterification of triglycerides with methanol, has become an attractive option [46, 47].

Transesterification is also an equilibrium-limited reaction. Usually, equilibrium constants are near unity and the reaction rates are low, so different process intensification methods that can drive reaction towards higher conversion are highly attractive. The transesterification process had been combined with reactive distillation [48-50] and reactive extraction [51, 52]. To the best of our knowledge, no one has applied reactive chromatography or SMBR technology to transesterification reaction except for biodiesel [20, 53]. Moreover, no one has applied SMBR for the transesterification production of glycol ether esters [18, 54].

The motivation to explore the transesterification reaction route for PMA production is to overcome the several disadvantages in the esterification reaction. First,

transesterification does not generate water as the byproduct, which forms multiple azeotropes with PM [55]. Consequently, the transesterification route does not require energy-intensive downstream operations, such as azeotropic distillation or extractive distillation [20], for water removal. Furthermore, in transesterification, there is easier removal of byproduct from the column for resin regeneration because ethanol is much less adsorbent to the resin than water is in esterification. Consequently, esterification has a high desorbent consumption to effectively elute the column of water [18]. Finally, transesterification can operate at a much lower temperature, 40-60 °C compared to the esterification's 110 °C [16, 18].

6.2 Results

6.2.1 SMBR optimization

The *initial model* is optimized according to the formulations given by Eq. 14-19. Three different values of ε in Eq. 19 are defined, which corresponded to 50%, 60%, and 70% conversion, while solving the maximization problem for ζ_1 (Eq. 14). These conversions are lower than that for the esterification case [24], but are within a range of practical interest. The highest conversions we can achieve experimentally require very small flow rates, and were limited by the lower limit of our pump flow rates; if smaller pumps were available that allowed us to operate at lower flow rates, then a higher conversion can be obtained experimentally. Each optimal solution of this optimization problem lies on the Pareto front of the multi-objective optimization problem (Figure 20). The operating conditions from this multi-objective optimization analysis are shown in Table 8.

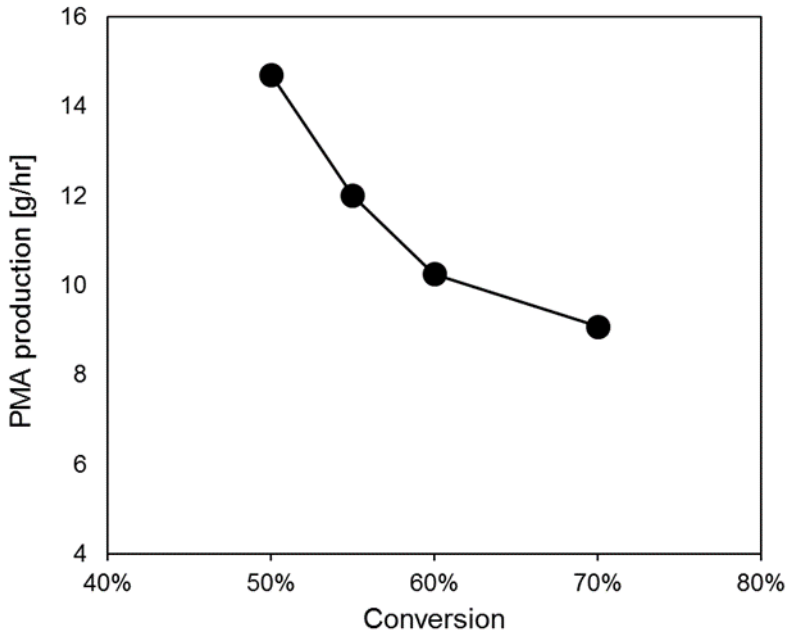

Figure 20 Pareto plot: model predicted PMA production rate against conversion of ethyl acetate.

Figure 20 shows the Pareto front between PMA production rate (Eq. 14) and conversion (Eq. 15). There is a trade-off relationship between these two objectives. A higher conversion is achieved when the residence time increases inside the SMBR. Consequently, the flow rates decrease and the switch time increases (Table 8). The slower flow rate results in the lower production rate as conversion increases.

Table 8 Optimal operating conditions form SMBR from the multi-objective optimization analysis for maximizing PMA production rate and ethyl acetate conversion using the *initial model*.

	Run 1	**Run 2**	**Run 3**
Target conversion [%]	50	60	70
Desorbent Flow rate [mL/min]	7.10	6.00	1.30
Extract Flow rate [mL/min]	6.00	5.30	0.80
Feed Flow rate [mL/min]	0.29	0.18	0.18
Raffinate Flow rate [mL/min]	1.30	0.90	0.70
Switch Time [min]	6.80	8.30	9.30

6.2.2 SMBR experiments

The SMBR operating conditions listed in Table 8 are implemented experimentally on the SMBR unit. The operating conditions implemented in experiments and the corresponding conversions predicted by the model are listed in Table 9. The reason there is a difference in the operating conditions and conversions between Table 8 and Table 9 is due to the deviations of the actual flow rates from the set points of the pump. The flow rates of the extract and raffinate were measured during the experiments, which are shown in Table 9. On the other hand, for the desorbent and feed flow rates, no direct measurements were possible. For these two pumps, we carried out pump calibration tests, in which the flow rates were indirectly calculated by the change in mass of the feed and desorbent bottles. These tests revealed that the desorbent pump exhibited an error of 2-3% from setpoint. The feed pump had even more deviation from setpoint, 3-8%, because the flow rates were near the lower limit of pump operation. For feed and desorbent flow rates, these flow rate corrections using the calibration curves are reflected in Table 9. The flow rates

implemented in the experiments are employed for all model simulation results and the model correction in Section 6.2.3.

After reaching cyclic steady state, concentration samples are collected from the extract and raffinate streams for each step of cycles 7 and 8. The concentrations are determined by GC. Figure 21 graphs the four component concentrations from the extract and raffinate streams at all three conversion conditions. The model accuracy is quantified by the squared error of the concentration (Eq. 28). These observations demonstrate that the inverse method used on the batch reaction experiments and single-column tests [17] to determine model parameters is a reliable method for developing a preliminary SMBR model. The remaining mismatch motivates parameter correction as discussed below.

Table 9 Experimentally implemented operating conditions for SMBR using the initial model. The flow rates reflect the setpoint correction and were rounded off to the nearest 0.1 ml/min when implemented experimentally.

	Run 1	**Run 2**	**Run 3**
Conversion predicted by initial model [%]	48.9	59.4	67.4
Desorbent Flow rate [mL/min]	7.30	6.10	1.30
Extract Flow rate [mL/min]	6.20	5.40	0.80
Feed Flow rate [mL/min]	0.30	0.19	0.16
Raffinate Flow rate [mL/min]	1.40	0.90	0.70
Switch Time [min]	6.80	8.30	9.30

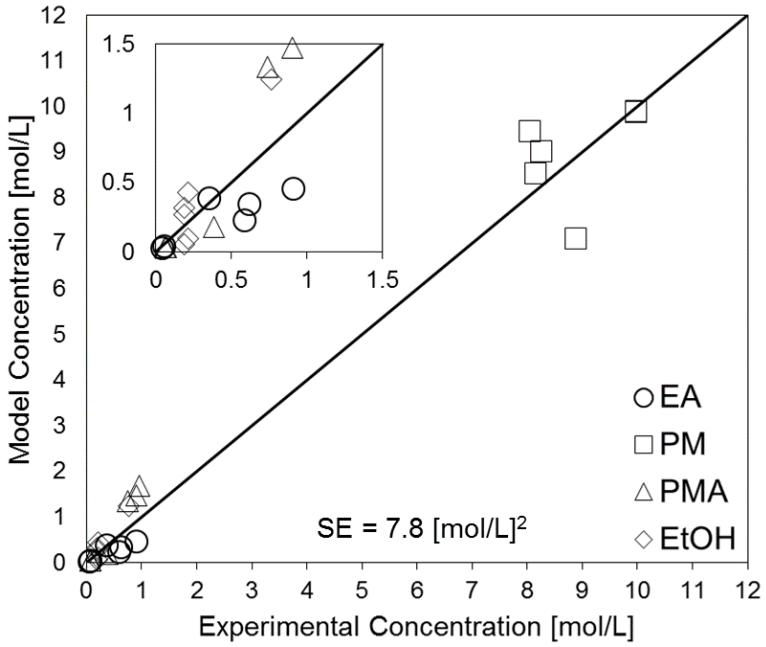

Figure 21 Comparison of the experiment to the initial model prediction for concentrations of all components in the extract and raffinate.

From our sample collection, we can calculate other performance indicators such as productivity, production rate, conversion, product recovery, byproduct content in the raffinate stream. Table 10 is a summary of the experimental performance indicators for all three conversion experiments. There is significant deviation in the conversion for Run 3 between model prediction and experimental result: 67.4% and 57.7%, respectively. This difference may be due to the model extrapolation; the model parameters were obtained only from single-column experiments, where the highest conversion achieved was only 63% [17]. The extent of the prior experiments may have limited the accuracy of the model for higher conversions.

Table 10 Summary of experimental performance indicators for all three conversions.

	Run 1	Run 2	Run 3
Conversion predicted by initial model [%]	48.9	59.4	67.4
Experimental conversion [%]	47.3	61.7	57.7
Productivity [kg/L/day]	1.26	1.08	0.78
Production rate [g/hr]	8.27	6.60	5.16
PMA recovery in raffinate [%]	72.3	68.7	67.4
Ethanol content in raffinate [wt. %]	1.09	0.95	1.99

6.2.3 SMBR parameter estimation

To improve the model accuracy and recalculate model parameters, parameter estimation was carried out using the SMBR experiments. As discussed in Section 4.3, there are 14 model parameters: ε_T, K_{eq}, k_1, H_{EA}, H_{PM}, H_{PMA}, H_{EtOH}, b_{PMA}, b_{EtOH}, D_{ax}, K_{EA}, K_{PM}, K_{PMA}, and K_{EtOH}. Each of the three conversion experiments generates samples for all four components from the extract and raffinate; hence, there are a total of 24 concentration data points. The objective function used to correct for the model parameter is:

$$\phi = \min_{\epsilon_T, D_{ax}, K_{eq}, k_1, H_i, K_i} \sum_{k=1}^{N_{exp}} \sum_{i=1}^{N_{comp}} (C_{i,k}^{model} - C_{i,k}^{exp})^2 \; + \; \rho \sum_{m=1}^{N_{param}} \left(\frac{\theta_m^{model} - \theta_m^{initial}}{\theta_m^{initial}}\right)^2 \tag{34}$$

$$\theta = \left(\varepsilon_T, D_{ax}, K_{eq}, k_1, H_{EA}, H_{PM}, H_{PMA}, H_{EtOH}, K_{EA}, K_{PM}, K_{PMA}, K_{EtOH}, b_{PMA}, b_{EtOH}\right)$$

Subject to equations 1-13

The term $\frac{\theta_m^{model}-\theta_m^{initial}}{\theta_m^{initial}}$ is non-dimensionalized by normalizing the parameter difference by the initial parameter value. A ρ value of 0.1 was chosen that is the best balance between model fitting and parameter deviations from the initial values [36].

Table 11 summarizes the SMBR parameter values from the *initial model* and the *corrected model*. The changes of recalculated parameter values are reasonable compared to the initial values

Table 11 Summary of SMBR parameter calculations.

	Total void fraction	**Reaction**		**Adsorption (Henry's Constant)**				**Adsorption (Equilibrium constant)**		**Dispersion and Mass Transfer**				
Parameter	ε_T	K_{eq}	k_1 $[\frac{L}{mol\ min}]$	H_{EA}	H_{PM}	H_{PMA}	H_{EtOH}	b_{PMA}	b_{EtOH}	D_{ax} $[\frac{m^2}{min}]$	K_{EA} $[\frac{1}{min}]$	K_{PM} $[\frac{1}{min}]$	K_{PMA} $[\frac{1}{min}]$	K_{EtOH} $[\frac{1}{min}]$
Initial model	0.50	0.17	0.105	0.396	0.457	0.206	1.33	0.77	0.296	1.17×10^{-4}	1.12	0.881	1.28	0.80
Corrected model	0.516	0.166	0.096	0.351	0.322	0.238	1.01	0.71	0.303	1.19×10^{-4}	0.304	0.846	1.16	0.19

The Henry's constants for PM and ethanol (H_{PM}, H_{EtOH}) changed to improve model fitting. These changes may be accounted for by some key differences in experimental conditions used to obtain the initial to corrected parameter values. First, there is more dead volume in the SMBR experiments that can be lumped into the Henry's constants [37] calculated for the *corrected model*. Contributing to the dead volumes include the column connection tubing, valves, and pumps. Second, due to the larger number of columns and experiments conducted for the SMBR experiments compared to only the single-column experiments, the variance (error and noise) may not have as great of an impact on the calculations for the *corrected model* values compared to the *initial model* values.

The mass transfer constants for ethyl acetate and ethanol (K_{EA}, K_{EtOH}) changed from their *initial model* values. These changes may be due to strong correlations with the axial dispersion and the Henry's constants.

A sensitivity analysis was conducted for all the model parameters (Figure 22). Each parameter was perturbed individually by a 20% increase and decrease from their *corrected* model values while all other parameters were unchanged. The perturbation that yielded the greater change in the squared error is plotted in Figure 22. There are several sensitive parameters, ε_T, k_1, H_{EA}, H_{PM}, and H_{PMA}, that caused noticeable increases in the squared error (*SE*) of the concentration (Eq. 28). A few of these parameters are also the same ones that changed by more than 10% from their *initial model* to the *corrected model* values.

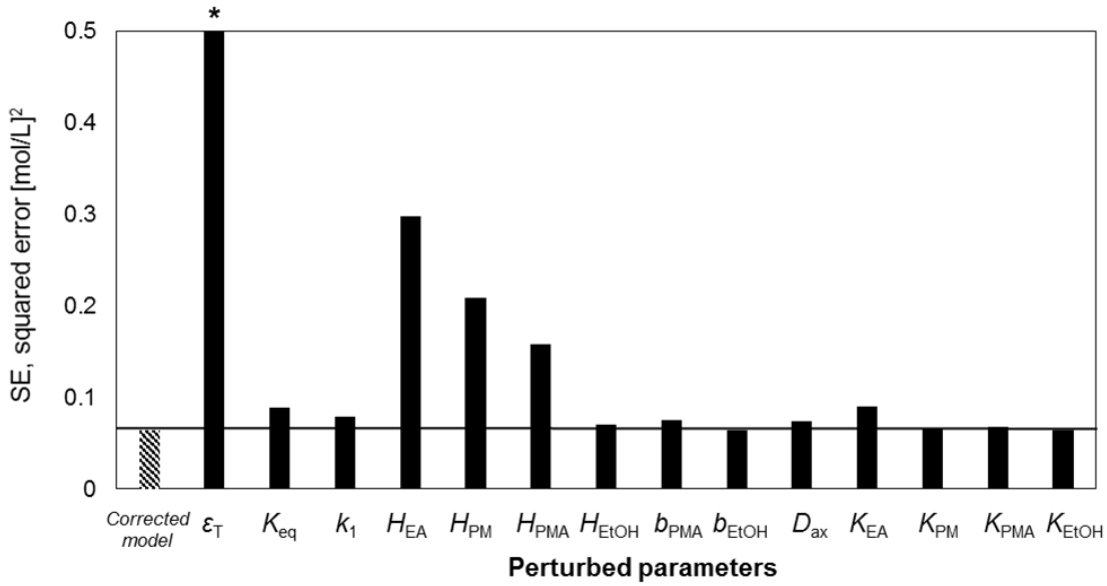

Figure 22 Summary of the sensitivity analysis. Each parameter was perturbed by 20% while all other parameters were unchanged. The total squared error of the concentration is reported for the corrected model along with each perturbed parameter. The asterisk above the bar for ε_T indicates the value extends beyond the maximum y-axis value.

There are also some parameters that are not very sensitive. Most of those parameters are the ones whose *corrected model* values remain very close in value to the *initial model* parameter values. Two exceptions are K_{EA} and K_{EtOH}. These two parameters changed greatly, by over 70% from their original *initial model* values, that in comparison, the 20% perturbation for the sensitivity analysis is small and the resulting squared error are close to the *corrected model* values.

After parameter recalculation, the *corrected model* simulated the operating conditions from Table 8, the same ones used to conduct the SMBR experiments, to obtain model predictions of the concentrations of all components. Figure 23 graphs the four component concentrations from the extract and raffinate streams at all three conversion conditions. The plot clearly illustrates the *corrected model* has better fit than the *initial model* and this is quantified by the lower squared error (*SE*) for the *corrected model*.

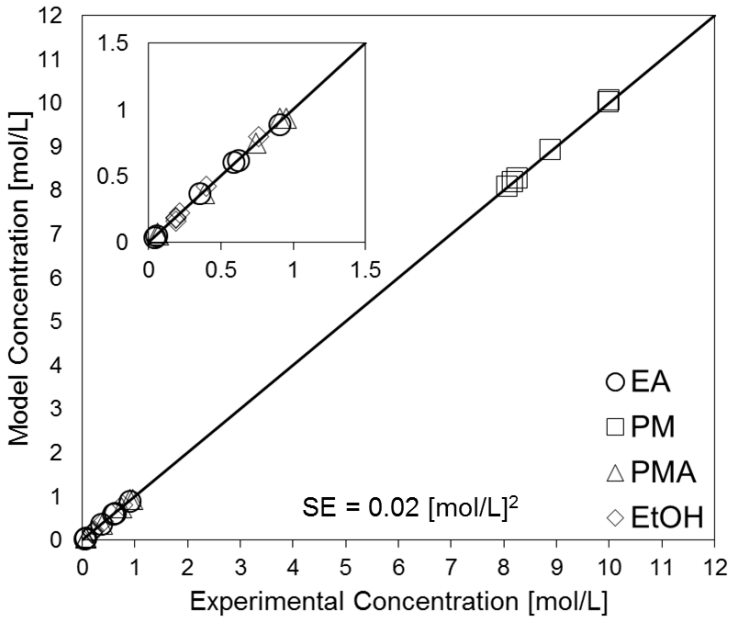

Figure 23 Comparison of the experiment to the corrected model prediction for concentrations of all components in the extract and raffinate

6.2.4 Model validation

The accuracy of the *corrected model* was verified by a validation experiment. The SMBR operating conditions listed in Table 12 were determined by optimizing the *initial model* to maximize PMA productivity and to achieve a conversion of 80%. We chose to optimize the *initial model* to maintain the consistency of the SMBR model used to determine the operating parameters for the 80% conversion to those of the prior three conversions. This conversion tested the model's predictability for an extrapolation from the conversion range of 50% to 70%. The operating conditions (Table 12) were implemented experimentally on the SMBR unit. Table 12 includes both the targeted flow rates, and the actual experimental implementations after correcting for pump flow deviations as described in Section 5.2.2. The conversion observed in the experiment was

74.6%, which was lower than the *initial model* prediction of 82.6%, but was predicted more accurately by the *corrected model* of 74.8%.

Table 12 Experimental operating conditions for maximized PMA production rate for validation experiment. The conversion obtained in the experiment was 74.6%.

Operating parameters	**Optimal operating condition**	**Experimental implementation**
Conversion predicted by initial model [%]	80.0	82.6
Conversion predicted by corrected model [%]	72.4	74.8
Desorbent Flow rate [mL/min]	0.40	0.41
Extract Flow rate [mL/min]	0.20	0.20
Feed Flow rate [mL/min]	0.040	0.030
Raffinate Flow rate [mL/min]	0.20	0.24
Switch Time [min]	29.4	29.4

Figure 24 compares the experimental observations and model predictions. The *corrected model* (Figure 24B) shows a greatly improved prediction of the experimental outcomes than the *initial model* (Figure 24A).

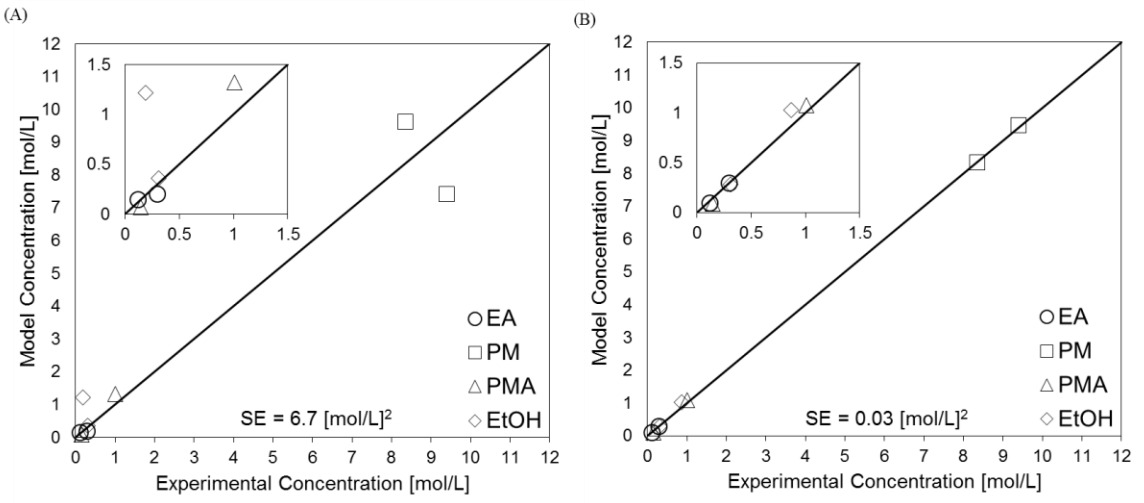

Figure 24 Comparison of the 80% conversion experiment to the model prediction for (A) initial model and (B) corrected model.

The *corrected model* is also able to describe the production rate (Figure 25A), conversion (Figure 25B), and PM to PMA ratio (Figure 25C) for each experiment significantly more accurately.

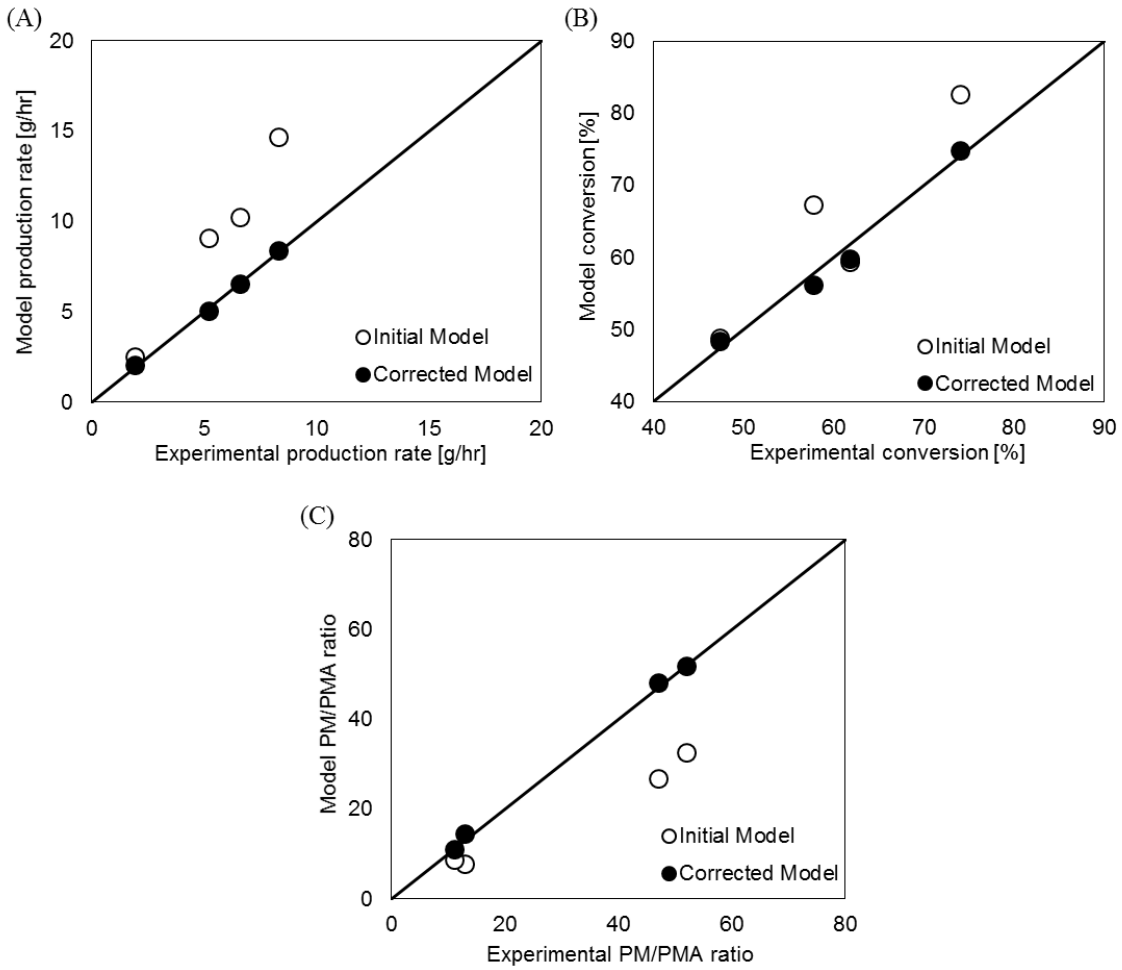

Figure 25 Comparison plots of (A) production rate, (B) conversion, and (C) PM to PMA ratio.

6.2.5 Potential sources of model mismatch

We made several model assumptions (summarized in Section 4.2) that may be the source of the remaining model mismatch. First, as discussed in Section 6.2.3, changes in the void fraction due to bed volume changes of the resin can contribute to model error. Second, the reaction may not be second order (Eq. 7) and thus calculations of conversion especially at the higher conversions may change.

6.3 Comparison of esterification and transesterification

With the *corrected model* developed for both the esterification and transesterification routes, a comparison of their relative performance can be made. Table 13 summarizes the findings. Esterification features superior productivity/production rate and lower PM to PMA ratio because of the faster reaction rate and higher selectivity of the adsorbent. On the other hand, transesterification has the advantage of shorter time to reach CSS and marginally better recovery and purity in the raffinate outlet.

Each of the two reaction routes has one significant limitation that has not yet been quantified, which are shown in the last two rows in Table 13; for esterification, it is the generation of water and thus the presence of azeotropes. The azeotrope challenge can be overcome by further processing the outlet streams of the SMBR through separation units [20, 21]. Addition of such separation units may offset the higher productivity due to the additional capital and utility cost, which would require further investigation. On the other hand, the transesterification route may have a disadvantage of catalyst deactivation, since base catalysts tend to be more unstable. While we did not observe deactivation of the anion exchange resin during the SMBR runs, deactivation was reported in past studies during accelerated stability studies in which an equal volumetric mixture of ethyl acetate and PM were pumped through a single reactive chromatography column and the PMA and the conversion were measured every hour [17, 18]. To overcome this potential deactivation, there has been work that demonstrated *in situ* regeneration of the resin for continuous reactors for biodiesel production [56-58]. In SMBR the regeneration step for the column can be performed by interrupting the production run, which would reduce the productivity. This interruption of production may be avoided by simultaneous regeneration and

production by adding the sodium hydroxide solution as a mixture with the solvent through the desorbent inlet [18, 59], or alternatively, offline regeneration of the SMBR columns such that there is periodic regeneration of resin in select columns within a cycle.

It should finally be noted in Table 13 that experimental SMBR conversion for transesterification has not achieved as high of a conversion as 90%. From the reliability of the corrected model we observed in the validation experiment, we assumed that the model prediction can be extrapolated to a higher conversion.

Table 13 Comparison of SMBR production of PMA via the esterification and transesterification routes.

Performance indicators	Esterification	Transesterification
Target conversion	90.0	90.0
Production rate [g/hr]	12.2	9.12
Productivity [kg/L/day]	1.87	1.39
PM to PMA (SMBR)	5.00	18.9
Time to cyclic steady state [hr]	19.8	5.66
PMA recovery in the raffinate	99.7	95.3
Byproduct content in raffinate	0.49	0.09
Azeotrope	Water	None
Catalyst stability	No deactivation observed	Potential deactivation

6.4 Conclusions

For production of PMA, we extended our previous work in SMBR optimization and model development to the transesterification reaction pathway. Utilizing the same model-based framework [24], the SMBR model is corrected using experimental results from three different conversion experiments. The *corrected model* is validated experimentally at a conversion outside the initial experimental range. This work

demonstrates the robustness and applicability of this model-based approach to other applications of SMBR.

The *corrected model* is optimized to target a 90% conversion and the results are compared to those from the esterification route. There are advantages and disadvantages to either production route for PMA. While the transesterification has lower conversion in our study, developments in resin or the use of alternative catalyst can improve conversion. Another potential route to overcome the limited degrees of freedom in operation of an SMBR is to have different material for the adsorbent and catalyst instead of relying on a single resin to have the ideal properties for both functions [18, 59]. In this way, a resin adsorbent and a homogenous catalyst can be optimally selected for separation and reaction. Finally, an overall process [60] that includes downstream separation units and recycle of unreacted reactants for the transesterification route needs to be conducted to allow for a better overall process understanding of this route. Such an investigation will enable a comparative study of the overall process operations between the esterification and transesterification routes.

CHAPTER 7. OPTIMIZATION OF OVERALL FLOWSHEET

7.1 Motivation

Some work has studied integration of SMB and SMBR into an overall process. Constantino et al. [61] evaluated an process integrated SMBR for butyl acrylate synthesis; their SMBR was coupled to a fixed-bed reactor to consume the remaining unreacted reactant. Similarly, Lee et al. [62] and Moraru et al. [63] evaluate a coupled reactor to SMB process. Nevertheless, to the best of our knowledge, an overall process evaluation with SMBR and downstream separation units has not been analyzed.

An important consequence of the purification steps in downstream separation units is the removal of water from the process. It is well documented that water forms an azeotrope with PM [55] that cannot be separated by conventional distillation methods. Alcohol dehydration at industrial scale is achieved via azeotropic distillation, extractive distillation, membrane pervaporation, and PSA. Azeotropic distillation is very energy intensive and requires an entrainer such as benzene or cyclohexane which are either carcinogenic or requires additional distillation steps to remove the entrainer from the product stream [64]. Extractive distillation is also highly energy intensive and costly and requires a suitable extractive agent such as ethylene glycol, which would require additional removal steps [65]. Membrane pervaporation is more suitable for alcohol dehydration at small scales and when a high organic purity is required [66]. Additionally, PSA processes have similar capital costs to membrane systems but have a longer operational life. Potential new methods for producing PMA at large-scale must consider less energy intensive alternatives that solves the azeotrope problem.

7.2 Configuration considerations

As described in Section 4.5.1, we evaluated three different process configurations- the standard (Figure 27A), the limited superstructure (Figure 27B), and full superstructure (Figure 27C). This required an approach called superstructure optimization. In this strategy, optimization of the configuration and operating conditions are executed simultaneously. Traditionally, the superstructure strategy requires the use of discrete variables and the formulation becomes mixed integer linear programing or mixed integer non-linear programming (MILP or MINLP) [25, 67]. In our study, the stream locations are not a fixed parameter, but are free variables that are determined by the optimizer. In our formulation, we do not use integer or discrete variables, but implement only the superstructure strategy using flow rates which are continuous variables [68]. Specifically, we explore the superstructure in how the downstream recycle stream can be connected to the inlet of the SMBR as well as how the feed, extract, and desorbent streams can be optimally configured.

7.3 Analysis

Cost of capital and operation must be analyzed carefully when designing this downstream process (Figure 26). The major capital cost comes from the SMBR columns, the distillation column, and the hot gas PSA unit. The major consumables are the resin, the hydrophilic adsorbent of the PSA, and the SMBR solvent. Finally, the operating costs are determined by the heat duty for the reactor's column heating jackets, the reboiler and condenser of the distillation column, and the vaporizer, heater, condenser, and vacuum

from the hot gas PSA. Our approach to handle the total process cost is by defining various "performance indicators" that are representative of the cost; the first indicator is *productivity*, which is the production rate of the product PMA per resin volume in the SMBR, which represents the capital cost of the SMBR; the second indicator is the *excess solvent ratio*, which reflects fresh solvent consumption for the process and the amount of waste generation through the *PSA purge* stream; third, the *single-pass conversion* is related to the extent of downstream processing that is needed to recycle unreacted reactants for maximum production; finally, we define *operating cost (OC) proxy* to evaluate the operation cost of PSA. These performance indicators are defined and discussed in Section 4.

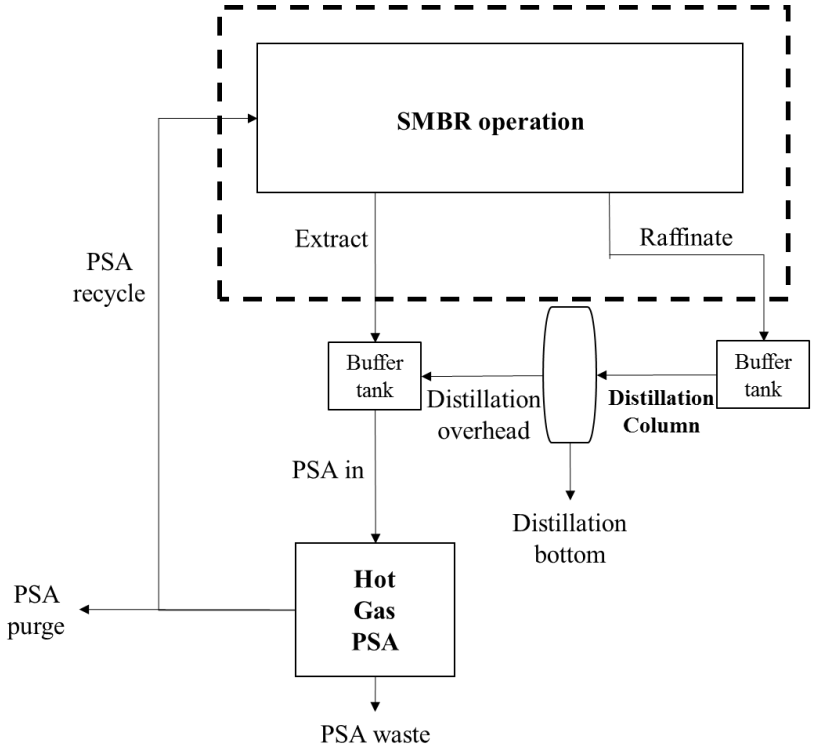

Figure 26 Reproduction of Figure 10; schematic for the overall flowsheet.

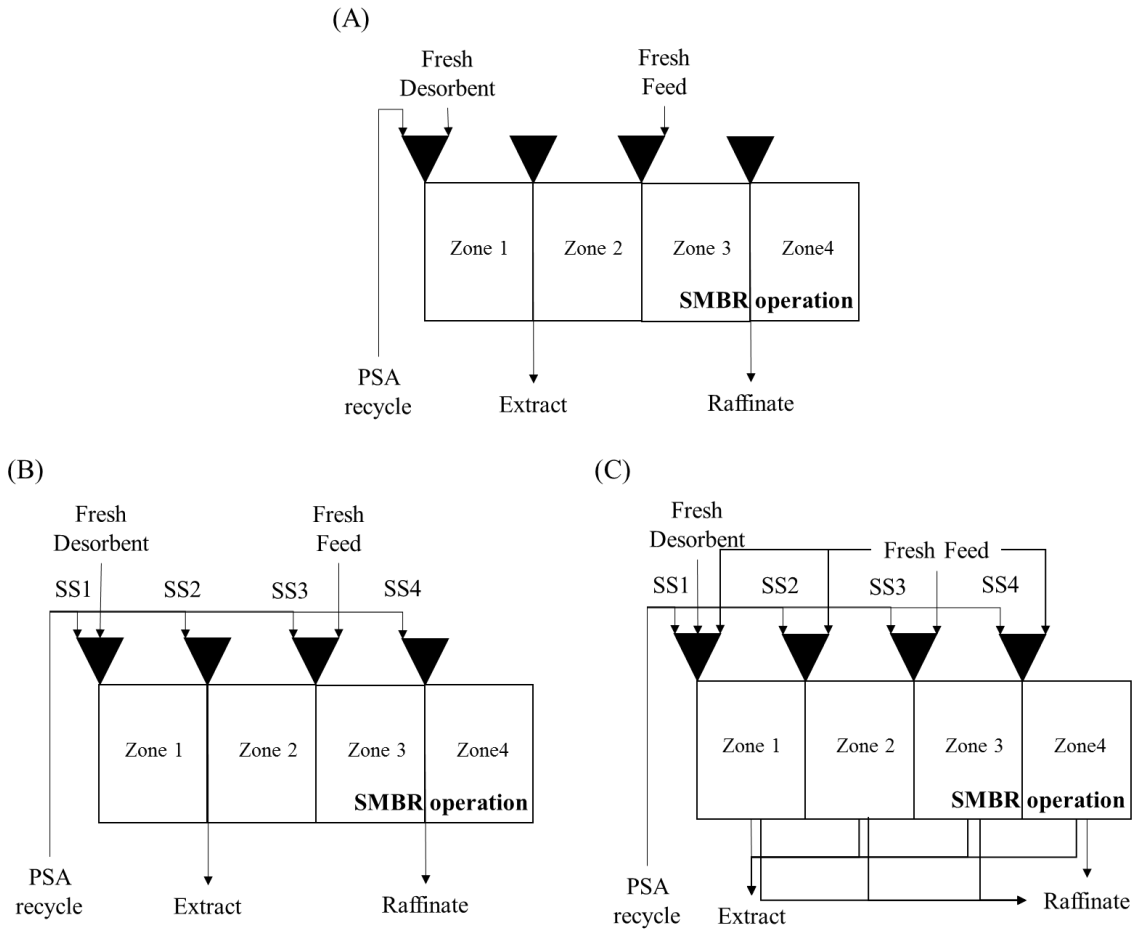

Figure 27 Reproduction of Figure 11; detailed schematic of the stream configurations around the SMBR for the (A) standard, (B) limited superstructure, and (C) full superstructure configuration.

7.4 Results

7.4.1 Feasibility of downstream units

We assume the distillation unit that processes the raffinate stream is capable of complete and pure PMA recovery in the *Distillation bottom* stream, due to PMA being the heaviest component (Figure 26). We demonstrate that this is technically possible through Aspen simulations. The method selected was NRTL-HOC (non-random two liquid model

with Hayden O'Connor). The method is good for azeotrope separations, mixtures of polar and nonpolar components, and systems containing organic acids (acetic acid).

Table 14 contains the details of the distillation unit operation simulated in Aspen for two conditions. We can operate the distillation columns for these different raffinate stream compositions to both achieve a PMA purity over 99 mol % and a PMA recovery over 98% in the distillation bottoms. Although there is some PMA loss in the *Distillation overhead* stream, especially for condition "2", the amount in comparison to the PMA composition in the extract is insignificant (lower than 3 mol%) and therefore does not alter the composition of the *PSA in* stream.

Table 14 Operating parameters for the distillation simulation in Aspen.

Condition	**1** (91% single-pass conversion, 1.2 excess solvent ratio)	**2** (72% single-pass conversion, 4 excess solvent ratio)
Method	NRTL-HOC	
Distillate to feed ratio	0.63	0.54
Feed stage	15	
Reflux ratio	5.0	
Number of stages	40	
Condenser	Total	
Reboiler	Kettle	
Pressure	5 atm (condenser and reboiler)	
PMA purity	99.6%	99.7%
PMA recovery	99.3%	98.4%

We assume the hot gas PSA completely removes all water produced by the SMBR operation through the *PSA waste* stream. This assumption is based on several papers that have applied a pilot PSA process for alcohol dehydration [66, 69, 70]. Liu *et. al.* [66] describe a hot gas PSA process that dehydrated isopropanol containing 35 mol% of water to less than the detectable limit for water (<500ppmv). Pruksathorn and Vitidsant [69] showed they achieved a purity of over 99.6 vol% for their ethanol dehydration from a feed

that contains 92 vol % of ethanol. Moreover, several patents detail the use of hot gas PSA for the dehydration of ethanol and methanol [71-73].

Additionally, a sensitivity analysis was conducted to evaluate the impact of recycling water through PSA recycle stream. In this analysis, water recovery in *PSA waste stream* is decreased from 100% to 90%. It was found that the productivity decrease of the overall process is only up to 8% even at the lowest water recovery of 90%. This analysis revealed that the process can handle recycling low concentrations of water (lower water recovery), although productivity decreases modestly with lower water recovery.

7.4.2 Trade-off relationships

The optimization results for the overall flowsheet reveal several trends. Figure 28 plots the results of the operating cost proxy against the productivity for the standard configuration. Each data line represents a specific single-pass conversion and within a given conversion, each point corresponds to an excess solvent ratio. The dashed line indicates the conditions that achieve the minimum operating cost proxy for any given conversion. Any point lying above the line is suboptimal operation and any point below that line is in the infeasible solution space in which no solution exists. This result highlights that there is a trade-off between achieving high productivity and low associated operating cost. The condition that corresponds to the minimum operating cost proxy is at 90% single-pass conversion and an excess solvent ratio of 1.5. The productivity corresponding to that point is 1.97 kg/L/day. This behavior can be explained by evaluating the definition of the operating cost proxy (Eq. 25). For all conversions lower than 90%, the operating cost is higher because of the dominating effects of the numerator contribution to the calculation of the operating cost proxy. A lower conversion increases the overall flow rates in the

process, including the *PSA in* stream, increasing the magnitude of the numerator in Eq. 25 and thus, the operating cost proxy is high. Conversely, at conversions higher than 90%, the operating cost is higher because of the dominating effects of the denominator contribution to the calculation of the operating cost proxy. A higher conversion decreases the PMA production because of the lower throughput, decreasing the magnitude of the denominator in Eq. 25 and thus, the operating cost proxy is high.

The results also illustrates some trade-off relationships between productivity and conversion and productivity and excess solvent ratio. The highest productivity is achieved when conversion is low and excess solvent ratio is high; conversely, the lowest productivity is when conversion is high and excess solvent ratio is low. This observation can be explained by individually evaluating the relationship between productivity and excess solvent ratio and productivity and conversion, which is discussed below.

In Figure 29A, we observe a direct relationship between productivity and excess solvent ratio while the conversion is held constant. In other words, the productivity decreases, often only slightly, with decreasing excess solvent ratio. This observation is true because with a lower excess solvent ratio, there is more downstream recycling of unreacted reactants; thus, requiring less external additions through the *Fresh Desorbent* and *Fresh Feed* streams (Figure 26). Less flow input into the overall process will result in lower outlet flows, which directly affects the productivity. Additionally, from the slopes of the curves, the effects of excess solvent ratio on productivity are more pronounced at lower conversions. The figure also reveals that to recycle the product stream entirely (excess solvent ratio close to one), single pass conversion needs to be very high (> 95%).

In Figure 29B, we observe an inverse relationship between productivity and conversion while the excess solvent ratio is held constant. As the conversion increases, productivity decreases. The slopes of each curve also change with different conversion; the slopes become steeper at the higher excess solvent ratios. This behavior was described for an isolated SMBR operation [24], and holds true in an overall process. This trade-off exists because to achieve a higher conversion, the fluid velocity must decrease to accommodate the longer residence time needed to achieve the higher conversion. A lower velocity results in a lower throughput and productivity.

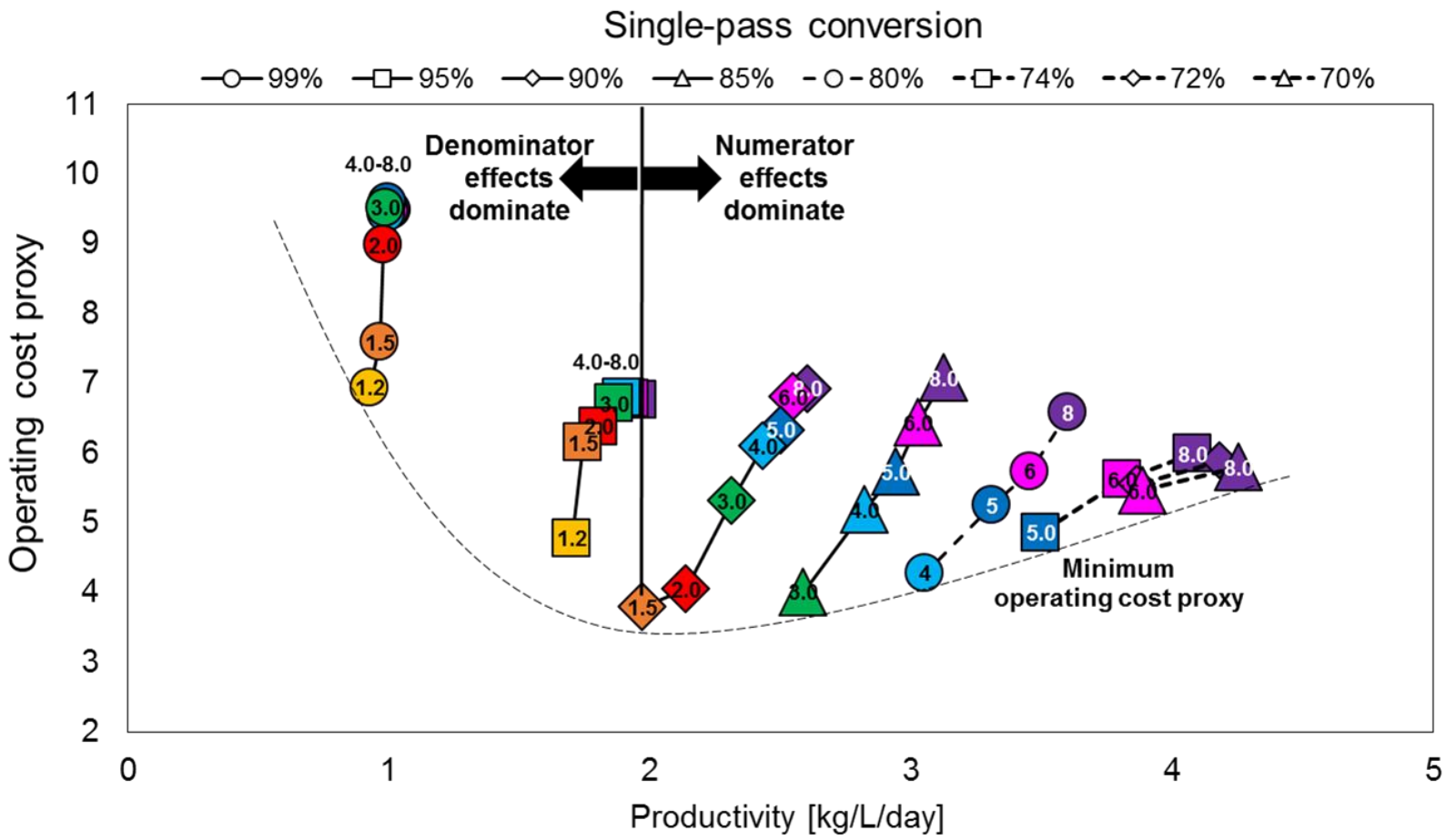

Figure 28 Results for the standard configuration. The operating cost proxy is plotted against the corresponding productivity. Each set of lines represent a specific single-pass conversion and within a given conversion, each point corresponds to an excess solvent ratio.

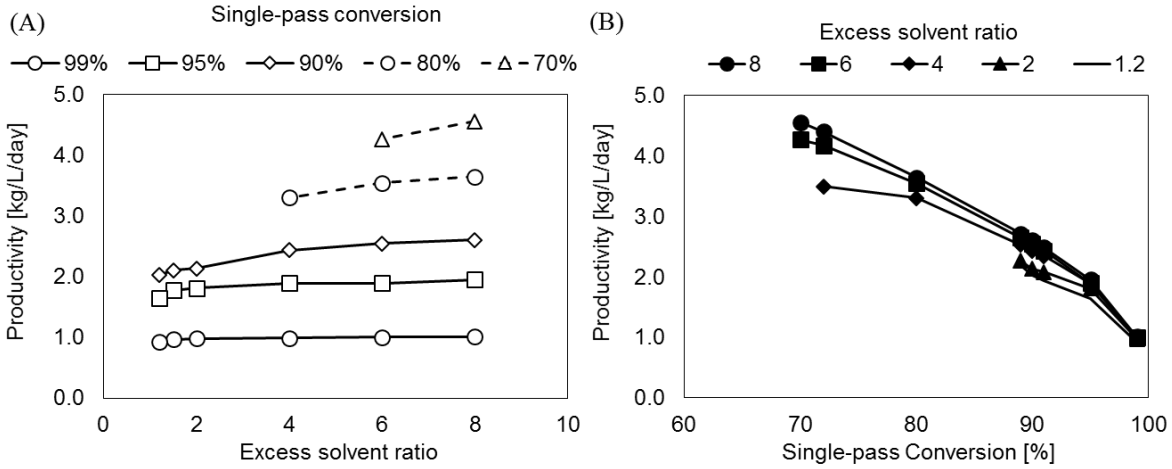

Figure 29 (A) Relationship between productivity and excess solvent ratio (B) Relationship between productivity and conversion.

The performance of the limited superstructure (Figure 27B) is evaluated using the same optimization formulation (Section 4.6) as the standard configuration. The observed trade-off relationships between productivity and conversion and between productivity and excess solvent ratio also apply to the limited superstructure configuration (Figure 30). Additionally, the same trend between operating cost proxy and productivity in the standard configuration is observed. The condition with the minimum operating cost proxy is at 90% single-pass conversion and an excess solvent ratio of 1.2. The productivity corresponding to that point is 2.02 kg/L/day.

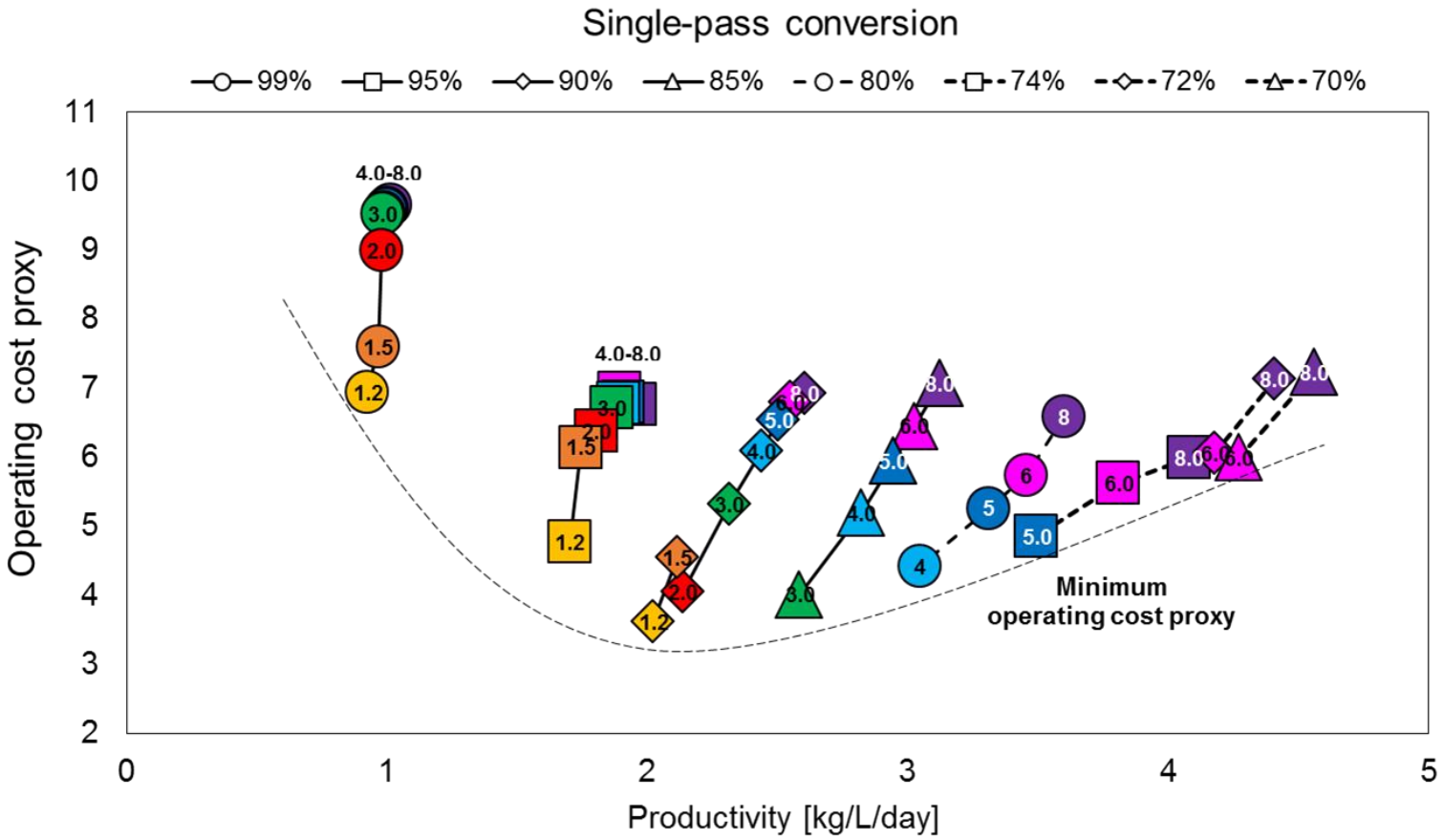

Figure 30 Results for the limited superstructure configuration. The operating cost proxy is plotted against the corresponding productivity. Each set of lines represent a specific single-pass conversion and within a given conversion, each point corresponds to an excess solvent ratio.

7.4.3 Comparison of performance among configurations

7.4.3.1 Evaluation of limited superstructure and standard configuration

The performances of the limited superstructure and the standard configuration are compared using the calculation of the ratios (Eq. 26 and 27). The productivity of the overall process between the two configurations are identical for all conditions examined except at 70% and 72% conversions. In Figure 31, the productivity and operating cost proxy ratios are plotted. There is a productivity advantage in the limited superstructure compared to the standard configuration. This productivity advantage occurs at extreme operating conditions, low conversions and high excess solvent ratios. As described in Figure 29, at these conditions, the trade-off effects between conversion, excess solvent ratio, and productivity are most pronounced (steeper slopes) and thus the superstructure's ability to mitigate these trade-offs is noticeable. The results also reveal that at a given conversion, the lower excess solvent ratio results in a greater productivity advantage for the limited superstructure over the standard configuration. Specifically for 70% conversion, excess solvent ratio of 6 has a higher productivity ratio and lower operating cost proxy ratio than compared to that at excess solvent ratio of 8. This behavior also extends to 72% conversion.

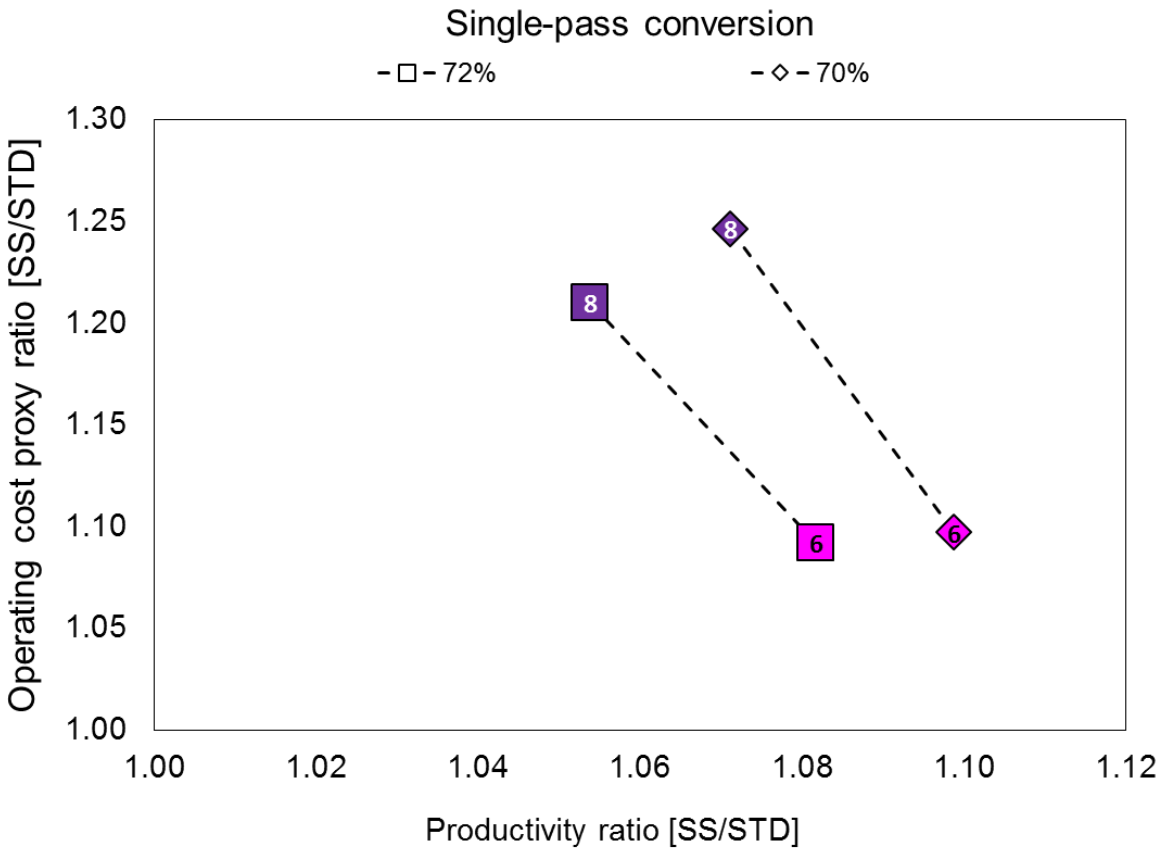

Figure 31 Comparison of the productivity and operating cost proxy ratios between limited superstructure and standard configurations at 70% and 72% conversion.

The condition at 70% conversion and an excess solvent ratio of 6 (Figure 32) is further analyzed because there is a productivity advantage for the limited superstructure configuration. There is a 9.8% productivity advantage in the limited superstructure over the standard configuration and a 9.5% increase in the operating cost proxy (Table 15). This suggests that the slight advantage in the superstructure configuration can be directly accounted by the increase in fresh desorbent and feed flow rate into the process. Specifically, the limited superstructure configuration (Figure 33B) has an approximate 9.5% increase in total flow rate than the standard configuration (Figure 33A).

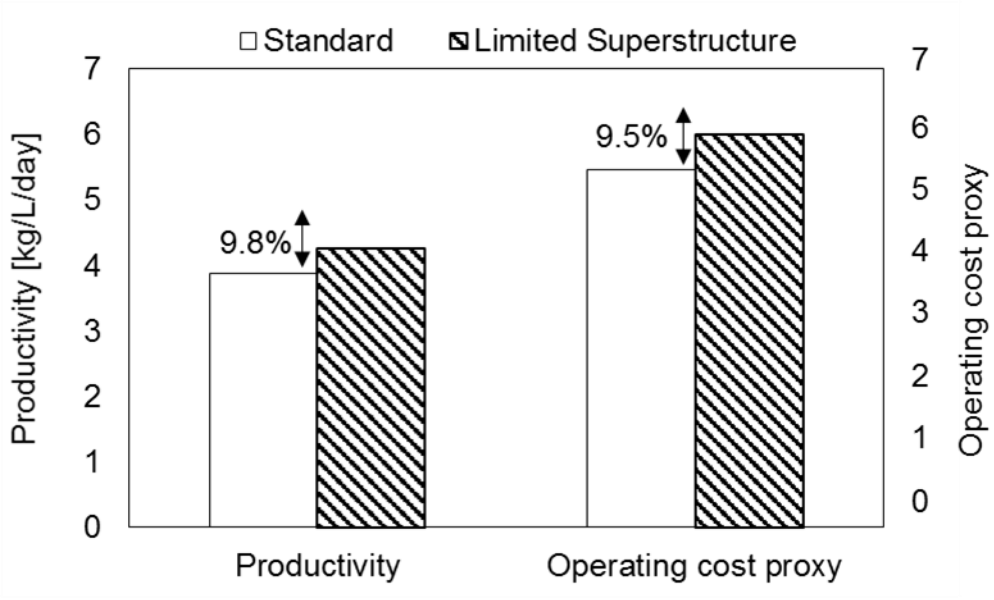

Figure 32 Comparisons for productivity and operating cost proxy for the 70% conversion and excess solvent ratio of 6.

Table 15 Summary of fresh flow into the overall process for the standard and limited superstructure configurations in Figure 32.

	Standard	**Limited Superstructure**
Fresh desorbent flow [m/hr]	1.405	1.571
Fresh feed flow [m/hr]	0.221	0.209
Total fresh flow in [m/h]	1.626	1.780

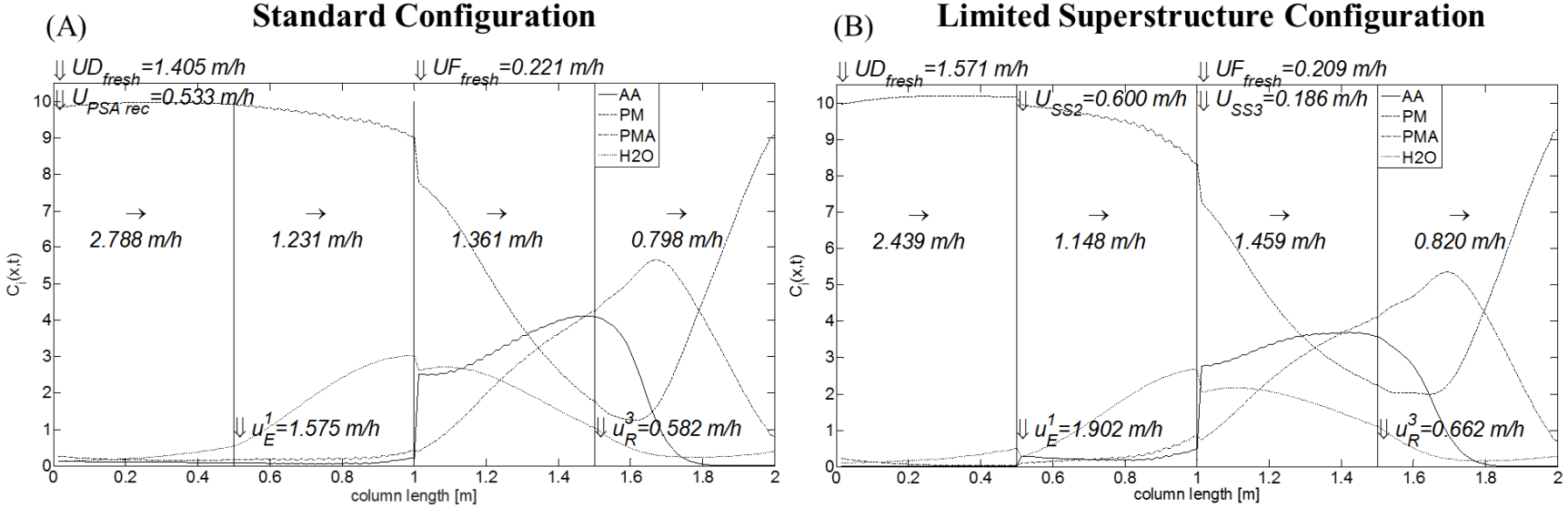

Figure 33 Internal concentration profile at the end of switch time corresponding to 70% conversion and excess solvent ratio of 6 for the (A) standard and (B) limited superstructure configuration.

7.4.3.2 Evaluation of full superstructure

We further explored the possibility of productivity enhancement for the full superstructure (Figure 27C). In the full superstructure, the feed, extract and raffinate streams are no longer fixed to a single inlet or outlet; instead, the locations of the streams are free and the optimal location and flow rate is determined by the optimizer. The problem formulation remains the same as that described in Section 4.6, in that we only optimize for the productivity of PMA and we only evaluate the operating cost proxy value. Figure 34 summarizes the configuration results from three different conditions, 99%, 95%, and 90% conversions for the excess solvent ratio of 1.2. The productivity (Figure 34A) is the highest for the full superstructure configuration at all three conversions. It can also be seen that the productivity increase by the full superstructure is achieved without a large increase in the operating cost proxy (Figure 34B).

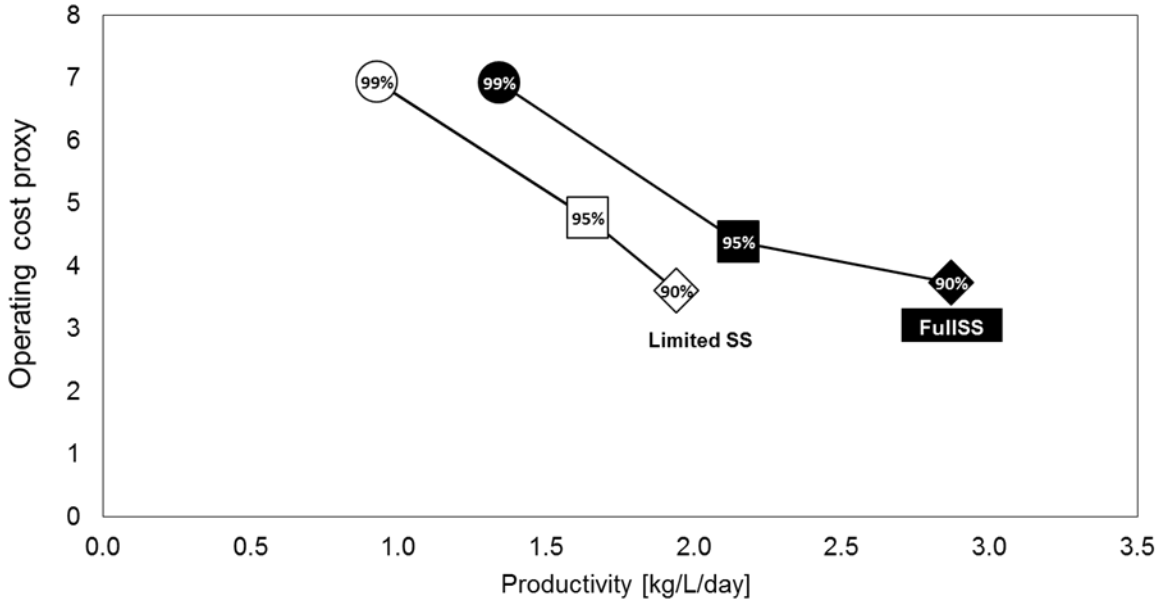

Figure 34 Comparison of operating cost proxy to productivity for the limited and full superstructure configurations.

The internal concentration profiles in Figure 35 explain why there is a productivity advantage in the full superstructure configuration (Figure 27C). The major difference between the full and the limited superstructure are that the full superstructure has different flow rate configurations, higher flow rates into the SMBR, and the reaction zone in column III extends into column IV.

For 99% conversion (Figure 35A and B), there are higher fresh feed and downstream recycle (U_{SS1}) flow rates into the SMBR. The higher flow rate into column III directly increases the amount of acetic acid fed and the raffinate flow rate (U_R^3). Subsequently, more PMA is produced and can be collected. The flow rate through column IV allows collection of an additional extract outlet (U_{Ex}^4). The internal recycle (from column 4 to column 1) of the SMBR is low (< 0.03 m/h), which resembles a 4-column packed bed instead of a standard SMBR operation.

For 95% conversion, (Figure 35C and D), a very similar behavior can be observed. The only difference is instead of an additional extract stream at the outlet of column IV, there is an additional raffinate stream (U_R^4). Raffinate is collected at the end of column IV because the PMA concentration is higher while the water content is lower, satisfying the process constraints for PMA recovery and water content in the raffinate stream (Eq. 6-8). The internal recycle flow rate of the SMBR is higher than that of the 99% conversion case (~ 0.30 m/h) making this operation resemble that of a standard SMBR operation.

Finally, for 90% conversion (Figure 35E and F), there is significantly higher fresh desorbent (U_D^1), feed (U_F^3), and downstream recycle (U_{SS1}, U_{SS2}, U_{SS3}) in the full superstructure compared to the limited superstructure configuration. The additional downstream recycle into column II (U_{SS2}) allows the collection of the additional raffinate outlet from column IV (U_R^4), increasing the productivity. The internal recycle flow rate of the SMBR is also higher than that of the 99% conversion case (~ 0.10 m/h) and this operation also resembles that of a standard SMBR operation.

The trade-off for the gain in productivity is the increased flow rate values of the downstream recycle (*SS*) streams for the full superstructure, and the need for additional pumps and valves to operate the different configurations.

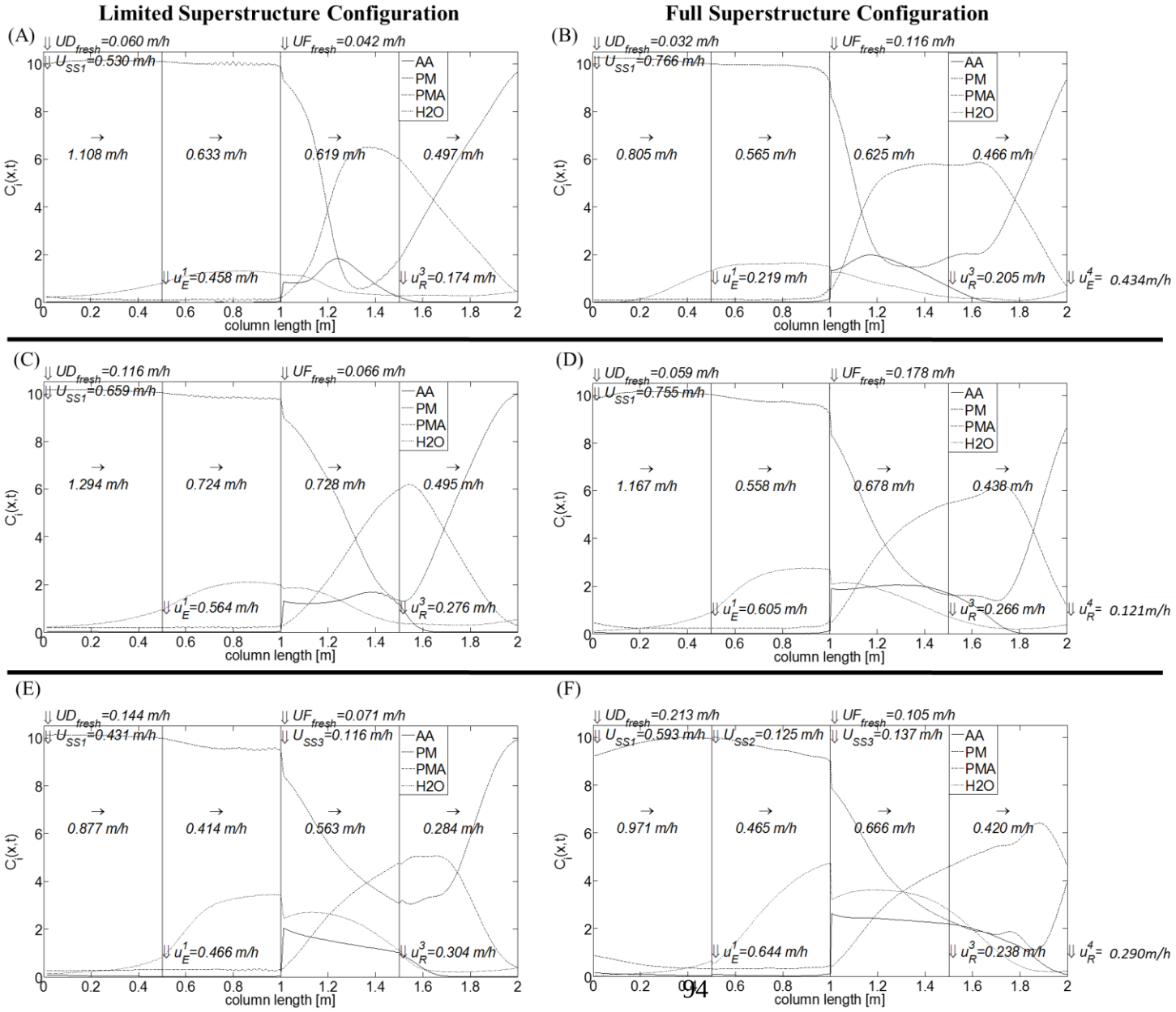
Limited Superstructure Configuration
Full Superstructure Configuration
(A)
(B)
(C)
(D)
(E)
(F)
AA
PM
PMA
H2O
column length [m]
C_i(x,t)
1.108 m/h
0.633 m/h
0.619 m/h
0.497 m/h
0.805 m/h
0.565 m/h
0.625 m/h
0.466 m/h
1.294 m/h
0.724 m/h
0.728 m/h
0.495 m/h
1.167 m/h
0.558 m/h
0.678 m/h
0.438 m/h
0.877 m/h
0.414 m/h
0.563 m/h
0.284 m/h
0.971 m/h
0.465 m/h
0.666 m/h
0.420 m/h

Figure 35 Internal concentration profiles at the end of switch time for the limited superstructure and full superstructure configuration. The left side shows the limited superstructure configuration and the right side is the full superstructure configuration. (A) and (B) are at 99% conversion, (C) and (D) are at 95% conversion, and (E) and (F) are at 90% conversion.

7.5 Conclusions

We developed a model of an overall process that examined the operation of an integrated SMBR along with two downstream processing units. Utilizing a modified version of an SMBR model developed from previous work [24], the process was optimized to determine the optimal operating conditions for the SMBR in the combined SMBR-downstream processing configuration. Three distinct process configurations were considered that increases with the degree of freedom: standard SMBR operation, limited superstructure, and full superstructure.

For each of the different configurations, the solution space is examined for maximum productivity while targeting specific product recovery, byproduct content, and purity while evaluating different conversions and excess solvent ratios. This evaluation elucidated the different trade-off relationships between the objective function and the system constraints; specifically, there is an inverse relationship between productivity and conversion and a direct relationship between productivity and excess solvent ratio. These relationships allow for the heuristic that if only high productivity is desired, operate at low conversions and high excess solvent ratios. However, within the context of operating a large process, an important consideration in addition to productivity is the cost to achieve the productivity. This cost is evaluated indirectly by selecting an indicator variable that is representative of the operating cost. To represent this cost approximately, the flow rate of the *PSA in* stream is used because it is the amount processed by the distillation column and the hot gas PSA. The operating cost proxy is evaluated to gain some insight into the solution space of the lowest operating cost. From this analysis, the relationship between operating cost proxy, productivity, conversion, and excess solvent ratio is determined. The

condition that minimizes the operating cost proxy at any given conversion is at the lowest excess solvent ratio. Additionally, there is a minimum when comparing the operating cost proxy against productivity of the conditions examined; the minimum operating cost occurs at 90% conversion and the lowest excess solvent ratio for the standard configuration and limited superstructure configuration.

Productivity and operating cost proxy is also compared between the different configurations. Comparing productivity between the limited superstructure and standard configurations reveal there is virtually no advantage in the limited superstructure except for at 70% and 72% conversion. Comparison between the limited superstructure and standard configuration for the operating cost proxy shows that there is no advantage in the limited superstructure performance. Comparison of the full superstructure to the other two configurations demonstrates an advantage of the full superstructure for both productivity and operating cost proxy at 95% conversion and 1.2 excess solvent ratio.

Our analysis of the operating cost proxy is not a direct cost analysis. The *PSA in* stream is assumed to be a surrogate indicator for the operating costs, but the only true and accurate manner for determining operating cost is to explicitly calculate for that term. Indeed, a future direction of this work is to formulate the optimization to consider operating cost by defining an objective function as the PMA productivity per cost of plant operation.

CHAPTER 8. CONCLUSIONS AND FUTURE WORK

8.1 Conclusions

The results presented in this thesis achieved the three main objectives outlined in CHAPTER 2:

1. Optimize the SMBR operation for the esterification route of PMA production using a mode-based framework
2. Determine if the model-based framework can be applied to the transesterification route of PMA production and compare the optimized operation between the two reaction routes
3. Optimize an overall process for the esterification route of PMA production

The first objective is discussed in CHAPTER 5 in which the model-based framework, also known as simultaneous optimization and model correction (SOMC) is introduced for the optimization of the SMBR operation for the esterification route of PMA production. This is the first time SMBR has been applied to the production of glycol ether esters. Starting from an SMBR model with model parameters obtained from simple kinetic and single column experiments, the optimization formulation allowed for the determination of the operating conditions of the SMBR. By performing only a few of these SMBR experiments at different operating conditions, samples were collected for both the raffinate and extract at every step in cycles 7 and 8 (total of 16 samples for each experiment) for the determination of experimental concentrations. A least-square minimization is performed using the experimental and model predicted concentration values to recalculate for the SMBR model parameters. After one round of model correction, model mismatch,

calculated as the sum of squared difference of concentration, is reduced by almost two orders of magnitude. The accuracy of the *corrected model* is validated at a new experimental condition. The *corrected model* can be re-optimized with new production specifications and it can be used to determine the corresponding optimal operating conditions to run the SMBR.

This work demonstrates that PMA can be successfully produced through SMBR. This model-based approach shows that without any model correction and using a model based on only batch experiments, the initial model can give good predictions of experimental outcomes. Additionally, it shows that with only minimal SMBR experiments, a much more accurate model can be achieved that can be a useful tool for guiding design and operating decisions for SMBR.

The second objective is described in CHAPTER 6, in which the SOMC approach is applied to the transesterification route of SMBR production. Due to the absence of previous work evaluating the transesterification in a SMBR operation outside of biodiesel production, much work was conducted to evaluate and select a suitable resin [17]. DOWEX^{TM} 22 resin used for the transesterification was selected from the resin screening. The process development approach for this reaction route is very similar to the one used for the esterification route. The objective function for the model correction allows for calculating new model parameters that effectively removed any observable model mismatch. More impressively, the model mismatch for the validation experiment shows almost perfect model predictions for the experiments. Furthermore, the model is able to accurately predict the two objectives, PMA production and conversion, as well as the PM

to PMA ratio. These results also confirmed that the model-based approach can be generalized to different chemistries and that it is robust and flexible.

The results from the esterification and transesterification enabled a direct comparison of the two reaction routes. At a given conversion, the esterification route achieved higher production/productivity and lower PM to PMA ratio. Both routes had comparable product stream recovery and byproduct content. The key difference in the two are azeotrope formation, sensitivity to water, and catalyst stability. The esterification route forms water as the byproduct and will need additional downstream processing to handle the azeotropes in the process. The transesterification route is extremely sensitive to water and requires extreme care in eliminating any water from the system. One approach was the addition of molecular 3Å to all feed and desorbent bottles. Another potential water mitigation strategy may be installing a guard column, packed with molecular 3Å, inline to the recycle line to absorb water in the system. Finally, the potential deactivation of the DOWEX^{TM} 22 catalyst may pose a challenge to SMBR operation. Future work will discuss some potential strategies to maintain catalyst activity for the transesterification route.

The final objective is described in CHAPTER 7, which explores the SMBR operation within an overall process. This is evaluated for the esterification pathway. There are two downstream units, a distillation column to further purify the product stream and a hot gas PSA to remove any water produced from the reaction and recycle nearly pure PM to the SMBR. The evaluation of an overall process can be conducted in many different ways depending on what performance indicators are considered. This work attempts to systematically evaluate the operation of an overall process by exploring the operating space around some key performance indicators and for different configurations. Productivity and

operating cost are evaluated against changes in conversion and solvent consumption (excess solvent ratio). Productivity increases as conversion decreases and as solvent consumption increases. Operating costs are the lowest along the boundary of feasible and infeasible solution space; this boundary is also the Pareto front between conversion and excess solvent ratio. Additionally, three different configurations of the SMBR unit are evaluated: standard, limited superstructure, and full superstructure. These results show that productivity increases with increasing degrees of freedom in the configuration, with the standard being the lowest and the full superstructure the highest. When the operating cost proxy is considered, the full superstructure is able to achieve the highest productivity without causing an increase in the operating cost proxy.

8.2 Future work

Completion of this thesis project has opened up questions and opportunities that may be explored and studied in future projects.

8.2.1 Refinement of the SMBR model

There remains limitations to the proposed method of model correction and parameter estimation. A systematic decision making process can be implemented like the ones found in other similar studies. For example, potential model modifications can be ranked based on order of simplicity and their potential impact on reducing the value of the objective function (Eq. 14) in parameter estimation.

The model equations used to describe the SMBR operations are often chosen based on considerations for modeling simplicity and predictive accuracy for experiments. Specifically, the equations describing the kinetic and adsorption behaviors were the

simplest equations that resulted in low model mismatch. Oh *et al.* [16] analyzed three different reaction mechanisms: Langmuir-Hinshelwood, Eley-Rideal, and the pseudo-homogenous models. The authors evaluated all potential equations for the esterification route and chose the pseudo-homogenous model considering the balance between model complexity and fitting. Future work can be to systematically evaluate the different kinetic models for the transesterification route to ensure that the pseudo-homogenous model remains the best choice. Similarly to kinetics, the simplest adsorption isotherm models are chosen due their relative simplicity. A linear isotherm is used for all components in the esterification and transesterification routes and only PMA and ethanol are modelled by a Langmuir isotherm. The linear isotherm is valid if the system is dilute, but with higher concentrations of components or overloading of the column, the linear isotherm assumption is no longer valid. Indeed, even the Langmuir isotherm used for the transesterification may not be sufficient at undiluted conditions because it is only a single-component model. Considerations for multi-component Langmuir and competitive isotherms may need to be explored for more fundamentally accurate models.

Furthermore, we demonstrated that an improved model can be obtained from a single iteration of model correction. This parameter correction step can be applied iteratively (Figure 36) that allows for the iterative calculation of the optimal SMBR operating conditions while carrying out model correction concurrently within a single framework [29, 37]. The major consideration for this scheme is defining an appropriate "termination criterion" (Step IV). This must be defined in order to determine when the iterative process can terminate and the corrected model is accepted. A good criterion requires both understanding of the system dynamics and some trial-and-error. This strategy

can be employed in the future to check the convergence of model parameters and make further improvements in the model fitting.

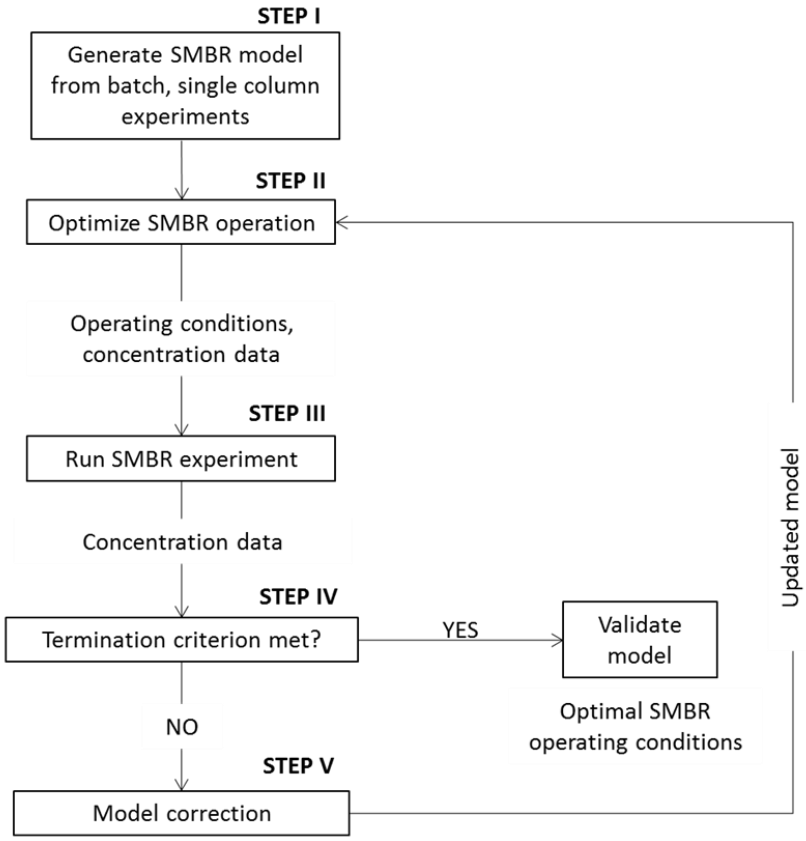

Figure 36 Iterative simultaneous optimization and model correction.

8.2.2 Model predictive control

In real processes, there are often process disturbances, either measured—equipment or physical properties of the system (flow rates, bed void volume, feed and desorbent concentrations etc.), unmeasured, or model errors. These disturbances require real-time and appropriate control inputs by the system in order to maintain the desired operation. Traditionally, process controls have been executed through PID controllers, but a more advanced method is through model predictive controllers. In this scheme, the controllers

depend on dynamic models of the process and is able to use those model to predict future events and take corrective action.

To successfully correct for perturbations in the process in a timely manner requires a system for detecting the current state (flow rates, pressure, temperature, concentration, etc.), a dynamic model, a computational system that can rapidly and accurately solve for transient profiles, optimal operations, and recalculated model parameters, and a responsive and effective control system to implement the corrective action. Currently, the model predictive controls combines process control to the SOMC method; the controller is capable of changing the operational setpoints and of continually optimizing and performing model correction.

There are some examples of model-predictive control for non-reactive SMB operations. Klatt *et al.* [74] developed a two-layer control architecture in which the optimal operating trajectory was calculated off-line and new model parameters were also calculated from online measurements. A model identification scheme identified simplified local linear models that when used in combination with local controllers could maintain the process along the desired trajectory. Neto *et al.* [75] presented a nonlinear model predictive control (NMPC) for a SMB process that optimized the separation of enantiomers while maintaining purities in the outlet streams. Their proposed control system was able to perform online corrective strategies in response to instrument malfunction and plant-model mismatch. Such work that combines modeling, simulation, optimization, and control strategies will prove to be extremely invaluable to SMBR operations.

The new control scheme will also need an optimization software that can calculate for transient states and not just cyclic steady states. AMPL for instance, is limited to

calculations for non-transient systems. Thus, a software that can handle a transient system, uses real-time concentration data, and perform calculations quickly will be necessary for the successful implementation of model predictive control.

8.2.3 Alternative SMBR operations

Different modes of SMBR operations have been developed that have shown enhanced performance. Some examples include: MultiFeed [76] examines multiple feed inlets; ModiCon [77] operation allows for control of the feed concentration; Varicol [9] allows for asynchronous switching of inlet and outlet positions; powerfeed [78] changes the inlet/outlet flow rates; and partial-feed and partial-withdrawal/discard [79] operations vary the feed and raffinate flow rates over time. Evaluation of the ModiCon operation has been conducted by Agrawal *et al.* [80] for the esterification route. Their modeling work showed that step inputs of feed increases the production rate as well as product purity and recovery. Additionally, he shows that less reactant is needed for the process because of the non-constant feed flow rate. Varicol allows for a more flexible use of different lengths for each zone of the SMBR. This method has shown up to 30% improvements in productivity for a given purity requirement. Powerfeed have shown similar operation advantages to that of Varicol but allows the external flow rates to change, which subsequently changes the internal flows.

8.2.4 Tuning separation and reaction separately

One of the major challenges in operating SMBR for new chemistries is selecting an appropriate resin that is capable of both separation and reaction. In the past, the approach was to mix two or more solid material within a column such that one serves mainly as the

adsorbent and the other acts as the catalyst [81]. This method fell out of favor once novel resins were developed that are capable of both reaction and separation. This was due to the fact that homogeneity of the mixed bed was difficult to achieve as well as the potential for differences in bed volume swelling and shrinking among the mixed resin materials. An alternative to this is to decouple the catalyst and adsorbent from being the same material. Instead, select a resin as the adsorbent and use a homogenous catalyst. Oh [17] demonstrated this method for the transesterification route for a single reactive chromatography column. An anion exchange resin is selected as the adsorbent while PM alkoxide is used as the catalyst. This operation can be implemented for the SMBR system.

8.2.5 Anion exchange resin development

An important factor to the success of any SMBR operation is selection of the appropriate stationary phase. The ideal resin must have low swelling ratios to different solvents, good catalytic stability and activity, and good selectivity between the product and byproduct. Designing a resin with these properties is challenging since it requires a quantitative model and understanding of how the adsorptive and catalytic properties are determined by the resin's chemical and physical properties. If such developments are made possible, design and optimization of SMBR operations can be faster and easier as it can alleviate the time and resource burden from the resin screening.

8.2.6 Overall process optimization

A new objective formulation for the overall process optimization is proposed for further study—maximize the productivity of PMA by the cost. This new objective can allow for better evaluation of optimal operating conditions. A part of this analysis will

require development of more detailed capital and operating cost models (Figure 37) for all units of operation that will include more rigorous evaluation of equipment (vessels, compressors, valves, piping), variable costs (raw material, consumables, utility, waste disposal/treatment), and fixed costs (rent, employee). These cost models will also enable a techno-economic assessment to evaluate the feasibility of the project, investigate cash flows over the plant's lifetime, evaluate the likelihood of other technologies, and compare economics of different technologies in producing PMA. Finally, to conclude the comparison of the two routes of producing PMA, optimization of the overall process should also be evaluated for the transesterification route.

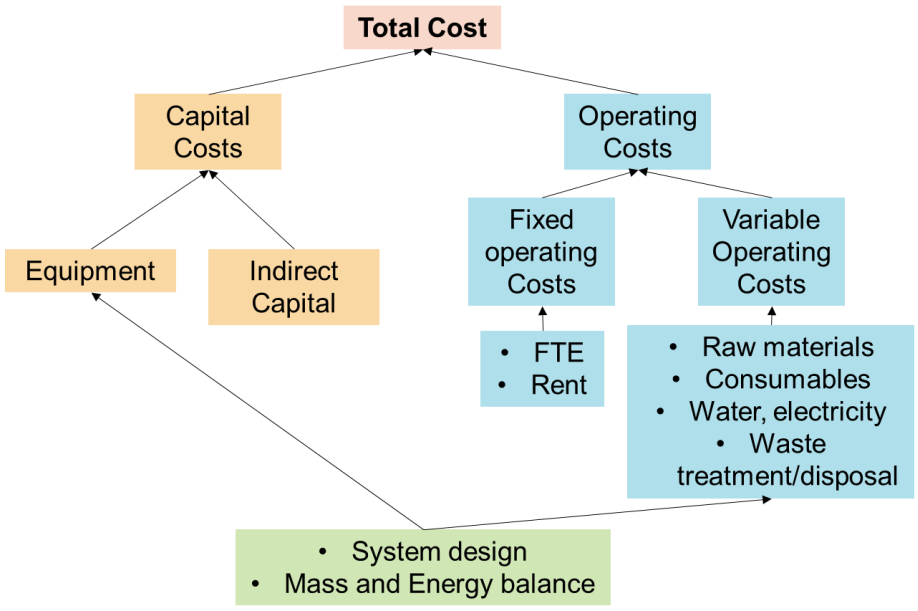

Figure 37 Cost considerations for a techno-economic analysis of the overall flowsheet.

REFERENCES

[1] A.I. Stankiewicz, J.A. Moulijn, Process intensification: transforming chemical engineering, Chemical Engineering Progress 96 (2000) 22-34.

[2] E. Borges da Silva, I. Pedruzzi, A. Rodrigues, Simulated moving bed technology to improve the yield of the biotechnological production of lactobionic acid and sorbitol, Adsorption 17 (2011) 145-158.

[3] A. Seidel-Morgenstern, L.C. Keßler, M. Kaspereit, New Developments in Simulated Moving Bed Chromatography, Chemical Engineering & Technology 31 (2008) 826-837.

[4] D.C.S. Azevedo, A.r.E. Rodrigues, Design methodology and operation of a simulated moving bed reactor for the inversion of sucrose and glucose–fructose separation, Chemical Engineering Journal 82 (2001) 95-107.

[5] A. Toumi, S. Engell, Optimization-based control of a reactive simulated moving bed process for glucose isomerization, Chemical Engineering Science 59 (2004) 3777-3792.

[6] A.K. Ray, R.W. Carr, Experimental study of a laboratory-scale simulated countercurrent moving bed chromatographic reactor, Chemical Engineering Science 50 (1995) 2195-2202.

[7] W. Yu, K. Hidajat, A.K. Ray, Optimization of reactive simulated moving bed and Varicol systems for hydrolysis of methyl acetate, Chemical Engineering Journal 112 (2005) 57-72.

[8] M. Minceva, Gomes, P. Sá, Meshko, V., Rodrigues, A. E., Simulated moving bed reactor for isomerization and separation of p-xylene, Chemical Engineering Journal 140 (2008) 305-323.

[9] H.J. Subramani, Hidajat, K., Ray, A. K., Optimization of Simulated Moving Bed and Varicol Processes for Glucose–Fructose Separation, Chemical Engineering Research and Design 81 (2003) 549-567.

[10] F. Lode, Francesconi, G., Mazzotti, M., Morbidelli, M., Synthesis of methylacetate in a simulated moving-bed reactor: Experiments and modeling, AIChE Journal 49 (2003) 1516-1524.

[11] W. Yu, Hidajat, K., Ray, A. K., Modeling, Simulation, and Experimental Study of a Simulated Moving Bed Reactor for the Synthesis of Methyl Acetate Ester, Industrial & Engineering Chemistry Research 42 (2003) 6743-6754.

[12] G. Dünnebier, Fricke, J., Klatt, K-U., Optimal Design and Operation of Simulated Moving Bed Chromatographic Reactors, Industrial & Engineering Chemistry Research 39 (2000) 2290-2304.

[13] M. Kawase, Suzuki, T. B., Inoue, K., Yoshimoto, K., Hashimoto, K., Increased esterification conversion by application of the simulated moving-bed reactor, Chemical Engineering Science 51 (1996) 2971-2976.

[14] C. Migliorini, Fillinger, M., Mazzotti, M., Morbidelli, M., Analysis of simulated moving-bed reactors, Chemical Engineering Science 54 (1999) 2475-2480.

[15] G. Agrawal, Oh, J., Sreedhar, B., Tie, S., Donaldson, M. E., Frank, T. C., Schultz, A. K., Bommarius, A. S., Kawajiri, Y., Optimization of reactive simulated moving bed systems with modulation of feed concentration for production of glycol ether ester, Journal of Chromatography A 1360 (2014) 196-208.

[16] J. Oh, Agrawal, G., Sreedhar, B., Donaldson, M. E., Schultz, A. K., Frank, T. C., Bommarius, A. S., Kawajiri, Y., Conversion improvement for catalytic synthesis of propylene glycol methyl ether acetate by reactive chromatography: Experiments and parameter estimation, Chemical Engineering Journal 259 (2015) 397-409.

[17] J. Oh, Development of reactive chromatography system for equilibrium-limited reactions, Chemical and Biomolecular Engineering, Georgia Institute of Technology, Atlanta, GA, 2016, pp. 158.

[18] J. Oh, B. Sreedhar, M.E. Donaldson, T.C. Frank, A.K. Schultz, A.S. Bommarius, Y. Kawajiri, Transesterification of propylene glycol methyl ether in chromatographic reactors using anion exchange resin as a catalyst, Journal of Chromatography A 1466 (2016) 84-95.

[19] The Dow Chemical Company, Product Safety Assessment: Propylene Glycol Methyl Ether Acetate The Dow Chemical Company, Midland, MI, 2008.

[20] S.H. Johnson, H.N. Wright, Process for the manufacture of glycol ether acetates, U.S. Patent S3700726A, 24 Oct. 1972.

[21] N. Kametaka, K. Marumo, K. Tokuda, K. Sekiguchi, Process for the continuous production of ethylene glycol monoethyl ether acetate, U.S. Patent 4260813A, 7 Apr. 1981.

[22] Rohm and Haas, Amberlyst 15 Industrial Grade Strongly Acidic Catalyst for Catalysis and Separation technologies, in: R.a. Haas (Ed.)Philadelphia, USA, 2003.

[23] The Dow Chemical Company, DOWEX 22 Ion Exchange Resin for Sweetener Applications, The Dow Chemical Company, Midland, MI, 2017.

[24] S. Tie, B. Sreedhar, G. Agrawal, J. Oh, M.E. Donaldson, T.C. Frank, A.K. Schultz, A.S. Bommarius, Y. Kawajiri, Model-based design and experimental validation of

simulated moving bed reactor for production of glycol ether ester, Chemical Engineering Journal 301 (2016) 188-199.

[25] Y. Kawajiri, L.T. Biegler, Nonlinear Programming Superstructure for Optimal Dynamic Operations of Simulated Moving Bed Processes, Industrial & Engineering Chemistry Research 45 (2006) 8503-8513.

[26] R. Fourer, Gay, D.M., Kernighan, W., MPL. A Modeling Language for Mathematical Programming, Brooks/Cole Publishing Company, CA, 2002.

[27] A. Wächter, Biegler, L. T., On the implementation of an interior-point filter line-search algorithm for large-scale nonlinear programming, Math. Program. 106 (2006) 25-57.

[28] A. Tikhonov, Goncharsky, A., Stepanov, V., Yagola, A., Numerical Methods for the Solution of Ill-Posed Problems, Kluwer Academic Publishers, Boston, 1995.

[29] B. Sreedhar, Y. Kawajiri, Multi-column chromatographic process development using simulated moving bed superstructure and simultaneous optimization – Model correction framework, Chemical Engineering Science 116 (2014) 428-441.

[30] M. Canonge, J.C. Joly, Process for the continuous preparation of acetates, U.S. Patent 4960927, 2 Oct. 1990.

[31] J. Jeong, H. Jeon, K.-m. Ko, B. Chung, G.-W. Choi, Production of anhydrous ethanol using various PSA (Pressure Swing Adsorption) processes in pilot plant, Renewable Energy 42 (2012) 41-45.

[32] S. Al-Asheh, F. Banat, N. Al-Lagtah, Separation of Ethanol–Water Mixtures Using Molecular Sieves and Biobased Adsorbents, Chemical Engineering Research and Design 82 (2004) 855-864.

[33] W. Yu, K. Hidajat, A.K. Ray, Determination of adsorption and kinetic parameters for methyl acetate esterification and hydrolysis reaction catalyzed by Amberlyst 15, Applied Catalysis A: General 260 (2004) 191-205.

[34] D. Gelosa, M. Ramaioli, G. Valente, M. Morbidelli, Chromatographic Reactors: Esterification of Glycerol with Acetic Acid Using Acidic Polymeric Resins, Industrial & Engineering Chemistry Research 42 (2003) 6536-6544.

[35] M. Mazzotti, B. Neri, D. Gelosa, M. Morbidelli, Dynamics of a Chromatographic Reactor: Esterification Catalyzed by Acidic Resins, Industrial & Engineering Chemistry Research 36 (1997) 3163-3172.

[36] P.C. Hansen, D.P. O'Leary, The Use of the L-Curve in the Regularization of Discrete Ill-Posed Problems, SIAM Journal on Scientific Computing 14 (1993) 1487-1503.

[37] J. Bentley, Sloan, C., Kawajiri, Y., Simultaneous modeling and optimization of nonlinear simulated moving bed chromatography by the prediction–correction method, Journal of Chromatography A 1280 (2013) 51-63.

[38] H. Schmidt-Traub, M. Schulte, A. Seidel-Morgenstern, Preparative Chromatography, Wiley2012.

[39] Sigma-Aldrich, Amberlite and Amberlyst Resins- Technical Information Bulletin, www.sigmaaldrich.com/chemistry/chemical-synthesis/learning-center/technical-bulletins/al-142/amberlite-amberlyst.html, 2015.

[40] V.M.T.M. Silva, A.E. Rodrigues, Novel process for diethylacetal synthesis, AIChE Journal 51 (2005) 2752-2768.

[41] J.M. Prausnitz, R.N. Lichtenthaler, E.G. de Azevedo, Molecular Thermodynamics of Fluid-Phase Equilibria, Pearson Education1998.

[42] A. Pal, S. Sharma, Y.P. Singh, Excess Molar Volumes of Binary Liquid Mixtures of 1-Propanol and of 2-Propanol + Propane-1,2-diol, 1-Methoxy-2-propanol, 1-Ethoxy-2-propanol, and 1-tert-Butoxy-2-propanol and Water + 1-Methoxy-2-propanol and 1-Ethoxy-2-propanol at 298.15 K, Journal of Chemical & Engineering Data 42 (1997) 1157-1160.

[43] M.T. Martello, A. Burns, M. Hillmyer, Bulk Ring-Opening Transesterification Polymerization of the Renewable δ-Decalactone Using an Organocatalyst, ACS Macro Letters 1 (2012) 131-135.

[44] G.P. Karayannidis, D.S. Achilias, I.D. Sideridou, D.N. Bikiaris, Alkyd resins derived from glycolized waste poly(ethylene terephthalate), European Polymer Journal 41 (2005) 201-210.

[45] D. Darnoko, M. Cheryan, Kinetics of palm oil transesterification in a batch reactor, Journal of the American Oil Chemists' Society 77 (2000) 1263-1267.

[46] L.C. Meher, D. Vidya Sagar, S.N. Naik, Technical aspects of biodiesel production by transesterification—a review, Renewable and Sustainable Energy Reviews 10 (2006) 248-268.

[47] H. Fukuda, A. Kondo, H. Noda, Biodiesel fuel production by transesterification of oils, Journal of Bioscience and Bioengineering 92 (2001) 405-416.

[48] T. Pöpken, S. Steinigeweg, J. Gmehling, Synthesis and Hydrolysis of Methyl Acetate by Reactive Distillation Using Structured Catalytic Packings: Experiments and Simulation, Industrial & Engineering Chemistry Research 40 (2001) 1566-1574.

[49] S. Steinigeweg, J. Gmehling, Transesterification processes by combination of reactive distillation and pervaporation, Chemical Engineering and Processing: Process Intensification 43 (2004) 447-456.

[50] I. Noshadi, N.A.S. Amin, R.S. Parnas, Continuous production of biodiesel from waste cooking oil in a reactive distillation column catalyzed by solid heteropolyacid: Optimization using response surface methodology (RSM), Fuel 94 (2012) 156-164.

[51] S.H. Shuit, K.T. Lee, A.H. Kamaruddin, S. Yusup, Reactive extraction and in situ esterification of Jatropha curcas L. seeds for the production of biodiesel, Fuel 89 (2010) 527-530.

[52] R. Zakaria, A.P. Harvey, Direct production of biodiesel from rapeseed by reactive extraction/in situ transesterification, Fuel Processing Technology 102 (2012) 53-60.

[53] D. Geier, J.G. Soper, Simultaneous synthesis and purification of a fatty acid monoester biodiesel fuel, U.S. Patent 7828978B2, 9 Nov. 2010.

[54] T.C. Frank, M.E. Donaldson, Reactive chromatography process for equilibrium-limited reactions, U.S. Patent 9630890 B2, 25 April, 2017.

[55] C.T. Hsieh, M.J. Lee, H.-m. Lin, Multiphase Equilibria for Mixtures Containing Acetic Acid, Water, Propylene Glycol Monomethyl Ether, and Propylene Glycol Methyl Ether Acetate, Industrial & Engineering Chemistry Research 45 (2006) 2123-2130.

[56] B. He, Y. Ren, Y. Cheng, J. Li, Deactivation and in Situ Regeneration of Anion Exchange Resin in the Continuous Transesterification for Biodiesel Production, Energy & Fuels 26 (2012) 3897-3902.

[57] Y. Ren, B. He, F. Yan, H. Wang, Y. Cheng, L. Lin, Y. Feng, J. Li, Continuous biodiesel production in a fixed bed reactor packed with anion-exchange resin as heterogeneous catalyst, Bioresource Technology 113 (2012) 19-22.

[58] N. Shibasaki-Kitakawa, H. Honda, H. Kuribayashi, T. Toda, T. Fukumura, T. Yonemoto, Biodiesel production using anionic ion-exchange resin as heterogeneous catalyst, Bioresource Technology 98 (2007) 416-421.

[59] J. Oh, B. Sreedhar, M.E. Donaldson, T.C. Frank, A.K. Schultz, A.S. Bommarius, Y. Kawajiri, Transesterification of propylene glycol methyl by reactive simulated moving bed chromatography using homogeneous catalyst, Adsorption, (Submitted for publication).

[60] S. Tie, B. Sreedhar, M. Donaldson, T. Frank, Y. Kawajiri, A. Bommarius, Process Integration for Simulated Moving Bed Reactor for Production of Glycol Ether Acetate, Chemical Engineering Journal (Submitted for publication).

[61] D.S.M. Constantino, R.P.V. Faria, C.S.M. Pereira, J.M. Loureiro, A.E. Rodrigues, Enhanced Simulated Moving Bed Reactor Process for Butyl Acrylate Synthesis: Process Analysis and Optimization, Industrial & Engineering Chemistry Research 55 (2016) 10735-10743.

[62] J.W. Lee, Z. Horváth, A.G. O'Brien, P.H. Seeberger, A. Seidel-Morgenstern, Design and optimization of coupling a continuously operated reactor with simulated moving bed chromatography, Chemical Engineering Journal 251 (2014) 355-370.

[63] M.D. Moraru, A. Milea, C.S. Bîldea, Design and Economic Evaluation of a Process for n-Butyl Acrylate Production, UPB Sci. Bull, Series B 78 (2016) 113.

[64] C.J. Wang, D.S.H. Wong, I.L. Chien, R.F. Shih, W.T. Liu, C.S. Tsai, Critical Reflux, Parametric Sensitivity, and Hysteresis in Azeotropic Distillation of Isopropyl Alcohol + Water + Cyclohexane, Industrial & Engineering Chemistry Research 37 (1998) 2835-2843.

[65] L. Zhigang, Z. Jinchang, C. Biaohua, Separation of aqueous isopropanol by reactive extractive distillation, Journal of Chemical Technology & Biotechnology 77 (2002) 1251-1254.

[66] Y. Liu, S.D. Feist, C.M. Jones, D.R. Armstrong, Isopropyl Alcohol Dehydration by Hot Gas Pressure Swing Adsorption: Experiments, Simulations, and Implementation, Industrial & Engineering Chemistry Research 53 (2014) 8599-8607.

[67] H. Yeomans, I.E. Grossmann, A systematic modeling framework of superstructure optimization in process synthesis, Computers & Chemical Engineering 23 (1999) 709-731.

[68] Y. Kawajiri, L.T. Biegler, Comparison of configurations of a four-column simulated moving bed process by multi-objective optimization, Adsorption 14 (2008) 433-442.

[69] P. Pruksathorn, T. Vitidsant, Production of pure ethanol from azeotropic solution by pressure swing adsorption, Korean J. Chem. Eng. 26 (2009) 1106-1111.

[70] M. Simo, C.J. Brown, V. Hlavacek, Simulation of pressure swing adsorption in fuel ethanol production process, Computers & Chemical Engineering 32 (2008) 1635-1649.

[71] J.D. Psaras, J.A. Zahniser, Dehydration of ethanol, US Patent 4351732A, 28, Sep. 1982.

[72] C. Brown, M. Simo, Adsorption process for the dehydration of alcohol, US Patent 8901359 B2, 2 Dec. 2014.

[73] C.J. Brown, M. Simo, Use of pressure swing absorption for water removal from a wet methanol stream, US Patent 8436202 B2, 7 May, 2013.

[74] K.U. Klatt, F. Hanisch, G. Dünnebier, Model-based control of a simulated moving bed chromatographic process for the separation of fructose and glucose, Journal of Process Control 12 (2002) 203-219.

[75] A.S. Andrade Neto, A.R. Secchi, M.B. Souza, A.G. Barreto, Nonlinear model predictive control applied to the separation of praziquantel in simulated moving bed chromatography, Journal of Chromatography A 1470 (2016) 42-49.

[76] P.S. Gomes, A. Rodrigues, Outlet streams swing (OSS) and MultiFeed operation of simulated moving beds, Separation Science and Technology 42 (2007) 223-252.

[77] H. Schramm, A. Kienle, M. Kaspereit, A. Seidel-Morgenstern, Improved operation of simulated moving bed processes through cyclic modulation of feed flow and feed concentration, Chemical Engineering Science 58 (2003) 5217-5227.

[78] Z. Zhang, M. Mazzotti, M. Morbidelli, Continuous chromatographic processes with a small number of columns: Comparison of simulated moving bed with Varicol, PowerFeed, and ModiCon, Korean J. Chem. Eng. 21 (2004) 454-464.

[79] Y. Zang, P.C. Wankat, SMB Operation Strategy−Partial Feed, Industrial & Engineering Chemistry Research 41 (2002) 2504-2511.

[80] G. Agrawal, Systematic optimization and experimental validation of simulated moving bed chromatography systems for ternary separations and equilibrium limited reactions, Chemical and Biomolecular Engineering, Georgia Institute of Technology, Atanta, GA, 2014.

[81] A.V. Kruglov, M.C. Bjorklund, R.W. Curr, Optimization of the simulated countercurrent moving-bed chromatographic reactor for the oxidative coupling of methane, Chemical Engineering Science 51 (1996) 2945-2950.